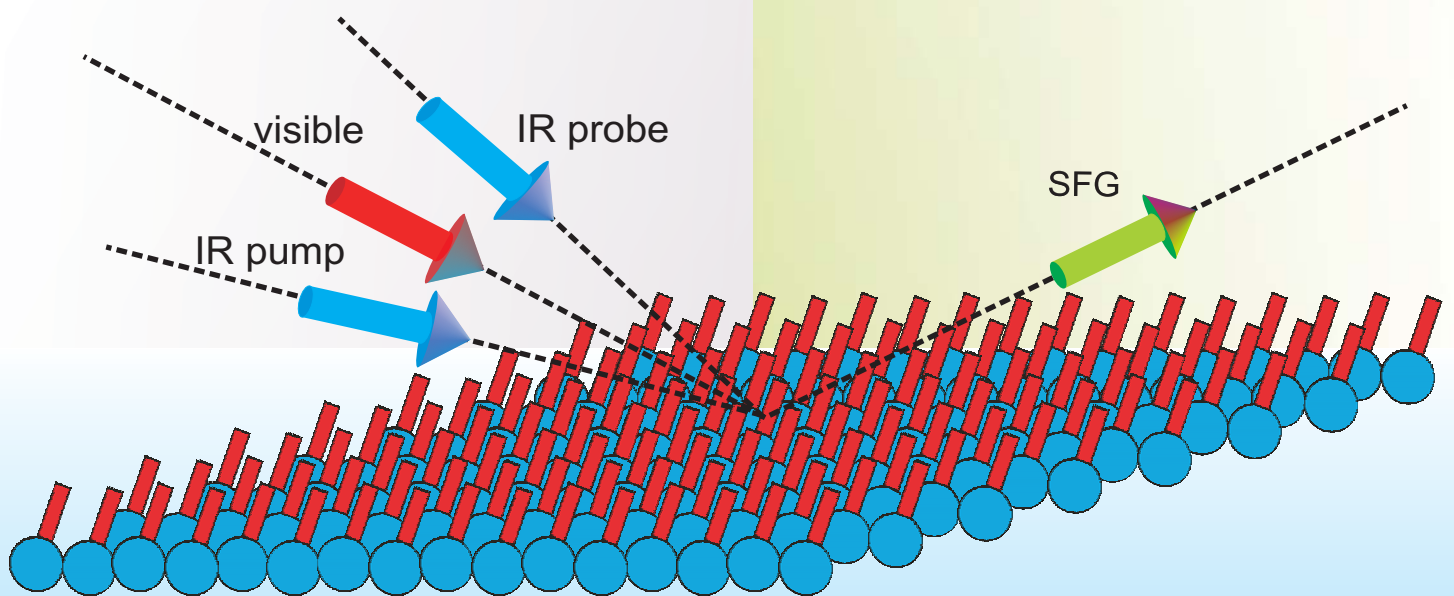


Ultrafast Spectroscopy of Model Biological Membranes



Avishek Ghosh

Ultrafast Spectroscopy of Model Biological Membranes

Ultrafast Spectroscopy of Model Biological Membranes

PROEFSCHRIFT

ter verkrijging van
de graad van Doctor aan de Universiteit Leiden,
op gezag van de Rector Magnificus,
Prof. Mr. Dr. Paul F. van der Heijden,
volgens besluit van het College voor Promoties
in het openbaar te verdedigen
op Woensdag 2 September 2009
klokke 13.45 uur

door

Avishek Ghosh

geboren op 20 Augustus 1979
te London, U.K.

Promotiecommissie

Promotor: Prof. Dr. Mischa Bonn

Overige leden: Prof. Dr. Aart Kleyn
Prof. Dr. Huib J Bakker
Prof. Dr. Marc Koper
Dr. Jens Bredenbeck
Dr. Sander Woutersen
Prof. Dr. Jaap Brouwer
Prof. Dr. Geert-Jan Kroes
Prof. dr. Marc C. van Hemert

This thesis is based on the following publications:

1. **Avishek Ghosh**, Marc Smits, Jens Bredenbeck, Niels Dijkhuizen and Mischa Bonn.
Femtosecond time-resolved and 2D vibrational sum frequency spectroscopy to study structural dynamics at interfaces. *Rev. Sci. Instrum.* *79*, 093907 (2008)
2. Marc Smits*, **Avishek Ghosh***, Martin Sterrer, Michiel Muller, Mischa Bonn.
Ultrafast Vibrational Energy Transfer between Surface and Bulk Water at the Air-Water Interface. *Phys. Rev. Lett.* *98*, 098302 (2007)
3. **Avishek Ghosh**, Marc Smits, Jens Bredenbeck, Mischa Bonn.
Membrane-bound water is energetically decoupled from nearby bulk water: An ultrafast surface-specific investigation. *J. Am. Chem. Soc.* *129*, (31), 9608-9609 (2007)
4. **Avishek Ghosh**, Marc Smits, Maria Sovago, Jens Bredenbeck, Michiel Muller, Mischa Bonn.
Ultrafast vibrational dynamics of interfacial water. *Chem. Phys.* *350*, (1-3), 23-30 (2008)
5. **Avishek Ghosh**, Maria Sovago, R. Kramer Campen and Mischa Bonn.
Structure and dynamics of interfacial water in model lung surfactants. *Faraday Discuss.* *141*, 1-15 (2008)
6. Marc Smits*, **Avishek Ghosh***, Jens Bredenbeck, Susumu Yamamoto, Michiel Muller and Mischa Bonn. Ultrafast energy flow in model biological membranes. *New J. Phys.* *9*, 390 (2007)
7. **Avishek Ghosh**, R.K. Campen and Mischa Bonn.
Ultrafast vibrational dynamics of water at various lipid-water interfaces. (*in preparation*)

Other Publications:

- Jens Bredenbeck, **Avishek Ghosh**, Marc Smits, Mischa Bonn.
Ultrafast Two Dimensional-Infrared Spectroscopy of a Molecular Monolayer. *J. Am. Chem. Soc.* *130* (7), 2152-2153 (2008)
- Jens Bredenbeck, **Avishek Ghosh**, Marc Smits, Han-Kwang Nienhuys and Mischa Bonn.
Interface-Specific Ultrafast Two-Dimensional Vibrational Spectroscopy. *Acc. Chem. Res.* (*in press*) (Web published: May 14, 2009).

*contributed equally to this work

Contents

Chapter 1	
Introduction	1
1.1 Interfaces - A General Perspective	1
1.2 Interfaces in Biology	3
1.3 Membranes and Interfacial Water	4
1.4 Challenges in probing interfacial water	6
1.5 Vibrational Sum Frequency Generation (VSFG) Spectroscopy - The Surface Probe .	7
1.5.1 Concepts in Nonlinear Polarization	7
1.5.2 Sum Frequency Generation	8
1.5.3 Vibrational Sum Frequency Generation at Interfaces	9
1.5.3.1 Properties of $\chi^{(2)}$ and surface-sensitivity of VSFG	11
1.5.3.2 VSFG - A surface-specific IR probe	12
1.6 Time-Resolved SFG Spectroscopy	13
1.7 Thesis Outline	15
Chapter 2	
Experimental Technique	16
2.1 Introduction	17
2.2 Generation of Mid-IR and Visible upconversion pulses for VSFG	17
2.3 Instrumentation at Sample	23
2.4 Detection Schemes and Data Acquisition	24
2.5 Software and Electronics	27
2.6 Getting Started	29
Chapter 3	
Ultrafast Energy Transfer between Interfacial and Bulk Water at the Air-Water Interface	31
3.1 Introduction	32
3.2 Static and Time-resolved VSFG experiments	33
3.3 Results and Discussion	36
3.3.1 Static SFG Results	36
3.3.2 Time-resolved SFG Results	37
3.4 Conclusions	42
Chapter 4	
Ultrafast Dynamics of Water at various lipid-water interfaces	43
4.1 Introduction	44
4.2 Surface-specific Vibrational Spectroscopy: Frequency- and Time-Resolved Sum Frequency Generation	44

Contents

4.3	Experimental Section	46
4.4	Results and Discussion	47
4.4.1	Frequency-resolved SFG experiments	47
4.4.2	Time-resolved SFG experiments	49
4.4.2.1	DPTAP/H ₂ O Interface	51
4.4.2.2	DMPS/H ₂ O Interface	54
4.4.2.3	DPPC/H ₂ O and DPPE/H ₂ O Interface	55
4.5	Conclusion	59
Chapter 5		
Structure and Dynamics of Water at Model Human Lung Surfactant interfaces		61
5.1	Introduction	62
5.1.1	Lung Surfactants and Interfacial Water	62
5.1.2	Frequency- and Time-Resolved SFG on model lung surfactant monolayers on water	63
5.2	Results and Analysis	65
5.2.1	Frequency-resolved VSFG measurements	65
5.2.2	Time-resolved SFG measurements	67
5.3	Discussion	70
5.3.1	Frequency-resolved SFG measurements	70
5.3.2	Time-resolved SFG measurements	70
5.4	Conclusions	72
Chapter 6		
Ultrafast energy flow in model biological membranes		74
6.1	Introduction	75
6.2	Time-resolved Surface Spectroscopy	77
6.2.1	Steady-state Sum Frequency Generation	77
6.2.2	Time-resolved Sum Frequency Generation	78
6.3	Experiment	79
6.3.1	Sample preparation	79
6.4	Results	80
6.4.1	Static SFG Spectra	80
6.4.2	Time Resolved SFG Spectra	82
6.4.2.1	DPPC	83
6.4.2.2	DOPC	85
6.4.2.3	Heat transfer across the monolayer	85
6.4.3	Data Analysis	87
6.5	Discussion	89
6.6	Conclusions and Outlook	90
Bibliography		91
Summary		104
Samenvatting		108
Dankwoord		112
Curriculum Vitae		114

Introduction

1.1 Interfaces - A General Perspective

Surfaces are ubiquitous in nature. Essentially, of everything we see around us, we observe the exposed surface. Surfaces define the boundary with the surrounding environment and influence interactions with that environment, and so it is no surprise that surfaces and interfaces have been intensely studied. We are confronted with interfaces almost every day through phenomena like corrosion, tarnishing of metals, friction, lubrication of moving parts, adhesives, surface tension in liquids and a variety of heterogeneous chemistry in atmospheric (e.g., aerosol chemistry), geological (e.g., mineral oxide-water interfaces) and biological processes.

The discipline 'Surface Science' deals with surfaces ranging from very well-defined single-crystal metal surfaces in ultra high vacuum to extremely complex surfaces of biological cells in living organisms. These efforts are prompted both by a fundamental interest in these intriguing systems, and by the technological importance of surfaces and interfaces: industrial-scale heterogeneous catalysis - whereby reactants (monomers) are adsorbed typically on a metallic surface which reduces the activation energy barrier and provides the essential reaction site - has revolutionized the polymer, petroleum, food and automobile industries today; large surface area materials have been essential for this development. Asymmetric heterogeneous catalysis has recently been used to synthesize enantiomerically pure compounds using chiral heterogeneous catalysts; implications of this development in drug discovery and medicinal chemistry can only be imagined. Metal-insulator interfaces are beginning to show their true power in emerging technologies, like spintronics - whereby the intrinsic electron spins can be used to transport information efficiently. For instance, a major breakthrough has recently been reported on transporting electron spins by efficient quantum-mechanical tunneling through a thin layer of insulator, interfacial with two flanking ferromagnetic layers - termed as Tunnel Magneto-Resistance [1]. So we see interfaces of different materials have remarkable properties that can truly revolutionize existing, and emerging technologies likewise.

Arguably one of the most important interfaces is the membrane surrounding living cells, which enclose a small volume of aqueous solution and separate it from the outside. However, membranes are not simply passive molecular barriers between the interior and the exterior; in fact, their active participation in a variety of natural phenomena is essential for life. In this thesis, we aim at getting

new insights into biological membranes using novel laser-based techniques.

There is a major challenge associated with obtaining a comprehensive understanding of the complex physics and chemistry of interfaces, owing to the difficulty in probing a few angstroms of matter. Nobel Laureate Wolfgang Pauli once said, *God made the bulk; the surface was invented by the devil*. Pauli explained that the diabolical properties of surfaces were due to the simple fact that surface atoms do not have an isotropic environment: they interact with three different types of atoms: those in the bulk below, other atoms from the same surface, and atoms in the adjacent phase. As a result, the properties of surface atoms are very different from those in the adjacent bulk media. With intense experimental pursuits and the advent of a wide variety of surface techniques over the past 50 years, like transmission electron microscopy [2, 3], low energy electron diffraction [4, 5], scanning tunneling microscopy [6–8], atomic force microscopy [6, 9], neutron reflectometry [10], neutron scattering [11] and X-ray diffraction [12, 13], complemented by powerful molecular dynamics simulation studies [14–20], our understanding of surfaces has been radically enhanced, as testified by a variety of emergent surface technologies and a better control over the variety of fundamental interfacial phenomena observed in nature.

The applicability of many surface science techniques is limited to surface samples that can withstand ultrahigh vacuum (UHV) conditions. These techniques are often invasive and generally set specific requirements on the samples, that limit the types of interfaces that can be studied. For instance, UHV conditions are not conducive to study solid-liquid and liquid-liquid interfaces. Probing surfaces by optical techniques is, in general, more flexible, non-invasive and is applicable to samples in their native environment. Indeed, optical techniques such as surface plasmon resonance [21, 22] and reflection absorption IR spectroscopy [23–25] have been insightful while probing surfaces non-invasively. In the past two decades, second-order nonlinear optical techniques of second harmonic generation (SHG) and sum frequency generation [26–30] (SFG) have proven to be versatile non-invasive tools for probing all kinds of interfaces with excellent molecular and surface specificities. The strength of these techniques for studying surfaces and interfaces lies in their inherent surface specificity. Although it was established in the mid-sixties that second harmonic and sum frequency generation could be used to investigate specifically the structures of surfaces and interfaces of centrosymmetric materials (under the electric dipole approximation), it was not until about 1980 that technical advances in laser sources enabled nonlinear optical spectroscopy of surfaces to become well established as a separate subfield¹

In this thesis I present briefly, the vibrationally-resonant sum frequency generation (VSFG) technique that we use to probe molecular processes at liquid-vapor interfaces but primarily introduce a novel time-resolved IR pump - VSFG technique in our continuing quest to unravel some of the mysterious dynamical phenomena associated with biological membranes.

¹For a historical perspective of surface nonlinear optics, I refer to the following review articles by Nobel Laureate, Nicolaas Bloembergen:

- Nonlinear optics and Spectroscopy. Reviews of Modern Physics, Vol. 54, No. 3, July 1982
- Surface nonlinear optics: a historical overview. (Invited Review) Applied Physics B, Vol. 68, 289-293, 1999

1.2 Interfaces in Biology

The main motivation behind the work presented in this thesis is the intriguing yet extremely complex biological interface - the cellular membrane - which compartmentalizes different cell organelles from the external environment and keeps them together for specific biological functions. The cartoon shown in figure 1.1 depicts some of the major constituents of a cell membrane: the lipid bilayer, forming the primary boundary of the cell and various integral and transmembrane proteins embedded in this lipid bilayer for selective transport across the membrane barrier or cellular signaling functions across the cell.

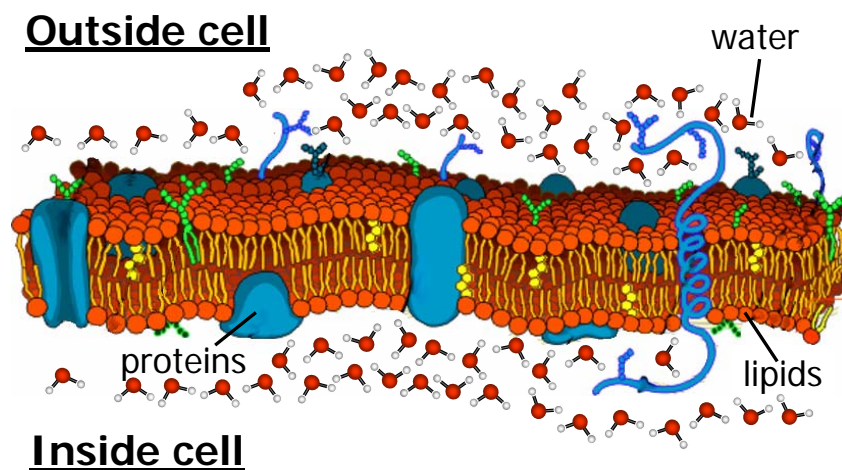


Figure 1.1. The cell membrane. (Courtesy: Wikipedia)

Membranes define the external boundaries of cells and regulate traffic across that boundary. These membranes are however, not merely passive observers of intercellular events. They chaperone and organize a variety of complex reaction mechanisms that control the cellular mass-energy balance and signaling. These membranes have some remarkable properties. Their flexibility permits shape changes that accompany cell growth and movement. They have the ability to break and reseal, causing two membranes to fuse (in exocytosis), or causing a single membrane-enclosed compartment to undergo fission to yield two sealed compartments (in endocytosis or cell division) without any gaping holes or leaks. The selective permeability of membranes allow them to retain certain ions and molecules within cells while excluding others, thus maintaining the ion-balance of the cell. The cell membranes thus participate in a multitude of biochemical processes either actively or by providing a scaffolding for various transmembrane proteins like sodium-potassium ion channels. These functionalities indicate that membranes are not merely a passive barrier but crucial for fundamental cell functioning. Different types of membranes with different compositions, are found even inside

the cells compartmentalizing different cell organelles; for instance, the inner and outer mitochondria, lysosomes, nucleus, rough endoplasmic reticulum (ER), smooth ER, golgi apparatus, etc.

1.3 Membranes and Interfacial Water

To understand the remarkable properties exhibited by membranes, one needs to consider their underlying molecular structure. Lipids, particularly phospholipids, are the basic building blocks of cellular membranes. The key property of lipid molecules is their amphiphilicity - lipids consist of a polar (hydrophilic) *head* and an apolar hydrocarbon (hydrophobic) *tail*, as shown in figure 1.2. As soon as the lipid molecules come in contact with water, the amphiphilicity of the lipids provides the driving force for the spontaneous self-assembly into monolayers and bilayers, with interfacial water molecules hydrating the hydrophilic headgroups² (see figure 1.2).

The lipid hydration process has important structural and functional consequences [31] for the membrane itself. For instance, hydration dynamics [32] and water-lipid interaction strengths [33] are closely related to the membrane fluidity and the molecular organization of the lipids.

The details of the mono-/bilayer self-assembly, including its mechanical properties, the lipid density in the bilayer and the thermodynamics of the process, depend strongly on the hydration of the hydrophilic lipid head groups. The biophysical processes at the cellular interface leading to proper cell functioning are thus dependent, not only on the lipid self-assembly *per se*, but also on the closely associated interfacial water molecules which dictate the mono-/bilayer functionalities. A detailed molecular level picture of the variety of biophysical processes occurring at biological membranes can only be gained by understanding how lipids, proteins and water interact among themselves and with each other. The molecular details of such interactions are expected to be crucial towards the functioning of particular membrane-bound proteins.

Our guess towards understanding of the complexity of membrane function has largely overlooked the role of water in membranes: water is still only efficiently represented as a dielectric medium [34]. Various prior studies imply that this view of water may not do justice to the complexity of its role in membrane function. For instance, studies of partially hydrated bilayers by X-ray scattering, neutron scattering and calorimetry suggest that the lipid phase - an essential parameter for membrane function - varies strongly with membrane hydration [31]. Further, NMR data from stacks of hydrated bilayers make clear that lipid head groups exhibit a strong influence on local water structure: the mobility of membrane-bound water is 100 times slower than that in bulk [35–37]. There is also a growing evidence for the importance of water in specific biochemical/biophysical functions: for example, recent computational studies have highlighted the possibility that water may mediate the interaction between some transmembrane proteins and the surrounding lipids [38, 39].

²In the presence of apolar (hydrophobic) tails, water tends to form ordered hydrogen-bonded *caged* structures around the apolar groups leading to a decrease in entropy of the water-hydrophobe system. Driven by this reduced entropy, the hydrophobic tails tend to aggregate in order to minimize their exposure to water. This phenomenon of aggregation of the hydrophobic tails in the presence of water, called hydrophobic interaction, together with the hydration of the hydrophilic headgroups, leads to the spontaneous assembly of the amphiphilic lipid molecules, forming a monolayer on the water sub-phase.

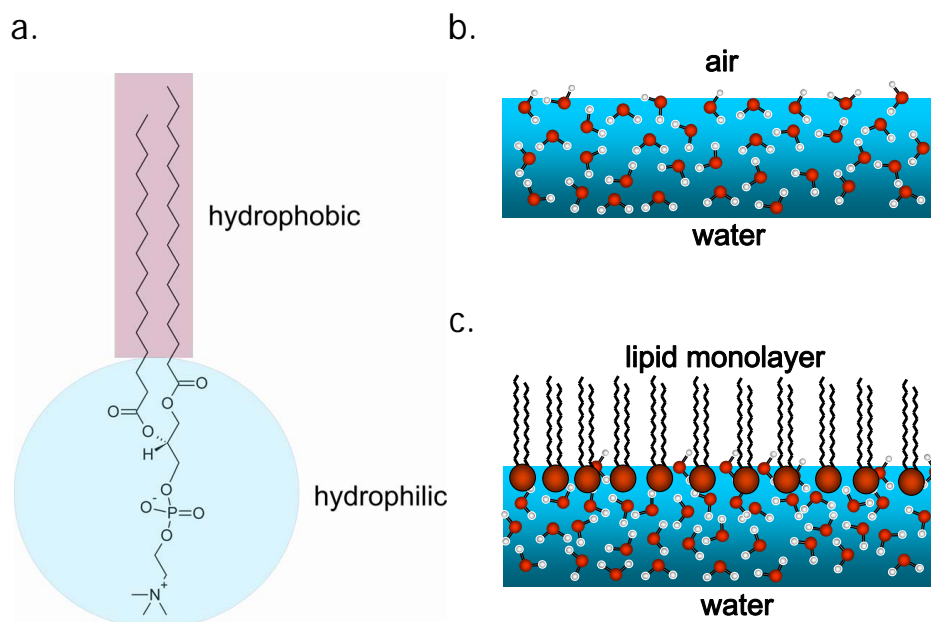


Figure 1.2. (a) Lipid molecule (1,2-dipalmitoyl-*sn*-glycero-3-phosphocholine, DPPC) with the indicated hydrophilic (blue) and hydrophobic (purple) groups. (b) Schematic of the water/air interface. (c) Schematic of a self-assembled monolayer of lipid on a water sub-phase.

The structural dynamics in membranes span timescales from picosecond to millisecond. The short timescales typically indicate fast structural processes like hydrogen-bond rearrangements of water, and the slower processes are associated with both conformational change in larger molecules (lipids and proteins) and collective processes like flip-flop dynamics in the membrane. Since the molecular level properties of small molecules, particular those of water, are known to be important for a number of biochemical/biophysical processes, these time scales are coupled. For instance, it is simply not sufficient to understand conformational rearrangements of transmembrane proteins as an event occurring in a static background of a dielectric continuum of local water molecules. Moreover, the underlying dynamic structure of the membrane along with its local environment (interfacial water molecules) has implications in the observed timescales of various biological events at the interface. Understanding the dynamics of bio-membrane systems on very short timescales is thus essential for a complete understanding of events occurring on longer timescales.

1.4 Challenges in probing interfacial water

Probing the interfacial water and their interactions with the membranes has always been an experimental challenge, as this layer of water is extremely thin. Although Berkowitz *et al* have shown, through molecular dynamics (MD) simulations, that this membrane hydration layer extends only up to ~ 5 Å from the membrane layer [20], these simulations depend heavily on the choice of model potentials used in the calculations. It is only imperative that the membrane hydration layer is directly observed through experiments to validate the true nature of these membranes. As a guideline, we can see from the water density profile calculated by MD simulations (shown in figure 1.3), the membrane bound water essentially has several locations along the surface normal as we move towards the bulk. The plot reveals the locations of buried water (region I) near backbone and carbonyl groups of the lipid headgroup, a first external hydration shell (region II) near the phosphocholine group, secondary hydration shells (regions III-IV) and the bulk water (region V).

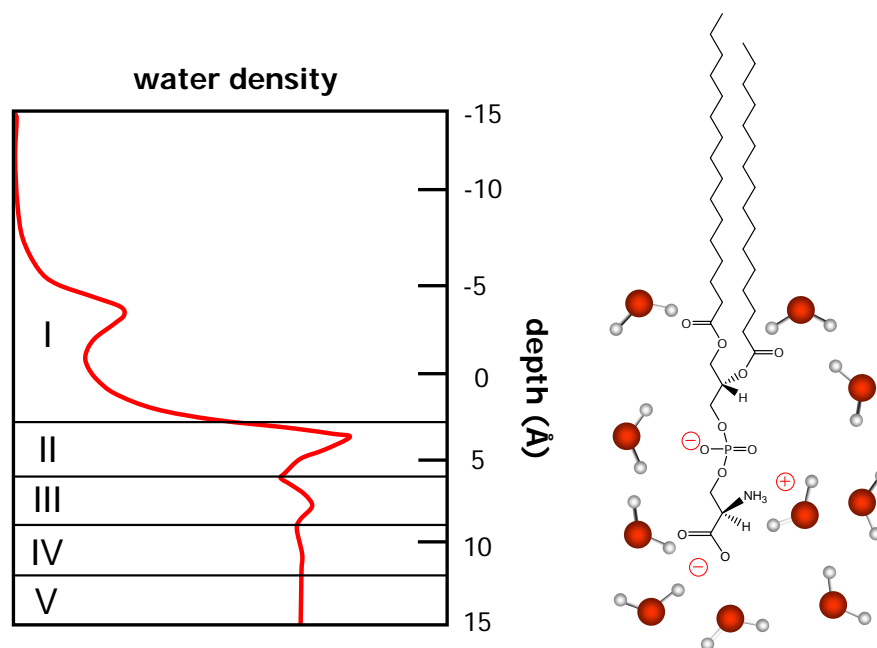


Figure 1.3. The water density profile at the DPPC/water interface from MD simulations [20], is shown on the left. Five distinct regions of interfacial water have been indicated as I-V as a function of the depth (in Å), starting from -15 Å (air), towards 0 Å (phosphate group of the lipid) and finally to 15 Å (bulk water). Region I (-5 to 3 Å) represents location and density of buried water near the carbonyl groups. Region II (3-6 Å) indicates first external hydration shell. Region III-IV (6-12 Å) indicates secondary hydration shells. Region V (>12 Å) indicates bulk water. The cartoon of the hydrated lipid on the right indicates the interfacial water regions, roughly corresponding to the depth scale on the left.

Since directly observing this interfacial water and its role in various complexities of membrane structure/function poses a great experimental challenge, there is no one *perfect* method for studying

such systems. Although it is beyond the scope of this thesis to describe in detail, the wide variety of methods that have successfully been applied to study biological membranes, include time-domain fluorescence (upconversion [40] or correlation [41]) spectroscopies, ESR/EPR [42–44] and NMR (see, e.g. Refs. [45–47]) studies of membrane dynamics, neutron [37, 48, 49] and X-ray scattering [50–52], conventional [53] and multidimensional infrared [54] spectroscopies and scanning probe microscopies [55]. Each of these techniques has its own unique strengths and limitations. In terms of limitations, some of the techniques require a perturbation of the sample due to the local environment necessary for the measurement, such as the elimination of an adjoining liquid water phase (for studies in vacuum), or the stacking of lipid bilayers (e.g. for NMR). Extrapolating such results to biologically relevant conditions clearly requires that the properties of interest do not change as a function of hydration level or headgroup-headgroup interaction. Other techniques may inherently perturb the sample by the means of measurement, for instance by adding a fluorescent label for microscopy, using the tip of a scanning probe microscope, or using high-energy neutrons, X-rays or electrons. Moreover with the existing surface techniques, directly probing such a complex membrane-bound interfacial water non-perturbatively, is almost impossible without compromising on the surface- or molecular-selectivity.

In the recent past, the second order non-linear optical techniques of second harmonic generation (SHG) and sum frequency generation [26–30] (SFG) have proven to be a versatile non-invasive label-free all-optical tool for probing interfaces, especially liquid-liquid interfaces, with excellent molecular and surface specificities. Using vibrational SFG (VSFG), one can probe the vibrational chromophores present in the interfacial molecular moieties, in a background-free, label-free manner. This, as we shall see, is our primary choice of technique to look at the interfacial water.

1.5 Vibrational Sum Frequency Generation (VSFG) Spectroscopy - The Surface Probe

Although a vast number of literature has been written on various nonlinear optical techniques, in this section I introduce some of the basic concepts behind VSFG and its surface and molecular specificity. A comprehensive theoretical treatment of nonlinear optics is beyond the scope of this thesis, but can be followed up in the textbooks of Boyd [56] and Shen [57].

1.5.1 Concepts in Nonlinear Polarization

In linear optical phenomena like reflection or refraction, the optical response of the material atoms is linearly proportional to the strength of the externally applied optical field. Nonlinear optical phenomena, on the other hand are *nonlinear*, in the sense that the optical response of the atoms/molecules in the material depends in a nonlinear manner on the strength of the applied optical field. For instance, second harmonic generation is one of the processes that may occur when the optical response of the material depends quadratically on the applied optical field strength. To quantify the material optical response as a result of the applied optical field, one needs to consider

the time-dependent polarization $\mathbf{P}(\mathbf{r}, t)$ induced in the material, which can be expanded in a Taylor series in terms of the applied field $\mathbf{E}(\mathbf{r}, t)$ to give, in a simplified notation:

$$\mathbf{P}(\mathbf{r}, t) \equiv \chi^{(1)}\mathbf{E}(\mathbf{r}, t) + \chi^{(2)}\mathbf{E}^2(\mathbf{r}, t) + \chi^{(3)}\mathbf{E}^3(\mathbf{r}, t) + \dots \quad (1.1)$$

$$= \mathbf{P}^{(1)}(\mathbf{r}, t) + \mathbf{P}^{(2)}(\mathbf{r}, t) + \mathbf{P}^{(3)}(\mathbf{r}, t) + \dots \quad (1.2)$$

where $\chi^{(1)}$ is the linear susceptibility (or polarizability) - responsible for all linear optical processes; $\chi^{(2)}$ and $\chi^{(3)}$ are the second-order and third-order optical susceptibilities, respectively - responsible for various nonlinear phenomena like SHG/SFG and third harmonic generation. The induced time-dependent polarization $\mathbf{P}(\mathbf{r}, t)$ in the material acts as a source term for generating new fields and is governed by the optical wave equation that follows directly from Maxwell's equations in the electric dipole approximation³

$$-\nabla^2\mathbf{E}(\mathbf{r}, t) + \frac{1}{c^2}\frac{\partial^2}{\partial t^2}\mathbf{E}(\mathbf{r}, t) = -\frac{4\pi}{c^2}\frac{\partial^2}{\partial t^2}\mathbf{P}(\mathbf{r}, t) \quad (1.3)$$

The term $\mathbf{E}(\mathbf{r}, t)$ in this equation 1.3, is the electric field generated in the material as a result of the induced polarization $\mathbf{P}(\mathbf{r}, t)$. This induced polarization is a sum of the linear and non-linear polarizations in the material as shown in equation 1.4

$$\mathbf{P}(\mathbf{r}, t) = \mathbf{P}^{(1)}(\mathbf{r}, t) + \mathbf{P}^{(NL)}(\mathbf{r}, t) \quad (1.4)$$

where $\mathbf{P}^{(1)}(\mathbf{r}, t)$ is the linear polarization and $\mathbf{P}^{(NL)}(\mathbf{r}, t)$ is the non-linear polarization. The non-linear polarization term is the driving field for various non-linear processes.

1.5.2 Sum Frequency Generation

Sum frequency generation (SFG) is a second-order non-linear optical process in which the second-order polarization $\mathbf{P}^{(2)}(\mathbf{r}, t)$ acts as the nonlinear source term $\mathbf{P}^{(NL)}(\mathbf{r}, t)$ (see eq. 1.4) in Maxwell's optical wave equation shown in equation 1.3. From equation 1.1, we have seen that the generic second-order polarization term is given by:

$$\mathbf{P}^{(2)} = \chi^{(2)}\mathbf{E}^2 \quad (1.5)$$

When two different optical fields \mathbf{E}_1 and \mathbf{E}_2 are applied in a material, the total electric field experienced by the system is:

$$\mathbf{E} = \mathbf{E}_1 + \mathbf{E}_2 \quad (1.6)$$

³Under the electric dipole approximation, the wavelength of the electromagnetic radiation which induces (or is emitted during) transitions between different energy levels, is much larger than the typical size of the material atom, approximated to a dipole. It is assumed that the dipole induced within a molecule is related solely to the applied macroscopic field and that contributions from the dipolar fields of neighbouring induced dipoles may therefore be ignored. In addition, within this approximation, the effects of optical magnetic fields and multipoles are neglected, in order to simplify the Maxwell's equations in the course of deriving the optical wave equation.

where the applied fields have optical frequencies ω_1 and ω_2 and have the form:

$$\mathbf{E}_1 = E_1 \cos \omega_1 t \quad (1.7)$$

$$\mathbf{E}_2 = E_2 \cos \omega_2 t \quad (1.8)$$

Now using the equations 1.6, 1.7 and 1.8 in equation 1.5,

$$\mathbf{P}^{(2)} = \chi^{(2)} [E_1 \cos \omega_1 t + E_2 \cos \omega_2 t]^2 \quad (1.9)$$

On expansion of equation 1.9, we get all the possible second order nonlinear optical processes:

$$\mathbf{P}^{(2)} = \frac{\chi^{(2)}}{2} [E_1^2 + E_2^2 - E_1^2 \cos 2\omega_1 t - E_2^2 \cos 2\omega_2 t + 2E_1 E_2 \cos(\omega_1 + \omega_2)t + 2E_1 E_2 \cos(\omega_1 - \omega_2)t] \quad (1.10)$$

In equation 1.10, the first two terms on the right-hand side, represent frequency-independent *optical rectification*, the next two represent *SHG* processes at $2\omega_1$ and $2\omega_2$ optical frequencies, the next one *SFG* at $\omega_1 + \omega_2$ frequency and the last term *difference frequency generation* at $\omega_1 - \omega_2$ frequency. Although the simple classical electromagnetic approach adopted here is sufficient to demonstrate the origins of various second-order nonlinear processes, an exhaustive definition is obtainable through rigorous calculations, such as those presented in the textbooks by Shen [57] or Boyd [56].

In the following section(s), I shall focus mainly on the SFG component of the second-order polarization, where the generated field has a frequency at the sum of the frequencies of the applied optical fields. We shall also show how to use this nonlinear optical technique as a surface-sensitive optical probe.

1.5.3 Vibrational Sum Frequency Generation at Interfaces

The VSFG experiment is schematically shown in figure 1.4. Experimentally, when two laser beams - one with a tunable mid-IR frequency ($\lambda_{\text{IR}} \sim 3000$ nm) resonant with a vibrational mode in the system and the other with a fixed near-IR (visible) frequency ($\lambda_{\text{vis}} = 800$ nm) - are overlapped in space and time at an interface and such that the energies and momenta (phase matching) of the incoming and outgoing photons are conserved, vibrational SFG (VSFG) is generated at a visible frequency ($\lambda_{\text{SF}} \sim 630$ nm). The energy and momentum conservation (phase-matching condition) of the photons involved in the VSFG process are shown in the relations:

$$\hbar\omega_{\text{SFG}} = \hbar\omega_{\text{IR}} + \hbar\omega_{\text{vis}} \quad (1.11)$$

$$\mathbf{k}_{\parallel}^{\text{SFG}} = \mathbf{k}_{\parallel}^{\text{IR}} + \mathbf{k}_{\parallel}^{\text{vis}} \quad (1.12)$$

where \mathbf{k}_{\parallel}^i is the component of the wavevector of the corresponding photon i parallel to the surface.

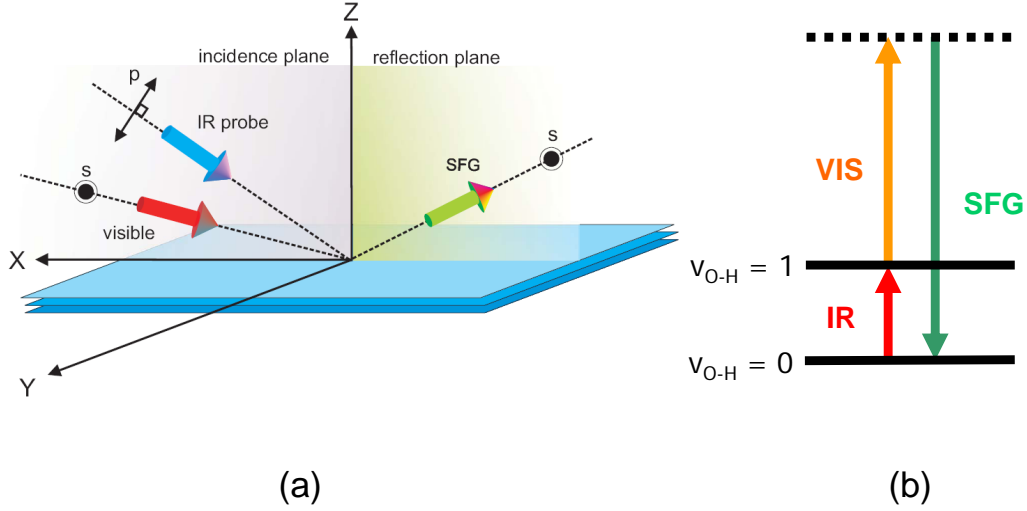


Figure 1.4. (a) Schematic of the Vibrational SFG (VSFG) experiment at an interface. (b) The energy level diagram depicting the VSFG process where the IR frequency is resonant with the $0 \rightarrow 1$ transition and the visible frequency is non-resonant and simply upconverts the $0 \rightarrow 1$ transition to generate the SFG signal.

The correct description of the second-order nonlinear polarization in the Cartesian co-ordinates of the lab frame, is given by:

$$\mathbf{P}_{i,\text{SFG}}^{(2)} = \chi_{ijk}^{(2)} \mathbf{E}_{j,\text{vis}} \mathbf{E}_{k,\text{IR}} \quad (1.13)$$

where i, j and k are indices that correspond to the Cartesian co-ordinates x, y and z (corresponding to the axes shown in figure 1.4). $\mathbf{P}_{i,\text{SFG}}^{(2)}$ denotes the induced polarization in the i^{th} direction due to the j^{th} and k^{th} components of the applied fields, $\mathbf{E}_{j,\text{vis}}$ and $\mathbf{E}_{k,\text{IR}}$, respectively and $\chi_{ijk}^{(2)}$ is the third-ranked second-order macroscopic susceptibility tensor.

In the VSFG process, the emitted SFG field, \mathbf{E}_{SFG} is phenomenologically related to the induced second-order polarization $\mathbf{P}_{i,\text{SFG}}^{(2)}$, through the equation:

$$\mathbf{E}_{i,\text{SFG}} = L_i \mathbf{P}_{i,\text{SFG}}^{(2)} \quad (1.14)$$

where L_i is the non-linear Fresnel factor associated with $\mathbf{P}_{i,\text{SFG}}^{(2)}$, and it takes into account the geometric (phase matching) considerations of the SFG process - for instance, the polarizations and the angles of the incident applied fields, define the direction of the emitted SFG field.⁴

⁴The electric fields also have Fresnel factors associated with them, usually denoted by K_j . Essentially equation 1.13 can be re-written while including the electric field Fresnel factors as:

$$\mathbf{P}_{i,\text{SFG}}^{(2)} = \chi_{ijk}^{(2)} K_j E_{p/s,\text{vis}} K_k E_{p/s,\text{IR}} \quad (1.15)$$

The SFG intensity I_{SFG} , which is the square of the emitted SFG field $\mathbf{E}_{\text{i,SFG}}$, is then simply proportional to the square of the induced polarization, as follows:

$$I_{\text{i,SFG}} = |\mathbf{E}_{\text{i,SFG}}|^2 \quad (1.16)$$

$$I_{\text{SFG}} = |L_i \mathbf{P}_{\text{i,SFG}}^{(2)}|^2 \quad (1.17)$$

$$= |L_i \chi_{ijk}^{(2)} \mathbf{E}_{\text{j,IR}} \mathbf{E}_{\text{k,vis}}|^2 \quad (1.18)$$

$$= |L_i \chi_{ijk}^{(2)}|^2 I_{\text{j,IR}} I_{\text{k,vis}} \quad (1.19)$$

Therefore, by simply measuring the SFG intensity using certain polarization combinations of the incoming and outgoing beams, one can estimate the value of $\chi_{ijk}^{(2)}$ for a given material.

1.5.3.1 Properties of $\chi^{(2)}$ and surface-sensitivity of VSFG

$\chi_{ijk}^{(2)}$ is a third-rank tensor, where i, j and k indices represent the Cartesian co-ordinates of the laboratory frame, thus leading to 27 possible susceptibility tensor elements. The macroscopic $\chi^{(2)}$ is related to the molecular second-order hyperpolarizability $\beta_{\lambda\mu\nu}^{(2)}$ (defined in the molecular frame), through:

$$\chi_{ijk}^{(2)} = N \sum_{\lambda,\mu,\nu} \langle (\hat{i} \cdot \hat{\lambda})(\hat{j} \cdot \hat{\mu})(\hat{k} \cdot \hat{\nu}) \rangle \beta_{\lambda\mu\nu}^{(2)} \quad (1.20)$$

where N is the number density of molecules, $(\hat{i}, \hat{j}, \hat{k})$ are the unit vectors in the laboratory frame and the $(\hat{\lambda}, \hat{\mu}, \hat{\nu})$ are the unit vectors in the molecular frame. The angular brackets indicate averaging over the molecular orientational distribution. Thus, $\chi_{ijk}^{(2)}$ is an orientationally- and number-averaged quantity of the molecular hyperpolarizability, $\beta_{\lambda\mu\nu}^{(2)}$ which is a product of the IR and the Raman transition moments of the molecule. [58] Both $\chi^{(2)}$ and $\beta^{(2)}$ are third-ranked tensors: third-ranked tensors have the property that they change sign upon an inversion operation in which $\hat{i} \rightarrow -\hat{i}, \hat{j} \rightarrow -\hat{j}, \hat{k} \rightarrow -\hat{k}$. Therefore,

$$\chi_{ijk}^{(2)} = -\chi_{-i-j-k}^{(2)} \quad (1.21)$$

For materials or systems possessing inversion symmetry, molecular properties do not change upon inversion operation. Therefore:

$$\chi_{ijk}^{(2)} = \chi_{-i-j-k}^{(2)} \quad (1.22)$$

The only solution that satisfies both the equations 1.21 and 1.22 is:

$$\chi_{ijk}^{(2)} = -\chi_{ijk}^{(2)} = 0 \quad (1.23)$$

For purposes of this section where the electric fields are represented as vectors and not scalar quantities, it is not necessary to discuss the electric field Fresnel factors exhaustively, although a thorough discussion can be found in [58].

This sets the selection rule that SFG is forbidden in any medium/material that possesses inversion symmetry, where the net $\chi_{ijk}^{(2)} = 0$ under the electric dipole approximation. The bulk of most liquids or solids is regarded as macroscopically random, i.e. possesses inversion symmetry, and is therefore SFG-inactive. However at surfaces and interfaces the inversion symmetry is broken, thus rendering the near-surface region SFG-active. This makes SFG a very attractive surface-sensitive, background-free probe, particularly for liquid-vapor or liquid-liquid interfaces, as there is no contamination of SFG generated from the bulk. In fact, the surface region probed by SFG can be as small as a few angstroms or less, of course depending on the details of the surface being studied.

Moreover, the non-zero $\chi_{ijk}^{(2)}$ values at the interface contain information about the macroscopic orientation of surface molecules. There are 27 possible $\chi_{ijk}^{(2)}$ tensor elements which reflect the molecular hyperpolarizability and molecular orientation at the interface. For an interface composed of non-chiral molecules, with an overall azimuthal symmetry, only seven of the 27 elements are non-zero due to symmetry considerations at the interface, of which several are degenerate, finally leading to only four distinct different sets:

$$\chi_{zzz}^{(2)}, \chi_{xxz}^{(2)} (= \chi_{yyz}^{(2)}), \chi_{xzx}^{(2)} (= \chi_{zyy}^{(2)}), \chi_{zxx}^{(2)} (= \chi_{zyy}^{(2)})$$

The magnitudes of the different tensor elements can be determined by using polarization-resolved measurements. Two different polarizations can be investigated for the two incident beams and the SFG beam: one with the electric field vector perpendicular to the plane of incidence, labeled "s", and one for the electric field vector parallel to the plane of incidence, labeled "p", as shown in figure 1.4.

Four polarization combinations of the 3 beams are sufficient to address the four distinct different sets of the seven non-zero tensor elements: PPP, SSP, SPS, PSS, with the letters listing the polarization of the three fields in the order of decreasing frequency, so the first is for the sum frequency, the second is for the visible beam, and the last is for the infrared beam. The four combinations give rise to four different intensities:

$$I_{PPP} \propto |L'_z L_z L_z \chi_{zzz}^{(2)} + L'_z L_i L_i \chi_{zii}^{(2)} + L'_i L_z L_i \chi_{izi}^{(2)} + L'_i L_i L_z \chi_{iiz}^{(2)}|^2 \quad (1.24)$$

$$I_{SSP} \propto |L'_i L_i L_z \chi_{iiz}^{(2)}|^2 \quad (1.25)$$

$$I_{SPS} \propto |L'_i L_z L_i \chi_{izi}^{(2)}|^2 \quad (1.26)$$

$$I_{PSS} \propto |L'_z L_i L_i \chi_{zii}^{(2)}|^2 \quad (1.27)$$

$$(1.28)$$

, where index i is of the interfacial xy -plane, and L and L' are the linear and nonlinear Fresnel factors, respectively which are essentially a function of the beam geometries and angles with respect to the surface normal (which is along the Z -axis in the figure 1.4).

1.5.3.2 VSFG - A surface-specific IR probe

As shown in the previous section, the SFG intensity is essentially a measure of the macroscopic $\chi^{(2)}$:

$$I_{\text{SFG}} \propto |\chi^{(2)}|^2 \quad (1.29)$$

In VSFG spectroscopy, the $\chi^{(2)}$ can be expressed as a function of the IR frequency ω_{IR} as:

$$\chi^{(2)} = A_{\text{NR}} e^{i\phi_{\text{NR}}} + \sum_j \frac{A_j (N_{0,j} - N_{1,j})}{\omega_{\text{IR}} - \omega_j + i\Gamma_j} \quad (1.30)$$

Here the nonlinear susceptibility $\chi^{(2)}$, and hence the VSFG signal, is enhanced when the IR frequency is resonant with a vibrational mode j of the surface molecules, as seen in the second term of equation 1.30. By scanning the IR over a range of frequencies, we get the VSFG spectrum of the interface. The amplitude of the resonant SFG signal is given by A_j , which is a function of the population difference between the ground and first excited vibrational states, $\Delta N_j = N_{0,j} - N_{1,j}$. ω_{IR} is the frequency of the incident IR pulse, ω_j is the vibrational resonance frequency, and Γ_j is the linewidth of the j^{th} resonance. Generally, there is also a non-resonant contribution to the overall SFG signal, characterized by amplitude A_{NR} and phase ϕ_{NR} . Although the non-resonant signal can exceed the resonant signal in case of metallic substrates, for the interfaces studied in this thesis, the non-resonant contribution from the sub-phase (either water or D₂O) is generally much smaller than the resonant modes at the interface.

Therefore VSFG spectroscopy, with its high sensitivity to molecular-specific vibrational resonances, makes it a surface analogue of IR spectroscopy. Together with its sub-monolayer sensitivity, VSFG technique has proven to be a highly desirable surface tool in the recent past. VSFG is further appealing to the surface science community owing to the relative simplicity in implementation of a basic VSFG setup, that has recently become available commercially [59]. As a result, the past two decades have seen much work in frequency- and polarization-resolved VSFG devoted to characterizing and understanding various solid-gas, liquid-gas, and liquid-liquid interfaces (see, e.g. [60–78].)

1.6 Time-Resolved SFG Spectroscopy

By providing the information-rich vibrational spectrum of interfaces in a surface-specific, label-free and background-free manner, frequency-resolved static VSFG studies have created a significant impact in the surface science community. However this static spectroscopy falls short of providing direct information on the dynamics of molecular structures and intra-/intermolecular vibrational coupling, which evolve at ultrafast time scales. IR pump-probe [79,80] and 2D-IR [81,82] techniques developed in the recent past, have shown their advantage over static spectroscopy in their ability to directly probe the ultrafast molecular dynamics in *bulk* systems. Although the first literature on pump-probe SFG experiments using picosecond pulses to probe vibrational lifetimes of adsorbates on semiconductor [83] and on metal surfaces [84] appeared in 1990, the time and frequency resolutions and the applicability of the technique to any interface were restricted to picosecond molecular dynamics. With the development of short amplified pulses (~ 100 fs) and better detection techniques, broad-

band IR pump - SFG probe experiments with sub-picosecond time resolution have now become a possibility. As a result, sub-picosecond surface vibrational lifetimes and dynamics can be interrogated directly. In the recent past, pump-probe SFG experiments have been performed to study the mechanisms of adsorption and desorption of gases on catalytic metals under UHV conditions [85]. Recently time-resolved electronic SFG studies have interrogated probe molecules at *buried* interfaces [86]. The work presented in this thesis, demonstrates a novel time-resolved SFG (TR-SFG) technique that was developed by combining static broadband SFG spectroscopy with IR pump-probe spectroscopy to study the ultrafast structural dynamics of molecules at the air-water interface and various water-lipid (model bio-membrane) interfaces: an attempt to elucidate the structure and dynamics of water at the model biological interfaces, under normal laboratory conditions. The development of our time-resolved SFG spectrometer was contemporaneous with that in the group of Y. R. Shen, which published the first IR pump - SFG probe results of interfacial water [87].

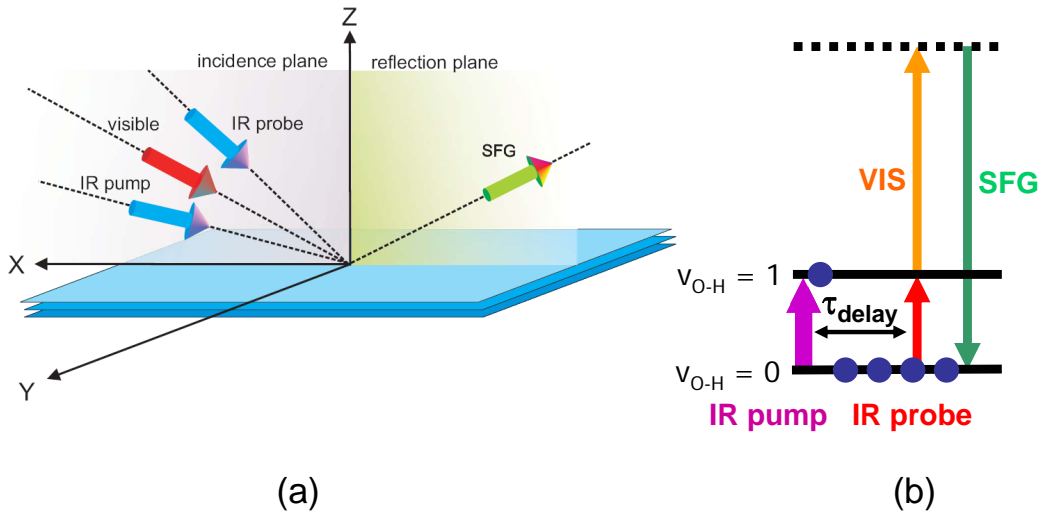


Figure 1.5. (a) Schematic of the TR-SFG technique with the indicated pump IR, probe IR, the visible and the SFG beams. (b) The energy level diagram in the presence of a pump pulse which excites molecules to the first vibrationally excited state. The pair of probe pulses generating the SFG beam is scanned in time τ_{delay} with respect to the IR pump pulse. By monitoring the modulation in the SFG signal as a function of time, the evolution of the system can be followed in real-time as molecules relax back to the ground state.

The basic schematic of the pump-probe TR-SFG technique and the energy level diagram is shown in figure 1.5. In a pump-probe TR-SFG experiment, the pump IR pulse excites molecules from the ground state $v = 0$ to the first vibrationally excited state $v = 1$ in a two-step process: high intensity IR pump pulse first prepares the two-level system by creating a vibrational coherence between the $v = 0$ and $v = 1$ and then population is transferred from $v = 0$ to $v = 1$. If the anharmonicity of

the vibration is larger than our experimental IR probe frequency window ($\sim 120 \text{ cm}^{-1}$), the excited state SFG signal ($v = 1 \rightarrow 2$) will not be observed. Moreover, this $v = 1 \rightarrow 2$ signal will be very small, given the fact that the SFG intensity depends on the square of the surface population density. This pump-induced population transfer from $v = 0 \rightarrow 1$, transiently reduces the effective $\chi^{(2)}$ of the system since $\chi^{(2)} \sim \Delta N$, where ΔN is the population difference between $v = 0$ and $v = 1$ states. This perturbation in the equilibrium population distribution is observed as a reduction in the SFG probe signal ('bleach'). As the molecules relax back to the vibrational ground state, the equilibrium population distribution is regained: the SFG signal returns to its original magnitude as a function of the delay time between the IR pump pulse and SFG probe pulse pair. In this mode, TR-SFG is fully analogous to the more widely applied transient IR absorption spectroscopy, except for the fact that the latter involves detection of a third-order coherence (two interactions with the pump IR field and one with the probe IR field), while the former involves the up-conversion of the third-order coherence created by the pump and probe IR fields, to a fourth-order coherence by the visible pulse. Hence the TR-SFG technique involves a $\chi^{(4)}$ optical interaction while static SFG spectroscopy is a $\chi^{(2)}$ process. The time dependence of the fourth-order signal is contained in the population densities of the ground (N_0) and the excited state (N_1), such that, in the absence of intermediate states:

$$I_{SFG} \propto [N_0(t) - N_1(t)]^2 \quad (1.31)$$

$$= [1 - 2N_1(t)]^2 \quad (1.32)$$

$$= 1 - 4N_1(t) + 4N_1^2(t) \quad (1.33)$$

$$\approx 1 - 4N_1(t) \quad (1.34)$$

This has some interesting consequences: for example, when the pump excites 10% of the ground state molecules to the excited state at zero pump-probe delay, the population difference amounts to $[N_0(t) - N_1(t)]^2 = (0.9 - 0.1)^2 = 0.64$. The SFG intensity level thus decreases to 0.64 and thus a bleach of 36% is observed. We further note that, for sufficiently small N_1 , the signal will decay with T_1 . This simplified analysis of TR-SFG data is dealt with, in greater detail in Chapter 3.

1.7 Thesis Outline

This thesis is essentially a compilation of various experiments performed using the novel TR-SFG spectroscopy technique. In the next chapter (Chapter 2), I describe the TR-SFG experimental setup in detail. In Chapter 3, I show the results of the first experiments performed using TR-SFG to study the vibrational dynamics of water molecules at the water-air interface. In Chapter 4, I discuss the TR-SFG experiments performed to elucidate the dynamics of water molecules at a variety of lipid-water interfaces. Chapter 5 deals with the TR-SFG studies of water on a model lung surfactant system. In Chapter 6, I describe the studies on the vibrational relaxation dynamics of C-H moieties and the energy flow dynamics across a model membrane system.

Chapter 2

Experimental Technique

Abstract

We present a novel setup to elucidate the dynamics of interfacial molecules specifically, using surface-selective femtosecond vibrational spectroscopy. The approach relies on a fourth-order nonlinear optical interaction at the interface. In the experiments, interfacial molecules are vibrationally excited by an intense, tunable femtosecond mid-infrared ($2500\text{--}3800\text{ cm}^{-1}$) pump pulse, resonant with the molecular vibrations. The effect of the excitation and the subsequent relaxation to the equilibrium state are probed using broadband infrared+visible sum frequency generation (SFG) light, which provides the transient vibrational spectrum of interfacial molecules specifically. This IR pump-SFG probe setup has the ability to measure both vibrational population lifetimes as well as the vibrational coupling between different chemical moieties at interfaces. Vibrational lifetimes of interfacial molecules are determined in one-dimensional pump-SFG probe experiments, in which the response is monitored as a function of the delay between the pump and probe pulses. Vibrational coupling between molecular groups is determined in two-dimensional pump-SFG probe experiments, which monitor the response as a function of pump and probe frequencies at a fixed delay time. To allow for one setup to perform these multifaceted experiments, we have implemented several instrumentation techniques described here. The detection of the spectrally resolved differential SFG signal using a combination of a charge-coupled device camera and a galvanic optical scanner, computer-controlled Fabry–Pérot etalons to shape and scan the IR pump pulse and the automated sample dispenser and sample trough height corrector are some of the novelties in this setup.

2.1 Introduction

In this chapter, the experimental setup for time-resolved sum frequency generation (TR-SFG) spectroscopy is presented in detail. The first section describes the scheme for generating high intensity mid-IR pulses ($2900\text{-}3500\text{ cm}^{-1}$) and the home-built pulse shaper for generating the narrowband visible upconversion pulse (12500 cm^{-1} ; 800 nm). The second section deals with the instrumentation and device controls at the sample stage. The third section discusses the novel instrumentation utilized in the detection path and acquisition schemes, followed by a fourth section that deals with the electronics, device synchronization and the data acquisition software. Finally, the chapter ends with a section that gets us started with the essentials to perform a TR-SFG experiment.

2.2 Generation of Mid-IR and Visible upconversion pulses for VSFG

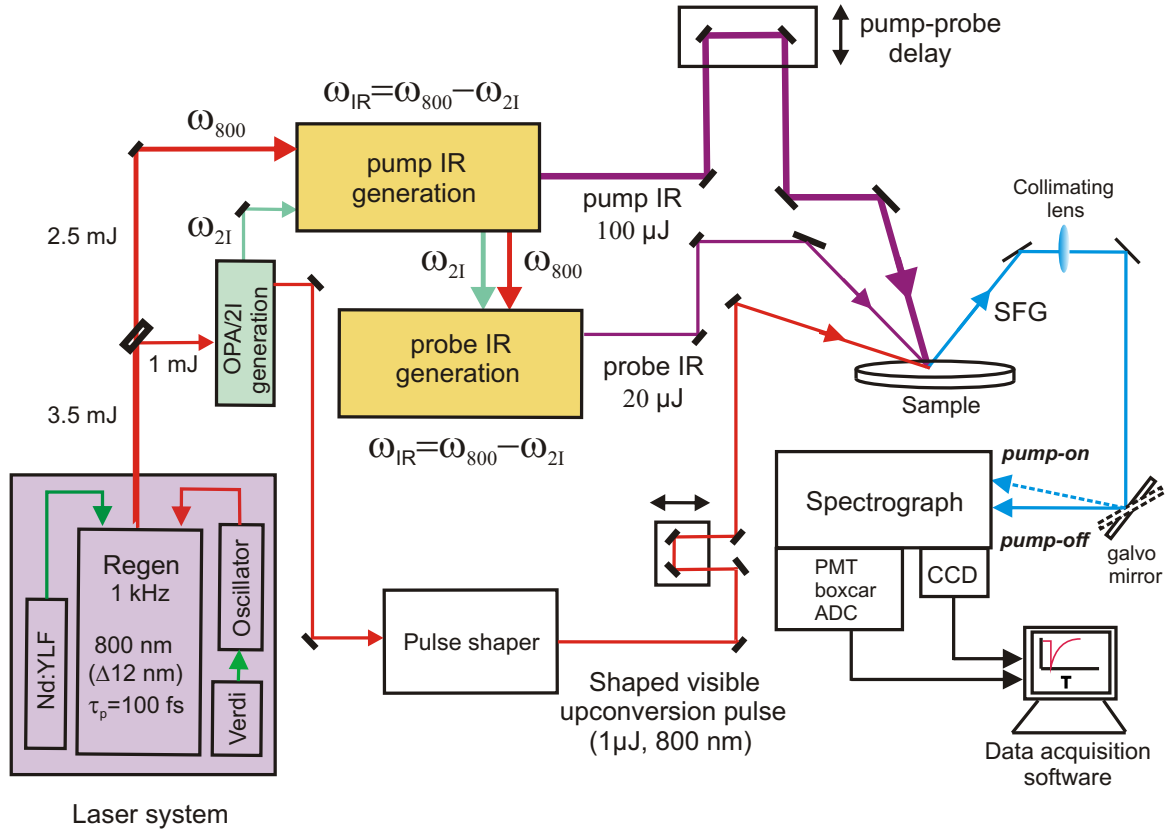


Figure 2.1. TR-SFG Experimental Setup.

The TR-SFG experimental scheme can be seen in figure 2.1. A conventional broadband SFG setup [77] requires a pair of probe laser pulses, i.e., a weak broadband IR ($\sim 10\text{ }\mu\text{J}$, FWHM ~ 150

cm^{-1}) and a narrowband visible upconversion pulse ($\sim 1 \mu\text{J}$, $\text{FWHM} < 10 \text{ cm}^{-1}$), to generate SFG at the interface. However for the TR-SFG experiments, an additional high intensity ($\sim 40 \mu\text{J}$) mid-IR pump pulse is required to excite ground state molecules to a higher vibrational state. This section will be used to describe the schemes adopted to generate appropriate mid-IR and visible pulses. The pulse generation scheme can be seen in Figure 2.2.

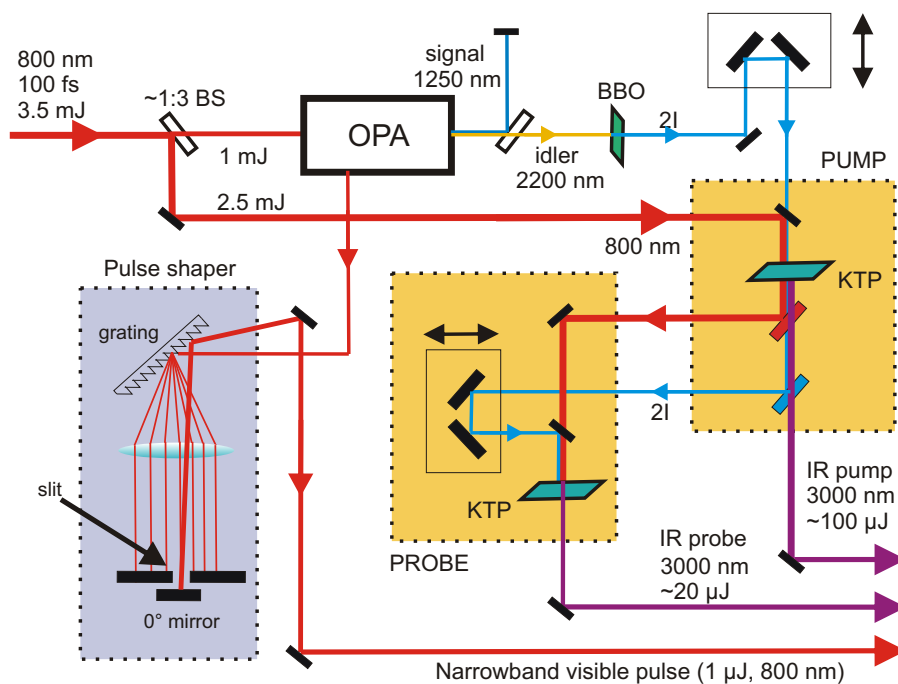


Figure 2.2. Generation of Mid-IR and narrowband visible pulse.

The Laser System

The laser system consists of a Verdi (diode-pumped Nd:YVO₄ CW laser from Coherent) which pumps a Ti:Sapphire based oscillator (Mira 900, Coherent) to generate mode-locked 800 nm pulses with sub-100 fs pulse duration. This provides the seed pulses for a Ti:Sapphire regenerative multipass amplifier (Titan, Quantronix), that is pumped by a high energy (18W, 100 ns) Nd:YLF laser (DQ-527, Quantronix). The multipass amplifier produces $\sim 3.5 \text{ mJ/pulse}$ centered at 800 nm with a bandwidth of $\sim 12 \text{ nm}$ with repetition rate of 1 kHz and 100-120 fs pulse duration. A commercial 5-pass *beta*-Barium Borate crystal (BBO)-based optical parametric amplifier (TOPAS, Light Conversion) is then pumped with 30% (1 mJ) of the amplified 800 nm beam to generate $\sim 350 \mu\text{J}$ of tunable signal ($\sim 1250 \text{ nm}$) and idler ($\sim 2200 \text{ nm}$) beams. The idler is then doubled in another type-I *beta*-Barium Borate crystal (BBO) (*beta*-BaB₂O₄, $5 \times 5 \times 3 \text{ mm}^3$, $\phi = 90^\circ$, $\theta = 22.2^\circ$) to generate $\sim 45 \mu\text{J}$ of $\sim 1100 \text{ nm}$ pulses.

Difference Frequency Mixing

Difference frequency mixing (DFM) of the doubled idler beam (1100 nm) with the remaining 70% (2.5 mJ) amplified 800 nm beam in a type-II parametric conversion process in Potassium Titanyl Phosphate (KTiOPO₄, KTP) crystal (10x10x3 mm³, $\phi = 0^\circ$, $\theta = 41.8^\circ$) produces $\sim 100 \mu\text{J}$ mid-IR pulses ($\sim 3000 \text{ nm}$). This scheme of DFM of the 800 nm and doubled idler, adopted from the scheme by Emmerichs et al. [88], not only generates a high intensity mid-IR beam but also amplifies the number of doubled idler photons as a result of an optical parametric amplification (OPA) process. This OPA can be viewed as an optical scattering process in which an 800 nm photon is scattered to two lower energy photons in KTP, while satisfying the requirement that energy be conserved:

$$\hbar\omega_{800} = \hbar\omega_{1100} + \hbar\omega_{3000} \quad (2.1)$$

In addition, photon momentum, \bar{k} must also be conserved (phase matching of the wavevectors):

$$\bar{k}_{800} = \bar{k}_{1100} + \bar{k}_{3000}. \quad (2.2)$$

This scattering of one 800 nm photon could, in principle, yield two photons with an infinite number of combinations of lower energy scattered photons while maintaining the conservation of energy. However the phase-matching conditions of the KTP crystal [89] limit the range of the desired wavelengths. To generate high intensities, 1100 nm photons are required to seed the DFM process, leading to a stimulated emission of 1100 nm and generation of 3000 nm photons. This DFM/OPA process can be easily understood from the energy level scheme as shown in figure 2.3. The generation of mid-IR beam is hence always associated with a substantial amplification of the doubled idler beam. The amplification of the 1100 nm beam can be used as a beam alignment diagnostic for mid-IR generation. By placing a Potassium Dihydrogen Phosphate (KH₂PO₄, KDP) crystal in the path of the doubled idler beam, the second harmonic of the doubled idler is generated - seen as a green beam (550 nm). At the correct phase matching angle of the KTP crystal and the correct temporal overlap of the 800 nm and the doubled idler beams, the second harmonic beam (550 nm) at the KDP, intensifies manifold, indicating the generation of the mid-IR beam.

Frequency tuning of the mid-IR pulse requires changing the fundamental idler frequency at the OPA stage (changing the phase matching angle of the BBO in the TOPAS) and subsequently optimizing the phase matching angles of the idler doubling crystal (BBO) and the KTP crystal. Using this approach of DFM, the centre frequency of the generated high-intensity mid-IR pulses is limited by the tuning curves of the KTP and the BBO crystals corresponding to the doubled idler and the NIR frequencies; generated mid-IR frequencies range from 2860 nm (3496 cm⁻¹) to 3570 nm (2801 cm⁻¹), with pulse energies in the order of 80-100 μJ . Typical full-width half maximum (FWHM) bandwidths of the mid-IR pulse amount to $\sim 150 \text{ cm}^{-1}$. This is used as the IR pump pulse; the intensity is typically attenuated using a neutral density filter to $\sim 40 \mu\text{J}$ to prevent cumulative heating of the interface which may affect the lipid phase and cause irreversible chemical changes of some of the lipid samples. The mid-IR transient SFG spectra used in our experiments typically

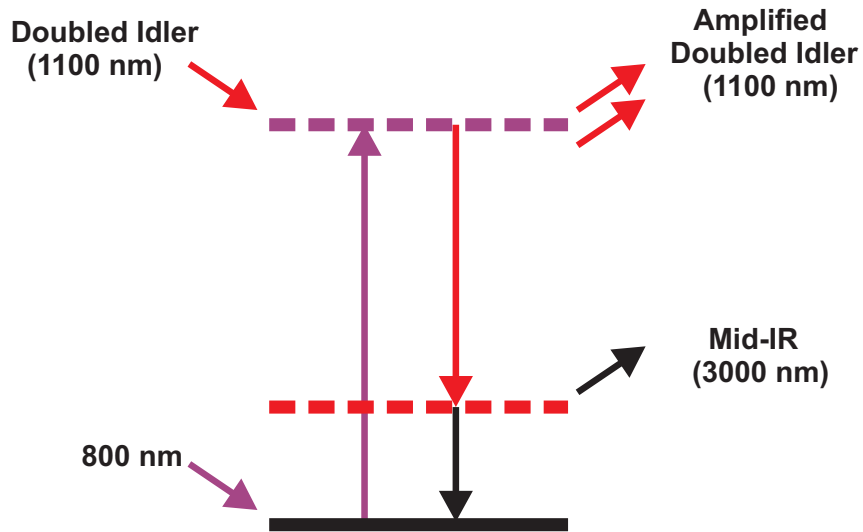


Figure 2.3. Energy level scheme for Difference Frequency Mixing. The levels with dotted lines represent virtual states in the photon scattering process.

range from 2900 to 3500 cm^{-1} and their corresponding spectra are shown in Figure 2.4.

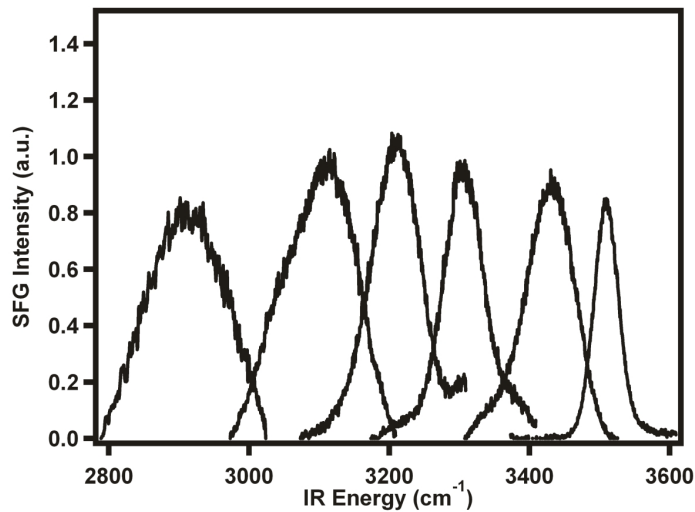


Figure 2.4. The range of mid-IR wavelengths generated by difference frequency mixing of 800 nm and doubled idler in the setup. The non-resonant SFG spectra shown here are generated at Au-air interface

The residual 800 nm pulse and the amplified doubled idler pulse after the pump IR generation, are separated using dichroic mirrors and recombined in a collinear fashion after appropriate time delays for the two pulses. The two pulses are then mixed in a second type-II KTP crystal ($5\times 5\times 3\text{ mm}^3, \phi = 0^\circ, \theta = 41.8^\circ$), to generate $\sim 25\text{ }\mu\text{J}$ of probe IR (FWHM $\sim 150\text{ cm}^{-1}$). In this manner, the probe IR wavelength can be tuned independently of the pump IR wavelength to a limited extent - the pump and the probe IR frequencies can be detuned by 200 cm^{-1} . With this scheme, we can perform

two-color pump-probe SFG experiments [90], but only to a limited extent. The limited detuning is caused by the fact that the doubled idler frequency which is used for IR pump generation is also used to generate the probe IR frequency.

Home-built pulse shaper for the visible upconversion pulse

The large frequency content of the broadband IR pulse allows us to investigate several vibrational resonances at once. The IR pulse sets up coherent polarizations, both in the bulk and at the interface. The interfacial polarization is upconverted using the visible laser pulse, to give a signal in the phase-matched direction. As such, the frequency resolution of the SFG depends on the bandwidth of the upconversion pulse. Shown in figure 2.5 is a home-built pulse shaper, that narrows the bandwidth of the visible pulse and thus allows us to maintain high frequency resolution in the experiment.

The pulse-shaper has a 4-f configuration (see figure 2.5a). In this configuration, the grating at the input disperses the incoming pulse. This frequency-dispersed pulse is imaged by a convex lens of focal length f onto its Fourier plane which is at a distance of $2f$ from the grating. Here all the frequency components of the pulse are spatially separated. A slit placed at the Fourier plane can be used to select a certain frequency range thus making the pulse narrow in the frequency domain. Fourier recomposition of this *shaped* pulse from the frequency to the time-domain is achieved by placing another grating at a distance of $2f$ from the lens, away from the first grating.

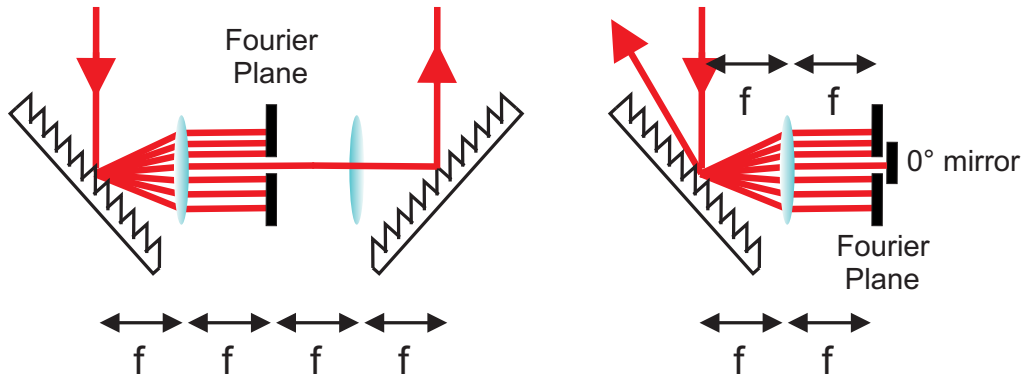


Figure 2.5. Our 4f-configuration pulse shaper: unfolded (a) and folded (b).

Our home-built pulse shaper has essentially a folded 4f-configuration (see figure 2.5b). The input for the pulse shaper is the residual of the 800 nm (FWHM ~ 12 nm) beam that is used to generate signal and idler pulses in the TOPAS. After the Fourier decomposition of the pulse and selection of a narrow frequency at the Fourier plane with a mechanical slit, a 0 mirror is placed very close to the slit. This mirror reflects the selected frequency back onto the input grating (only slightly displaced in the vertical plane), for Fourier recomposition of the narrowband pulse back into the

time-domain. Typical bandwidth of the shaped pulse is $\sim 0.3\text{-}0.6\text{ nm}$ or $5\text{-}10\text{ cm}^{-1}$) FWHM. Figure 2.6 shows different spectra obtained with the pulse-shaper, at different slit-widths.

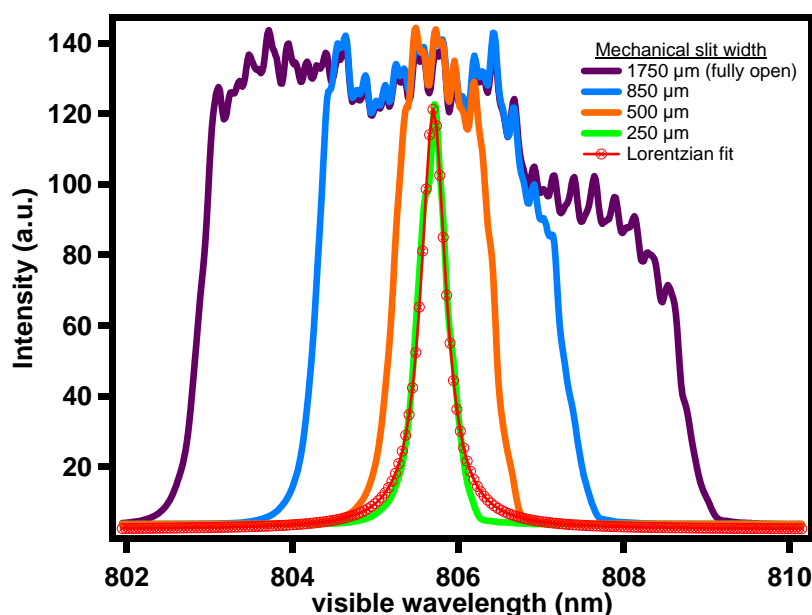


Figure 2.6. Frequency shaping of visible pulse at various slit widths of the pulse-shaper.

Since this visible pulse is used to up-convert a vibrational resonance to generate the SFG spectrum, a narrow band visible pulse (much narrower than the bandwidth of a typical vibrational mode $\sim 15\text{ cm}^{-1}$), ensures a high resolution of the spectrum acquired. However this high resolution comes at a cost. Due to the time-bandwidth product, the narrower the bandwidth is, the longer is the pulse duration, leading to a reduced peak intensity. This limits the high-resolution SFG spectral intensity usually between 0.1 and 10 detected photons per laser shot. Of course, maintaining high resolution of the SFG spectrum makes sense only when the vibrational resonances are narrow; for instance while probing the CH_3 symmetric stretch mode which has a linewidth of $\sim 12\text{ cm}^{-1}$. However in case of the hydrogen-bonded O-H vibrational modes in H_2O , which span $\sim 400\text{ cm}^{-1}$, the spectral resolution can be safely compromised on, and a spectrally broader and hence a more intense visible pulse can be used to up-convert the resonance.

Note: Frequency shaping of the mid-IR pump is also a possibility in this experimental scheme, which have been used in 2D-SFG experiments reported in [91]. The 2D-SFG instrumentation involves placing a piezo-controlled Fabry-Pérot etalon (ThorLabs) in the pump IR path of the existing TR-SFG scheme (see figure 2.7). By adjusting the voltage on the piezoelectric actuators, one can

control the parallelism and the distance between the mirrors of the etalon, thus controlling the center frequency and width of the pulse. The etalon shapes the broadband pump IR pulse (FWHM $\sim 200 \text{ cm}^{-1}$) into a narrowband pulse (FWHM $\sim 20 \text{ cm}^{-1}$). Typical energies of the shaped pump IR pulses is $\sim 10 \mu\text{J}$, due to the inherent reflective losses in the Fabry-Pérot etalon. As shown in figure 2.7, a small part (1%) of the pump IR and the visible upconversion pulse are mixed in a Lithium Niobate (LiNbO_3) crystal to generate a sum frequency signal which is used to calibrate the excitation frequency.

2.3 Instrumentation at Sample

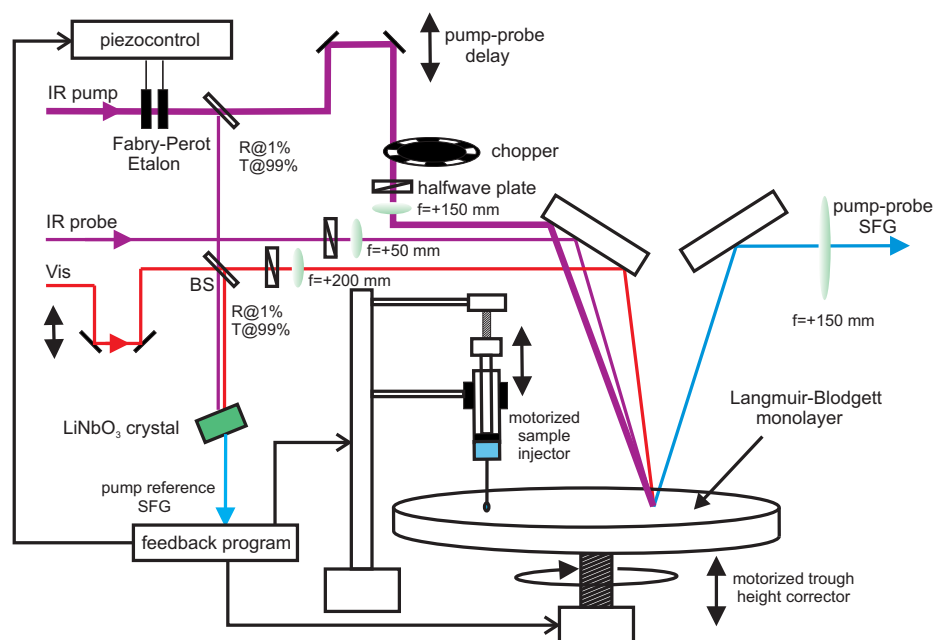


Figure 2.7. Instrumentation at the sample.

In figure 2.7, a schematic overview of the instrumentation at the sample is shown. The pump IR, probe IR and the visible beams are kept in the same vertical plane of incidence and focused down to beam waists of 150, 100 and $100 \mu\text{m}$, respectively. The beams are overlapped at the sample interface, at incidence angles of 56° , 46° and 50° , respectively with respect to the surface normal. The probe IR and the visible beam generate the SFG spectrum at the interface when the two incident fields are temporally and spatially overlapped. The temporal overlap can be achieved by scanning

the delay of the visible pulse. The spatial and temporal overlap of the pump IR with the SFG probe pair can be optimized by monitoring the third-order (bulk-allowed) nonlinear optical process of infrared-infrared-visible-SFG (IIV-SFG) [92], which occurs only when all the three incident pulses overlap. The energy level scheme for such an IIV-SFG process is shown in figure 2.13. Also in the figure, a typical pump-probe cross-correlation IIV signal from an interface is shown (discussed later). The sample is held in a home-built TeflonTM trough (~ 5 cm radius) which is rotated at ~ 5 rpm to reduce cumulative heating. The sample is effectively refreshed every ~ 5 laser shots. This trough is supported on a motorized lab-jack, specially designed to damp mechanical vibrations while rotating the trough or while moving the trough vertically. To account for the evaporation of the water sub-phase, the vertical position of the SFG spectrum on the CCD chip is monitored by the measurement software throughout the experiment. Due to evaporation of the water sub-phase over long data acquisition times, the surface height changes and moves out of the foci of the incident beams. As a result, the SFG signal decreases in intensity and is displaced vertically on the CCD chip. The latter effect is used as a feedback to correct the trough height for evaporation, by a motorized (Standa stepper motor controller 8SMC1-USBh) lab-jack, to restore the signal (and intensity) at the original position on the CCD. Some of the experiments require hours of SFG signal acquisition. Over this period, the surface pressure of the lipid monolayer tends to drop, leading to a drop in signal intensity. One possible reason for this is that the TeflonTM trough becomes coated with lipids. The effect of the pressure drop can be circumvented by the addition of small amounts of fresh surfactants onto the monolayer. The shape of the SFG spectra of a *repaired* monolayer was identical to that of a freshly prepared one. The monolayer repair during data acquisition is performed when the probe SFG signal intensity drops by 20% of the original SFG intensity at the start of the experiment. The computer-controlled feedback program uses a motorized lipid sample injector (syringe filled with the lipid solution in chloroform, attached to a Standa stepper motor) to add a few drops of the lipid solution onto the water sub-phase, and allowing the system to equilibrate. This automation of sample control allows to perform many hours of scanning without human intervention.

2.4 Detection Schemes and Data Acquisition

The pump-probe SFG signal generated from the interface is collected and collimated by a 150 mm positive lens (see figure 2.7) and then sent to either a photomultiplier tube (PMT, Acton Research, PD438) or a monochromator/CCD camera depending on the application. The PMT is used to record the spectrally integrated pump-probe SFG signal in the photon-counting mode [93, 94]. The electronics used for the PMT detection is shown in figure 2.8 with green lines. The PMT signal is averaged on a boxcar integrator, with typical electronic gate widths of $3 \mu\text{s}$. The averaged PMT signal is then sent to the PC through an analog-to-digital converter (ADC, National Instruments, 16-bit). To separate the pump-on and pump-off SFG photons, a diode laser (continuous wave) is transmitted through the same hole in the chopper as the pump beam and onto a photodiode (PD) as schematically shown in figure 2.8. The PD signal is sent to the PC via the ADC; this provides the information as to which laser shot corresponds to pump-on and which one to pump-off SFG signal.

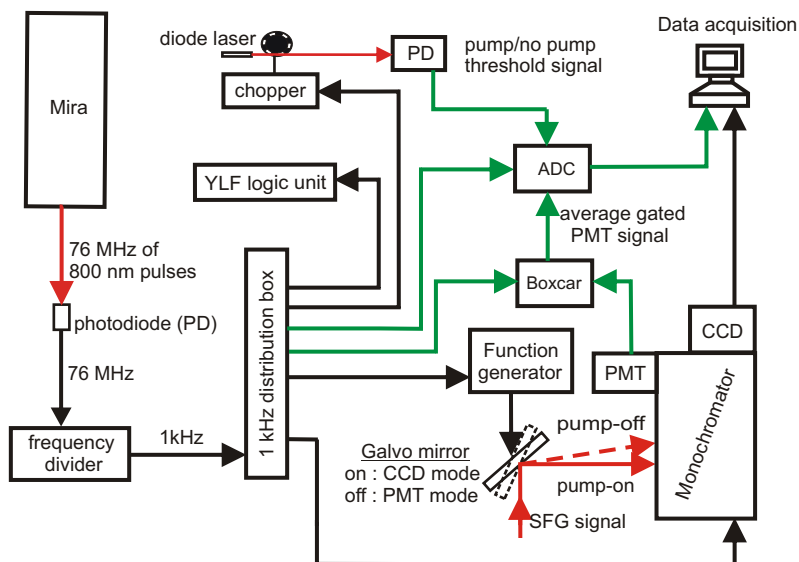


Figure 2.8. Electronics.

For obtaining spectral information during a pump-probe SFG experiment, the SFG signal is dispersed by a monochromator (Acton SpectroPro 300i) and the image is recorded on a CCD chip (512x512 pixels, 24 μm /pixel). In a typical spectrally-resolved TR-SFG experiment we have used two kinds of CCD cameras. Originally an intensified CCD (Princeton Instruments, PI-MAX2:512 Gen III) was used and then an Electron-Multiplying CCD (Andor, iXon^{EM+}). In an intensified CCD (iCCD), the frequency-dispersed SFG photons are incident on a multichannel plate (MCP) that creates an avalanche of photoelectrons for every incident photon - this is the intensifier. These photoelectrons then fall on a phosphor screen creating fluorescent photons which are then incident on the CCD chip. By applying a trigger gate voltage on the MCP, the intensifier gate opens only for a few nanoseconds for CCD image acquisition for SFG. This way, one can record large SFG photon fluxes with minimal shot noise. At high SFG signal photon counts (for example from Au-air or water-charged lipid interface), the iCCD works better than a non-intensified CCD as it cuts down on the ambient noise significantly. However at very low SFG signal limits (e.g., neat water-air interface), an EM-CCD (thermo-electrically cooled down to about -100°C) seems to be a much better choice as the iCCD at low signals has such a large read-out noise that it overwhelms the SFG signal. In the EM-CCD, every photon is converted to an electron on the CCD. All the electrons in an image frame are first binned vertically onto a single shift register (1×512) which is then amplified

in a multiplication register and then read out. This way for a 512×512 chip the read-out noise corresponds to only 512 pixels. In contrast, the iCCD image is read out line-by-line and the read out noise corresponds to 512×512 pixels. Apart from this, the quantum efficiency of an EMCCD at lower photon fluxes is larger than that of an iCCD¹

In order to record the SFG spectra with and without the effect of the IR excitation, before sending the SFG signal to the monochromator, the pump-on and pump-off SFG signals are spatially separated using a galvanometric servo-controlled optical scanning mirror (GSI Lumonics, VM2000) synchronized with the 1 kHz laser repetition rate. The galvano mirror is supplied with a 500 Hz sinusoid voltage from a function generator (Agilent Technologies, 20 MHz/Arbitrary Waveform Generator), by which the mirror oscillates with an angle of $\sim 1^\circ$ about the mirror axis. This translates to a spatial separation of ~ 4 mm on the CCD chip (total chip size: $12 \text{ mm} = 512 \text{ pixels}$) between the pump-on and pump-off SFG signal. Figure 2.9 shows the detection path optics and the use of the galvano mirror to spatially separate the pump-on/pump-off SFG signals.

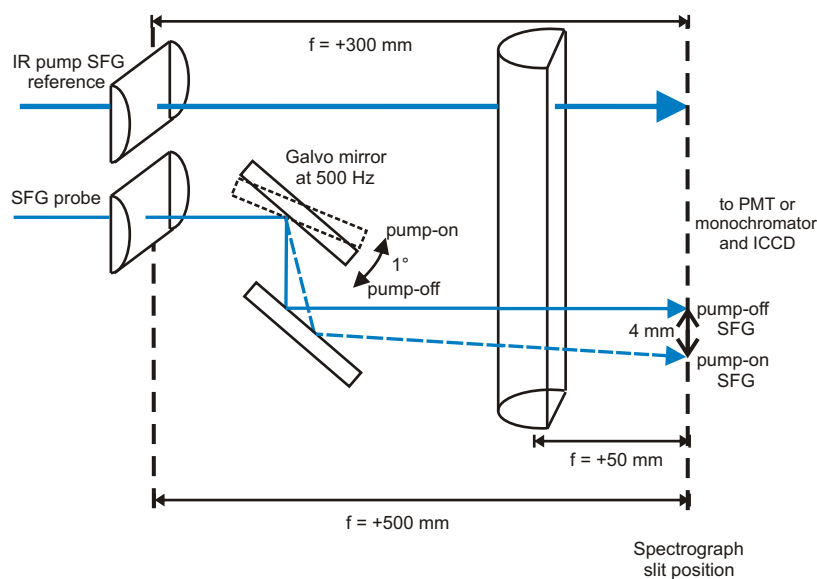


Figure 2.9. Detection optics

To ensure that the pumped shot always falls onto the same position on the chip, the phase of the scanning mirror is synchronized with the phase of the chopper output signal (figure 2.10). The diode signal through the chopper has a square waveform as shown in the upper diagram. The sinusoidal

¹For a more detailed discussion on EMCCDs and iCCDs, please refer to the websites of Andor (www.andor.com) and Princeton Instruments (www.princetoninstruments.com)

waveform supplied to the galvo mirror is shown in the lower diagram. Each crest and trough on the sinusoid function correspond to two fixed mirror positions. The chopper waveform phase must then be adjusted with respect to the sinusoid waveform to synchronize the pump-on/pump-off SFG positions on the CCD chip.

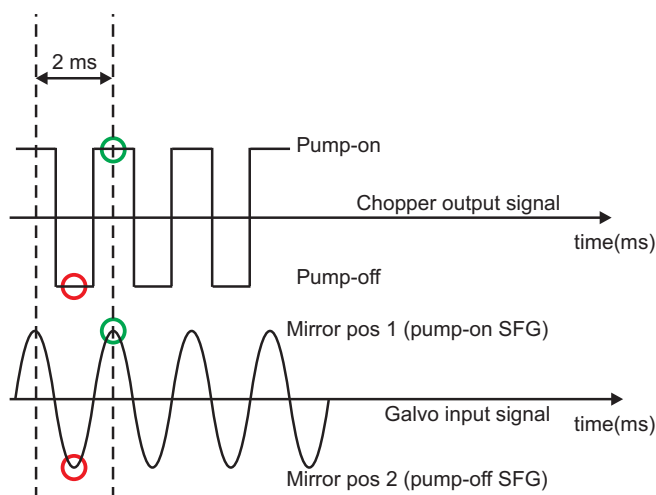


Figure 2.10. Galvo/chopper synchronization.

By binning the individual pump-on and pump-off SFG spectra, vertically on the CCD chip, we can obtain the spectral information with and without the IR excitation. A typical screenshot, shown in figure 2.11, includes the pump-on SFG and the pump-off SFG images on the CCD chip with the galvano mirror in action, which spatially separates the two images.

Note: For the 2D-SFG experiments, the reference SFG (generated by mixing a small fraction of the narrowband visible and the narrowband pump beams in an LiNbO_3 crystal) is sent to the monochromator and the CCD via the detection path shown in figure 2.9). Image of this reference SFG on the CCD chip can also be seen in figure 2.11; the computer program uses this image as a feedback for the piezo-controller of the Fabry-Pérot etalons to adjust the bandwidth and center frequency of the shaped IR pump pulse.

2.5 Software and Electronics

The electronics scheme for this setup have been shown earlier in figure 2.8. A small fraction of the 76 MHz 800 nm seed pulses from the oscillator is detected by a fast photodiode. This photodiode

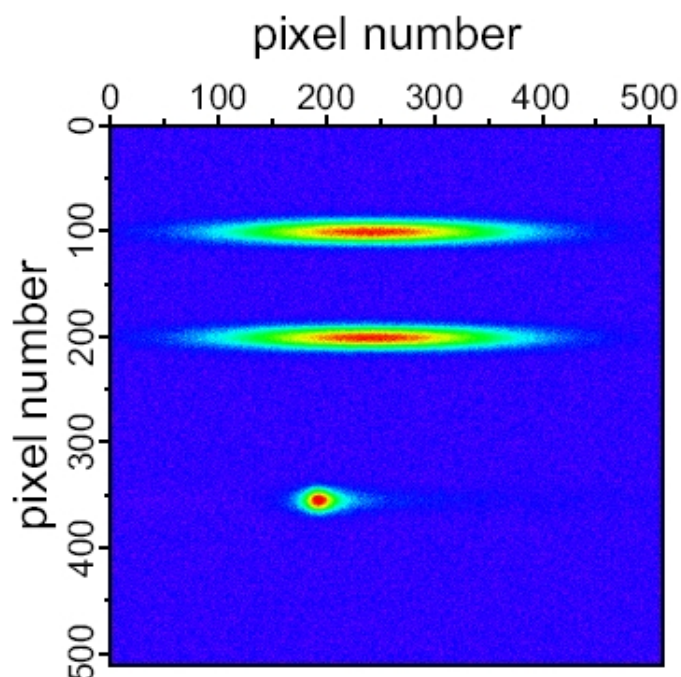


Figure 2.11. CCD screenshot.

signal is then divided by an electronic frequency divider to generate a 1 kHz signal which is used to trigger the Nd:YLF laser and all the electronics in the setup, including the phase-locked optical chopper, the boxcar integrator, the A-to-D converter, the function generator for the galvano mirror and the CCD camera.

The data acquisition software was written in LabView 8. Typical CCD readouts such as presented in Figure 2.11 contain the spectrally dispersed pump-on, pump-off and pump reference SFG signals. The software controls the pump-probe delay line and analyzes the CCD images in real-time to establish whether specific action should be taken, such as trough height modification or adjustment of the Fabry-Pérot piezo voltage.

The ratio between the pump-on/pump-off spectra is instantaneously calculated to monitor in real-time any spectral shifts during a pump-probe SFG experiment. The pump-probe delays for the TR-SFG, the Fabry-Pérot voltages for the 2D-SFG, the spectrograph settings and the function generator settings for the galvanic mirror can all be set in specific panels in the software shown in figure 2.12. The spectrograph settings include the grating, the center wavelength of detection, the pixel-wavelength calibration, intensifier gain and the signal acquisition times. A function generator is included to set phase, the amplitude of the oscillation and the offset position of the scanning galvano mirror. The number of scans, the sample height control and the pump polarization (controlling the

motorized halfwave plate in the pump IR path) may also be adjusted in the software.

The ratio between the integrated pump-on and pump-off SFG spectra, is plotted as a function of pump-probe delay during the scan, for real-time monitoring purposes. The feedback to the sample control program is taken from the CCD image (figure 2.11) after every scan. The signals are fit to Lorentzians as a function of the vertical pixel position to reliably determine the vertical position of the spectra on the CCD camera. As soon as the spectrum is observed to have been shifted vertically by a pre-set number of pixels (typically 10), the feedback control program moves the trough height motors to re-position the signal. As discussed earlier, to account for sample degradation over long acquisition times, when the amplitude of the Lorentzian falls by 30% of the original amplitude, the sample injector dispenses a pre-calibrated number of drops required to restore the original signal amplitude. This way the SFG signals are maintained at their initial conditions before every scan, throughout the experiment, typically consisting of 100 scans. A typical scan is performed from -1.8 ps to 100 ps, in linear steps of 50 fs till 500 fs and logarithmic thereafter.

2.6 Getting Started

Before starting a TR-SFG experiment, apart from generating the appropriate mid-IR frequencies, one needs to characterize the temporal durations of these mid-IR pulses, since this defines the instrument response of our experiments and hence the accuracy in our time-resolved dynamics measurements. Also maintaining the protocol for preparing the model biological interfaces, has proven to be extremely crucial in the success of a TR-SFG experiment.

Instrument Response

To determine the time-resolution of a typical TR-SFG experiment, one needs to characterize the pulse duration (FWHM) of the IR pulses by cross-correlating the pump IR with probe IR pulses at the interface. This is done by scanning the delay of the pump IR with respect to the probe SFG pair (IR probe+visible) and recording the third-order nonlinear process of infrared-infrared-visible-SFG (IIV-SFG) intensity [92]. Figure 2.13(a) shows the energy-level schematic for the IIV-SFG process, while figure 2.13(b) shows a typical pump-probe IIV-SFG cross-correlation trace at the DMPS-water interface [94]. In this cross-correlation, the narrowband visible pulse has a duration of ~ 1 -2 ps (10 times longer than the IR pulse durations). This makes the cross-correlation trace essentially a convolution of only the two IR pulses. Now since the time envelopes of two IR pulses can be approximated as Gaussians, the actual time-resolution (τ_p) of the individual IR pulses can be extracted from the cross-correlation FWHM (τ_{cc}) as,

$$\tau_p = \frac{\tau_{cc}}{\sqrt{2}} \tag{2.3}$$

The pump and probe IR for all the TR-SFG experiments are reasonably described as Fourier-limited pulses with typical widths of ~ 120 -140 fs.

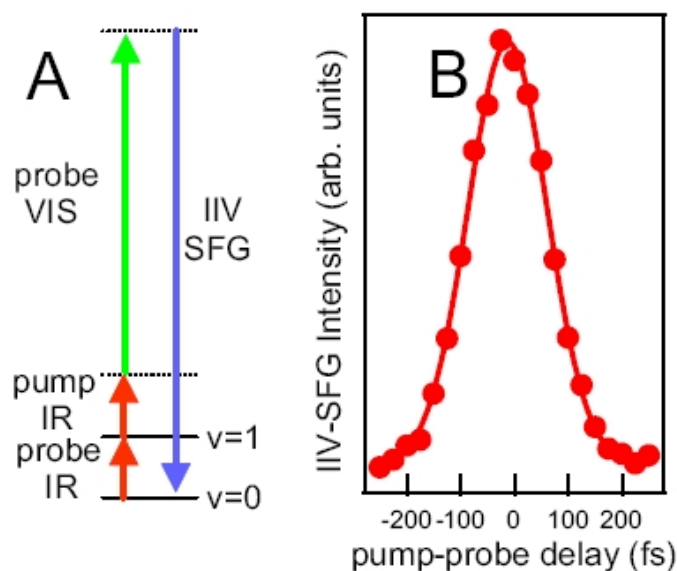


Figure 2.12. (a) Energy level scheme for the third-order nonlinear optical process of IIV-SFG. (b) Cross-correlation trace of pump-probe IR.

Preparing the model biological interface

Time-resolved SFG experiments are typically performed at various model biological interfaces which shall be dealt with in detail in the later chapters. For most interfacial water studies, ultra pure water is used (Millipore-filtered, 18 M Ω -cm resistivity) as the sub-phase, supported in a home-built Teflon trough. For the interfacial lipid studies, D₂O (DLM-6 Deuterium Oxide 100%, Cambridge Isotopes) is used as the sub-phase, in order to reduce the heating effects due to absorption of mid-IR (~ 2900 cm⁻¹) radiation by water. The lipids used to prepare the model biological interfaces were always purchased from Avanti Polar Lipids. Typically a solution of lipid is prepared in 90% chloroform and 10% methanol (Sigma Aldrich) and a Langmuir monolayer film of lipid molecules is prepared by careful addition of drops of the lipid solution in steps of 0.5 L on the water subphase while monitoring the surface pressure of the monolayer with a Wilhelmy-plate based tensiometer (model Kibron DeltaPi). The surface pressure is maintained such that all experiments are performed in the liquid condensed phase of the lipid monolayer (~ 40 mN/m).

Ultrafast Energy Transfer between Interfacial and Bulk Water at the Air-Water Interface

Abstract

In the previous chapter we developed a femtosecond time-resolved SFG spectroscopy scheme to study the vibrational dynamics of interfaces. In this chapter we shall be using this scheme to study the O-H stretch vibrational lifetime of hydrogen-bonded water molecules at the neat water/air interface. The vibrational lifetime in the frequency range of 3200 to 3500 cm^{-1} is found to closely resemble that of bulk water, indicating ultrafast exchange of vibrational energy between surface water molecules and those in the bulk.

3.1 Introduction

Interfacial water plays an important role in many biological, chemical and physical processes (see e.g. [95–97] and references therein). The air-water interface, owing to the asymmetric nature of its terminated hydrogen bond network, has been shown to play an eminent role in the heterogeneous chemistry of a variety of atmospheric and geochemical processes. For instance, through a number of simulations and experiments on simple aqueous salt solutions (eg, NaCl), the anions (particularly halides) have been found to be present at the air-water interface at enhanced concentrations than in the bulk water itself; the cations on the other hand, prefer to remain solvated in the bulk phase [98]. This is consistent with observations of hydrogen bonding in aqueous ionic clusters. Cations form hydrated clusters in which the ion binds to water oxygen atoms. The water molecules are distributed fairly symmetrically around the ion. In contrast, anions bind to water hydrogen atoms. The water molecules are arranged asymmetrically around the ion, enabling hydrogen bonding between them. This behavior is seen for the larger anions Cl^- , Br^- , and I^- [99]. Hence, sodium cations should prefer the homogeneous environment in the bulk liquid, whereas large anions should form asymmetric structures near the interface. This observation indicates the potential of the terminated H-bond network at the air-water interface to cause preferential adsorption of a number of reactive species at the interface and subsequently enhance the surface reactivity. Halide ions at the surfaces of atmospheric aerosol particles play an important role in controlling oxidant levels in the marine boundary layer of the atmosphere. Even a number of gases, like Cl_2 and Br_2 have been shown to have higher adsorbed concentrations at the air-water interface than in the bulk of solvent [100]. The air-water interface has also shown to be a preferential adsorption site for biologically important species like single-stranded DNA [101]. Therefore one can only imagine, the immense potential the air-water interface has, in a variety of natural or artificial heterogeneous chemical reactions. However, because of the experimental difficulties in investigating liquid interfaces in general, and the most prevalent water-air interface in particular, knowledge of the structural and dynamical interface properties has not yet reached the same degree of sophistication that has been attained for bulk water. [102]

Non-linear optical techniques, such as Second Harmonic Generation (SHG) and Sum Frequency Generation (SFG) [26, 103] spectroscopy are generally surface specific and have been shown to be selectively sensitive to the outermost few monolayers of water molecules [104–106]. Vibrational SFG (VSFG) is a particularly powerful tool, as it allows the molecular vibrations of surface water to be probed, which are known to be sensitive reporters of the hydrogen-bonding water environment. Briefly, VSFG relies on the coherent interaction of infrared (IR) and visible (VIS) fields at the surface, to produce a field with a frequency that is the sum of the two incident fields. This surface-specific process is resonantly enhanced by surface vibrations. Indeed, the application of SFG to investigate water at the water/air interface has revealed important new insights in the interfacial water structure [61, 62] and orientation. [107]. It has been shown, for instance, that a significant fraction of surface water molecules ($\sim 20\%$) have a free O-H group sticking into the vapor. These *free*, non hydrogen-bonded O-H groups are characterized by a relatively high vibrational frequency of the

O-H stretch. For the H-bonded interfacial water molecules, the spectrum is broad and featureless, a situation reminiscent of the vibrational spectrum of bulk water. A typical SFG spectrum of water at the neat water-air interface is shown in figure 3.1.

In studies of bulk water, a wealth of information about the properties of water has been obtained by the study of the vibrational dynamics of the O-H stretch vibration through the use of non-linear infrared (pump-probe) spectroscopy (see e.g. [108–112]). The motivation for much of this work lies in the realization that the ultrafast femtosecond behaviour of water molecules contains additional information on the structural and dynamic behaviour in its hydrogen-bonded environment. In pump-probe spectroscopy, by exciting certain vibrational modes with a pump IR pulse, a non-equilibrium perturbation is introduced in the molecule and with the delayed probe pulse, one can essentially take snapshots of the excited vibrational mode in time, as it relaxes back to its original equilibrium state. Such non-linear spectroscopies have been shown to be extremely useful in unraveling different aspects of water dynamics, including intermolecular energy transfer, reorientational motion, and the effects of ions thereon. In addition to investigations of bulk water, there has been much interest in how the water vibrational dynamics are affected by confinement and/or the binding to molecules that mimic a biological environment [113–115].

In this chapter, we shall present our pump-probe studies on water molecules at the air/water interface by using the novel femtosecond IR pump-VSFG probe spectroscopic technique. In these studies, the frequencies of the IR pump and probe pulses are resonant with a symmetric stretch vibrational mode¹ of the hydrogen-bonded interfacial water molecule. The pump pulse excites this vibrational mode and the modulation of the interfacial SFG spectrum originating from the IR probe and up-conversion visible pulses, is monitored as a function of the pump-probe delay [83, 84, 87, 103, 116]. The time evolution of recovery of the SFG signal then reflects the vibrational relaxation of the interfacial water molecules. The femtosecond time-resolved SFG study that is presented here, is thus a one-colour pump-probe experiment that allows us to selectively probe the lifetime dynamics (T_1) of the O-H stretch vibration and provide new insights in the structure and dynamics of water at the neat water-air interface.

3.2 Static and Time-resolved VSFG experiments

Two independent setups have been used in this study: one for static SFG spectroscopic studies and one for the time-resolved studies. We used the easily tunable static SFG setup to record the broadband (2000-2900 cm^{-1}) SFG spectrum of heavy water D_2O at the neat water-air interface as shown in figure 3.1. In this setup, the IR frequency can be easily scanned from 2000 cm^{-1} to 2900 cm^{-1} , which is why D_2O was used for the static measurements, instead of H_2O . The D_2O spectrum ranges from $\sim 2250 \text{ cm}^{-1}$ to $\sim 2850 \text{ cm}^{-1}$ and resembles the frequency-shifted H_2O spectrum.²

¹The fundamental O-H symmetric stretch mode being isoenergetic with the overtone of the water bending mode, leads to Fermi resonance coupling of the two modes

²The features of the D_2O spectrum are essentially the same as the H_2O spectrum, only red-shifted in frequency due to a larger reduced mass of the O-D oscillator. Assuming the O-H and O-D force constants to be the same, $\bar{\nu}_{\text{OH}}/\bar{\nu}_{\text{OD}} = \sqrt{\mu_{\text{OD}}/\mu_{\text{OH}}} \simeq 1.374$

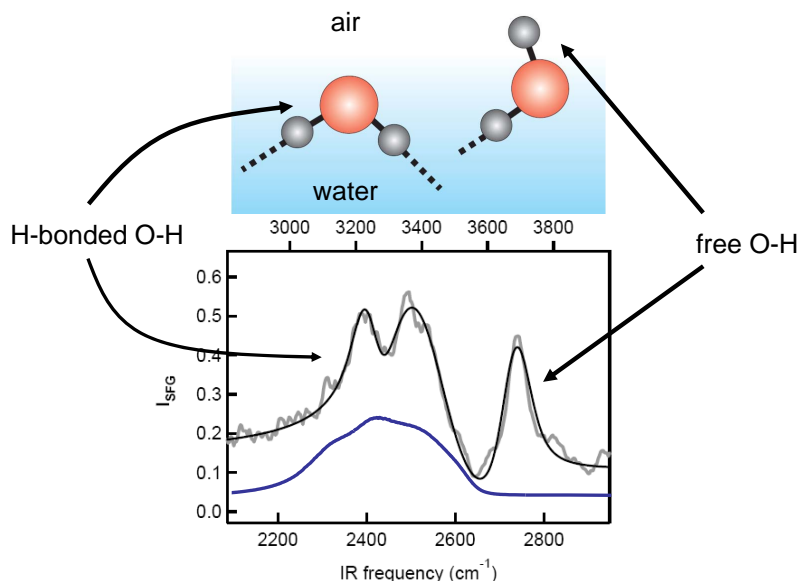


Figure 3.1. The SFG spectrum of O-D at the neat D_2O -air interface is shown in light grey. The top axis represents the IR frequency scaling for the equivalent H_2O spectrum. The solid line is a fit to the observed SFG spectrum, assuming two inhomogeneously broadened resonances and a single Lorentzian for the dangling O-D vibration. The linear infrared absorption spectrum of H_2O is also shown here (solid blue line), to show the contrast between the O-H in bulk and at the surface.

In the static SFG experiment, the SFG signal is spectrally dispersed by a monochromator and detected by a CCD camera. The spectral resolution is limited by the bandwidth of the visible beam and is $\sim 20 \text{ cm}^{-1}$. The reduced spectral resolution explains, as discussed in chapter 2, why the intensity of the spectrally narrow free O-D peak is relatively low compared to the H-bonded peaks, when comparing the results of figure 3.1 to other reports in literature.

The TR-SFG setup is much more involving owing to the requirement of generating high energy mid-IR pump pulses, which limits the tunability to the O-H stretch region ($2900\text{-}4000 \text{ cm}^{-1}$), with a bandwidth³ of $\sim 150 \text{ cm}^{-1}$. In the experiments, the central frequency of pump and probe pulses are set at fixed positions within the $\sim 400 \text{ cm}^{-1}$ SFG resonance as indicated by the arrows across the SFG spectrum in figure 3.2

In the TR-SFG experiments on neat water-air interface, distilled Millipore-filtered water (H_2O , $18 \text{ M}\Omega\text{-cm}$ resistivity) at pH 7 was used in a home-built Teflon trough. The trough was rotated at 5 rpm to suppress the effect of sample heating. The one-colour TR-SFG experiments were performed at fixed IR pump and probe frequencies across the hydrogen-bonded spectrum ($3200\text{-}3500 \text{ cm}^{-1}$) as indicated by the dotted arrows in figure 3.2. The foci of the pump IR, the probe IR and the visible pulses were overlapped spatially and temporally at the surface of the water. The temporal overlap

³For transform-limited Gaussian pulses, one can simply compute the bandwidth that can be covered with a pulse of duration, $\Delta\tau$ (in s) by using the equation, $\Delta\bar{\nu} = 0.441/c\Delta\tau$ where $c = 3 \times 10^{10} \text{ cm/s}$ and $\Delta\bar{\nu}$ is the bandwidth in cm^{-1}

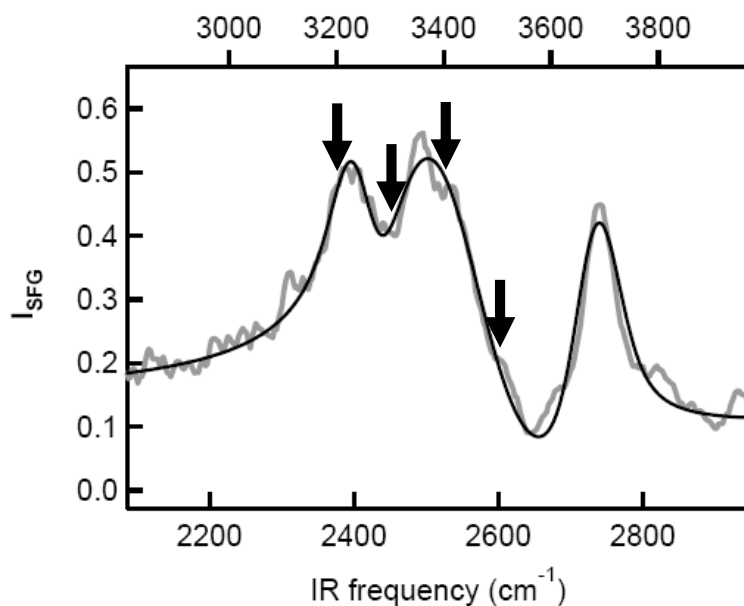


Figure 3.2. One-colour pump and probe frequencies for the TR-SFG experiments are indicated by the solid arrows across the O-H spectrum.

of all three beams was optimized by monitoring the IIV-SFG signal (see *Getting started* in Chapter 2). Subsequently, the TR-SFG experiment was performed by monitoring the SFG signal while delaying pump pulse with respect to the probe (IR + visible) using a mechanical delay line. These experiments were performed from -0.5 ps to 3 ps pump-probe delays in steps of 100 fs. The SFG signal was filtered using bandpass filters and a monochromator and was detected in a spectrally-integrated manner with a Photo Multiplier Tube (R9910, Hamamatsu). Because the SFG signal is less than 0.1 detected photon per laser shot, and the pump-induced modulation typically 10% thereof, 25 scans were averaged, each consisting of 20 points (10,000 laser shots per point). The 1 kHz pump beam was chopped to 500 Hz and the normalized, differential SFG signal was computed as the ratio between the signals with and without the pump.

At the neat water-air interface, the largest resonant VSFG signal is generated by the $\chi_{xyz}^{(2)}$ ($= \chi_{yyz}^{(2)}$) components of the stretch dipoles of the H₂O molecule. If the xz-plane (see figure 3.3) is defined as the plane of incidence for the IR probe and visible beams (and plane of reflection for the SFG beam), then the polarization vector in the xz-plane (and perpendicular to direction of beam propagation) is defined as P and the polarization vector perpendicular to the xz-plane is defined as S . In this beam geometry, the polarization combination required to probe the $\chi_{xxz}^{(2)}$ ($= \chi_{yyz}^{(2)}$) component is S,S and P for SFG, visible and IR probe beams, respectively. TR-SFG experiments were also performed with two different pump polarizations (P and S, parallel and perpendicular to the surface normal) in order to investigate anisotropy effect on the pump-probe SFG signal. The polarizations of all beams could be rotated independently using $\lambda/2$ -plates mounted on a motorized

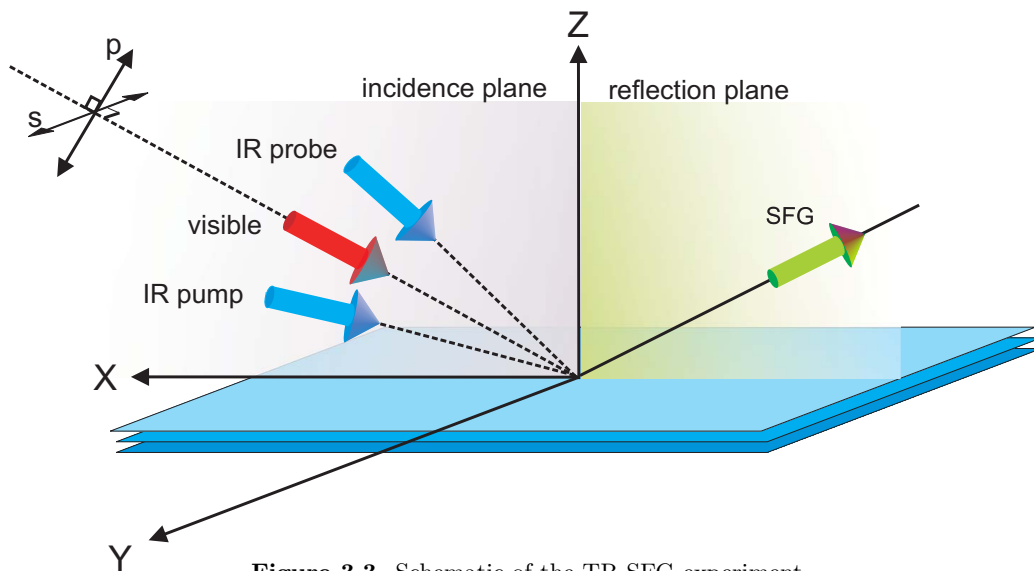


Figure 3.3. Schematic of the TR-SFG experiment.

rotation stages controlled by the measurement software.

3.3 Results and Discussion

3.3.1 Static SFG Results

Except for the shift in frequency due to the mass difference, the D_2O spectrum is equivalent to previous reports of SFG spectra of H_2O [62, 63]. The narrow resonance in the SFG spectra at $\nu=3690$ (2730) cm^{-1} has been shown to be due to the dangling O-H (O-D) bond. The hydrogen-bonded O-H however, is represented by a broad, double peaked spectral feature spanning from ~ 3100 to 3550 cm^{-1} (see figure 3.1). The solid line shown in the spectra, is a fit to the data assuming two inhomogeneously broadened resonances and a single Lorentzian for the dangling O-D vibration. Figure 3.1 also shows the linear infrared absorption spectrum of H_2O (dotted lines), which reveals that the infrared response of the H-bonded part of the surface spectrum is markedly different from that of the bulk.

The assignment of the broad double-peaked feature, however has been a subject of intense debate in recent literature: on the one hand, in analogy with the IR spectrum of liquid water and ice, it has been argued that the two apparent peaks at ~ 3200 and at ~ 3450 cm^{-1} are the result of strongly hydrogen bonded ('ice-like') water, and weakly hydrogen bonded ('liquid-like') water, respectively. This argument has been bolstered by a series of MD simulations that have been interpreted to suggest that each spectral feature is actually a combination of multiple, distinct, water structures [117–124].

However, on the other hand, it has also been argued based on analogy to gas phase water molecules, other simulations and interpretations of the spontaneous Raman spectra of bulk water, that the two peaks can largely be explained as the symmetric and asymmetric vibrational modes of the water molecule [104, 125]. Recently published work, however, by showing that each peak has a similar dependence on IR and VIS polarization, has demonstrated that both peaks result from vibrational modes with the same symmetry thus ruling out the latter interpretation [126]. Recent isotopic dilution experiments show that a third mechanism best explains the double peaked nature of the interfacial water spectrum. At both the air/water and lipid/water interfaces the two peaks collapse to one upon isotopic dilution, showing that the two-peak structure is not the result of a distribution of H-bonded structures [127]. Owing to the frequencies and polarization dependencies of the SFG response [126], the interpretation in terms of symmetric and asymmetric vibrational modes can also be discarded. The variety of experimentally observable characteristics of the double peaked spectral feature can be thus best explained if the visible *dip* in the spectrum is the result of a Fermi resonance between the bend overtone and the stretch fundamental [127]. Such coupling has been demonstrated to exist, using two-colour IR pump-probe experiments in bulk water [111, 128, 129].

3.3.2 Time-resolved SFG Results

The typically broad and featureless time-averaged SFG spectra of the hydrogen-bonded O-H species almost immediately prompts us to ask whether the underlying dynamic structure of water is indeed different. The results of the pump-probe measurements of the relaxation of O-H stretching modes of hydrogen-bonded water after pumping at frequencies $\nu_{pump} = 3200, 3300, 3400$ and 3500 cm^{-1} , are depicted in figure 3.4. Also shown in figure 3.4 is the third-order IR+IR+VIS (IIV) SFG signal, which is used to determine time zero ($\Delta t = 0$) and quantify the time resolution in each experiment.

The normalized pump-probe SFG signal of the water-air interface reveals a pump-induced decrease in the signal that is observed after $\Delta t = 0$. At 3400 and 3500 cm^{-1} , this is followed by a recovery of the signal that deviates from the level before $\Delta t = 0$; at lower frequencies, it is followed by an additional, slower decrease. The initial decrease in SFG is due to excitation of the O-H stretch mode to its first excited state by the pump pulse. Owing to the large vibrational anharmonicity of $\sim 300 \text{ cm}^{-1}$ [130], SFG generated from the excited state ($v = 1 \rightarrow 2$) is shifted out of the spectral window. The recovery at 3400 and 3500 cm^{-1} reflects vibrational relaxation, and the long-time offset is caused by an increase in the local temperature due to the energy deposited by the pump pulse, which is eventually converted to heat. The pump-induced temperature increase in the focus has been calculated to be approximately 15 K. As observed in the transients, this offset goes from ~ 0 at $\nu_{pump} = 3500 \text{ cm}^{-1}$ to much smaller than 0 at $\nu_{pump} = 3200 \text{ cm}^{-1}$, in accordance with an expected blue shift of the spectrum due to the pump-induced heating that results in a weaker hydrogen-bonded network.

From the data in figure 3.4, two timescales seem apparent: a fast (~ 100 fs) relaxation time corresponding to the recovery of the pump-induced bleach signal (most clearly evident at $\nu = 3500 \text{ cm}^{-1}$, and the slower (~ 500 fs) timescale by which the final SFG level is reached (most apparent at

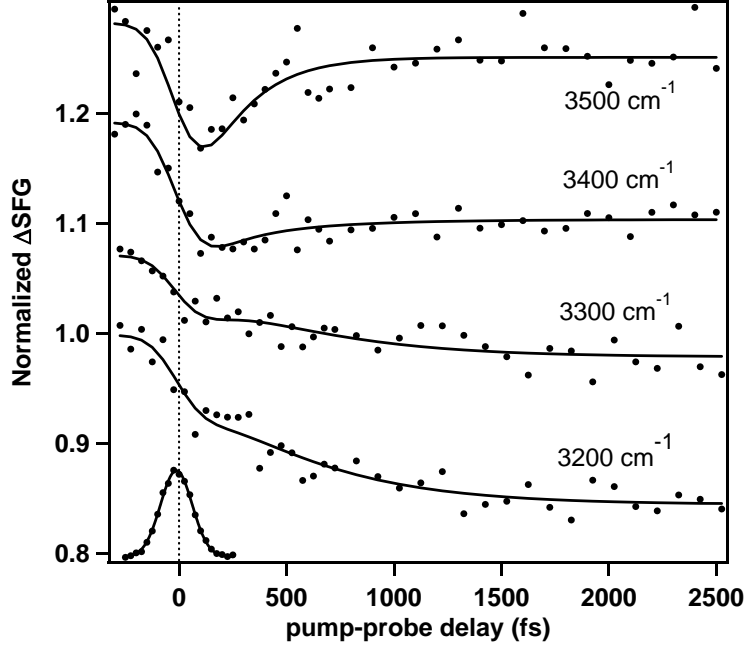


Figure 3.4. TR-SFG one-colour pump-probe transients across the hydrogen-bonded H₂O spectrum. Time-resolved SFG data for interfacial water for $\nu_{pump} = 3200, 3300, 3400$ and 3500 cm^{-1} (traces are offset for clarity). Polarizations of the SFG, VIS probe, IR probe and IR pump were S, S, P and S. The solid lines are the fits based on a four level system explained in the text. The lower trace is the third-order IR+IR+VIS SFG signal (shown for $\nu = 3300 \text{ cm}^{-1}$).

$\nu = 3200 \text{ cm}^{-1}$). Indeed, a four-level energy scheme characterizing such a system shown in figure 3.5 provides a very good description of the experimental data.

In bulk studies it was shown that vibrational relaxation from $v=1$ occurs through an intermediate state v^* , which is a mixed state of the ground state of the stretch vibration and other modes that accept energy from the $v=1$ state [131]. From v^* relaxation then occurs to the system at elevated temperature, which is a long-lived state with optical properties different from the original ground state. This explains the observed long-time signal offset in the data. The following physical picture thus emerges: the ground state ($v=0$) is depleted by the pump, and relaxation from the excited state ($v=1$) occurs to an intermediate state (v^*), before reaching the new ground state ($v'=0$) at elevated temperature. We calculate the population in each level by solving the coupled differential equations,

$$\frac{dN_0(t)}{dt} = -I(t, \tau_{fwhm})\sigma_0(N_0 - N_1) \quad (3.1)$$

$$\frac{dN_1(t)}{dt} = I(t, \tau_{fwhm})\sigma_0(N_0 - N_1) - \frac{N_1}{T_1} \quad (3.2)$$

$$\frac{dN_{v^*}(t)}{dt} = \frac{N_1}{T_1} - \frac{N_{v^*}}{\tau_{eq}} \quad (3.3)$$

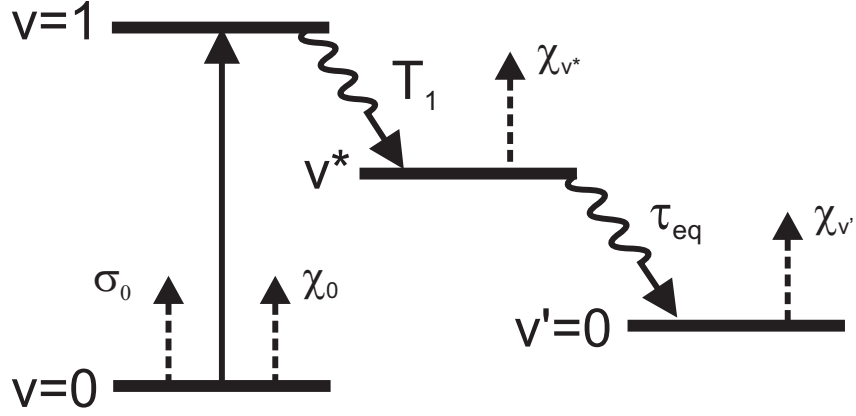


Figure 3.5. A four-level energy description for intermolecular vibrational relaxation.

$$\frac{dN_{v'}(t)}{dt} = \frac{N_{v^*}}{\tau_{\text{eq}}} \quad (3.4)$$

where,

$$\begin{aligned} \frac{dN_x(t)}{dt} &= \text{the rate of population change in level } x \text{ at time, } t \\ I(t, \tau_{\text{fwhm}}) &= \text{the Gaussian pump pulse with a certain pulse duration, } \tau_{\text{fwhm}} \\ \sigma_0 &= \text{is the absorption cross-section for the } 0 \rightarrow 1 \text{ transition,} \end{aligned}$$

We know that the SFG intensity is proportional to the square of the population difference between the ground (N_0) and the excited vibrational state (N_1). Therefore,

$$I_{\text{SFG}} \propto (N_0 - N_1)^2 \quad (3.5)$$

At room temperature the thermal excitation of the vibrational excited state is very low, so that, $N_1 \sim 0$. If we define ΔN as the population that is transferred from the ground to the excited state by the pump pulse, then $N_0 \rightarrow (N_0 - \Delta N)$ and $N_1 \rightarrow \Delta N$, so that:

$$I_{\text{SFG}} \propto (N_0 - 2\Delta N)^2 = N_0^2 - 4N_0\Delta N + 4(\Delta N)^2 \quad (3.6)$$

This demonstrates that the technique is relatively sensitive to population changes, as the differential signal is dominated by the second term, which is proportional to 4 times the population transfer. The third term is quadratic in the population difference and can generally be neglected, since the degree of pump-induced population transfer is generally small. The pump-probe differential TR-SFG signal can then be approximated as:

$$I_{\text{SFG}}(\Delta t)/I_{\text{SFG}}(0) \propto 1 - 4\Delta N/N_0 \quad (3.7)$$

$$\text{or } \Delta I_{\text{SFG}} \propto 1 - 4\Delta n \quad (3.8)$$

where Δn is the normalized excited state population and ΔI_{SFG} the differential TR-SFG signal. Considering the populations in all four levels of the 4-level system, the effective, time-dependent susceptibility $\chi_{\text{eff}}^{(2)}$ reads:

$$\chi_{\text{eff}}^{(2)} = [N_0(t) - N_1(t)]\chi_0 + N_{v^*}(t)\chi_{v^*} + N_{v'}(t)\chi_{v'} \quad (3.9)$$

where the time dependence is contained in the time-dependence of the occupation of the different levels, each with their own SFG activity χ_x .

Note that the differential TR-SFG signal (ΔI_{SFG}) is then proportional to the population difference ΔN , between the ground and excited state. The time constant reflecting population decay in the experiments is T_1 . The two time constants obtained from the four level model describe the vibrational relaxation to the intermediate state (T_1) and the thermalization process (τ_{eq}). Such dynamics are reminiscent of observations for bulk water [130,132] and observations for water at the water-silica interface [87]. The TR-SFG data can be described very well using $T_1=190$ fs obtained from bulk water measurements [130] and a $\tau_{\text{eq}}=400 \pm 100$ fs (solid lines in figure 3.4). We found no evidence for a frequency dependence of T_1 , in analogy with the recent hole burning experiments of water at the water/silica interface [87].

Moreover, we also performed polarization-resolved pump-probe experiments whereby the pump polarization was altered between P and S polarizations, and the pump-probe signal was acquired at all delay times as in the TR-SFG transients. From the data presented in figure 3.6, it is apparent that within the time resolution of the experiment, pumping with either horizontal (S-) or vertical (P-) polarized light results in the same efficiency of excitation of the surface molecules. This randomization of the excitation polarization is the first clear and direct indication of a very fast energy transfer between the isotropic bulk molecules and the surface molecules: although we selectively probe the outermost few molecular layers of water molecules, the excitation depth is determined by the absorption length of IR light in water (a few μm). A large *reservoir* of isotropic excitations is therefore present right below the surface, which exchanges rapidly with excitations at the surface. Further evidence for ultrafast energy exchange with the bulk comes from the observed timescales as noted earlier, which correspond very well to the timescales observed in bulk water. Hence, it is clear that the vibrational dynamics of the hydrogen-bonded water at the surface are dominated by ultrafast vibrational energy transfer processes. For bulk water, the fast spectral diffusion has been attributed to extremely fast Förster energy transfer [132]; the same mechanism is apparently operational at the water-air interface. The cartoon shown in figure 3.7 depicts the Förster energy transfer-type relaxation mechanism.

This also explains the similarity between the dynamics at the water-air interface and those at

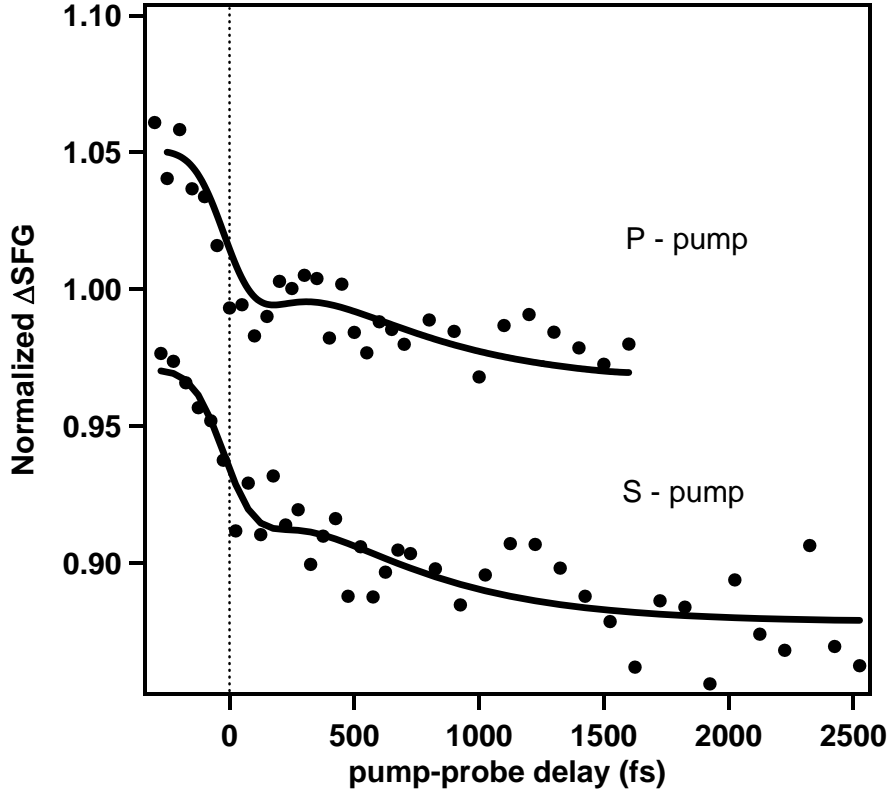


Figure 3.6. P- and S-pump dependence on TR-SFG at 3300 cm^{-1}

the hydrophilic and hydrophobic silica/water interface recently reported using SFG in total internal reflection (TIR) geometry [87]. For the latter interface, McGuire *et al.* reported somewhat similar dynamics, with $T_1=300$ fs and $\tau_{eq}=700$ fs. Although the rigid silica surface (required for TIR-SFG) has been shown to induce order in the interfacial water compared to water at the water/air interface [107], the effect of the increased order on the vibrational dynamics is limited due to the ultrafast energy transfer processes that dominate the observed relaxation behaviour. Future experiments with isotopically diluted water to suppress the energy transfer will enable answering the question to what extent the vibrational dynamics at the surface are intrinsically different from those in bulk.

A Note about Coherent Artifacts: It has been demonstrated that coherent artifacts may contribute to a pump-probe signal [133]. This can result in a change in the SFG signal unrelated to the vibrational dynamics. These artifacts should be more pronounced when the pump and probe IR polarizations are parallel. When comparing results for orthogonal and parallel pump and probe polarizations (as shown for $\nu_{pump} = 3300\text{ cm}^{-1}$ in figure 3.6), the results are very similar. Since coherent artifacts are expected to be much larger in the situation of parallel polarization, the resemblance of the two data sets indicate that the data represent the true dynamics and is not influenced

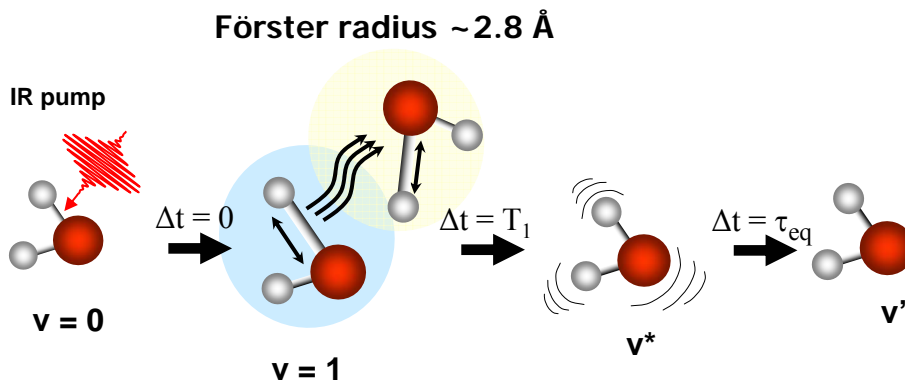


Figure 3.7. Cartoon depicting Förster-type intermolecular energy transfer. After excitation of the O-H oscillator, a very fast Förster-type energy transfer randomizes the excitation energy and polarization; subsequently relaxing to an intermediate state (v^*) and finally to a thermally equilibrated state (v').

by coherent artifacts. This check was performed for all frequencies. A second argument against coherent artifacts is the observation that the first minimum in the signal (corresponding to the maximum population of the excited vibrational state) is always found at positive delay times. This is most clearly visible in the data for 3500 and 3400 cm^{-1} . This clearly indicates that the decrease of the signal is due to population being transferred to the excited state.

3.4 Conclusions

In conclusion, we have demonstrated ultrafast energy transfer between surface and bulk water at the air-water interface using a novel pump-probe TR-SFG experiment. Although the spectral response differs appreciably for bulk and surface water, the O-H stretch vibrational dynamics at the surface are indistinguishable from that in the bulk, in the $3200\text{-}3500 \text{ cm}^{-1}$ hydrogen-bonded region.

Ultrafast Dynamics of Water at various lipid-water interfaces

Abstract

We present results of a comparative study of surface vibrational dynamics of interfacial water at various model membrane systems. We employ tr-SFG spectroscopy to probe the surface dynamics of water molecules at the monolayers of DPTAP, DMPS, DPPC and DPPE on a water sub-phase. DPTAP is chemically very different from DMPS, DPPC and DPPE and has a positively charged head-group. DMPS, DPPC and DPPE are chemically similar but differ in the details of their polar head-group: DMPS is negatively charged whereas DPPC and DPPE have zwitterionic head-groups; DPPC and DPPE differ in that in PC the terminal amine group is tri-methylated. The static vibrational SFG spectra of interfacial water in these systems reveal subtle differences in linewidths, but are very broad and quite featureless and therefore difficult to interpret in detail. TR-SFG allows us to excite specific sub-ensembles within the distribution of O-H oscillators of water in the monolayer system and subsequently follow the SFG response of this perturbation in time. The resulting time-dependent SFG response provides information about the structure and structural dynamics of these interfacial water molecules.

4.1 Introduction

As noted in the previous chapter, the aqueous interfaces are of paramount importance in a variety of chemical, biological and physical processes. An important factor in determining the adsorption and reactivity characteristics of these interfaces, is the interruption of the hydrogen bonded network at these interfaces. As the local hydrogen bond characteristics also determine the vibrational properties of the water high-frequency O-H stretch, these vibrations can provide useful information about the interfacial water structure and dynamics. In this chapter, we report investigations on a biologically ubiquitous interface: the lipid/water interface. As a model system, we use a lipid monolayer on water. This is a reasonable model for a real biological membrane, as in a real membrane the two leaflets that constitute the lipid bilayer are relatively weakly coupled. A multitude of different types of lipids exist in nature. These lipids vary in the details of their polar head groups (small, large; strongly or weakly hydrogen bonding; neutral, zwitterionic, charged) and apolar alkyl chains (link, degree of saturation). For the interaction with the water it is apparent that the details of the polar head group are the most important. Here, we present a systematic study of water interacting with four distinct types of lipids. We investigate similarities and differences between water interacting with pure monolayers of these for lipids. A comparison with the results obtained for the water-air interface is used to separate 'trivial' effects due to termination of the water hydrogen bond network, with specific effects due to the interaction with the lipids. Our results provide new insights on, lipid/water and interfacial water/water interactions. These interactions are themselves important for understanding membrane function.

4.2 Surface-specific Vibrational Spectroscopy: Frequency- and Time-Resolved Sum Frequency Generation

The main challenge in understanding interfacial water is largely a technical one, since the interfacial water extends upto only within ~ 1 nm from the membrane molecules. To overcome the challenge of specifically investigating this ultra-thin layer of water molecules, we use our non-invasive, label-free, all-optical surface-specific spectroscopic techniques of VSFG and TR-SFG. As the frequency of the O-H stretch is known to vary strongly as a function of hydrogen-bond strength [134], vibrational spectroscopy provides an attractive approach. The measurement of the O-H stretch frequency of membrane-associated interfacial water might, therefore, provide useful insight into the interaction of this water both with itself and various other membrane components. Measurement of the frequency of the O-H stretch of membrane bound water using conventional linear spectroscopies (e.g. IR) is challenging in that it requires the cancellation of a large bulk signal. This obstacle was largely overcome 20 years ago with the first measurements of interfacial water in the air/water and quartz/water systems using vibrational sum frequency generation spectroscopy (VSFG) [62, 117, 118]. Briefly, in VSFG a pulsed visible and IR beam are overlapped at an interface and the emission of photons at the sum of the frequencies of the two incoming beams measured. In the dipole approximation the sum frequency process is prohibited in environments with local inversion symmetry and is thus,

for many systems, VSFG provides an interface-specific probe (inversion symmetry is always broken at the interface). The SFG emission intensity increases when the IR energy matches a vibrational transition in the interfacial species. These characteristics make VSFG an ideal optical probe for the vibrational spectrum of water-membrane interfaces. The sum-frequency generation (SFG) intensity is essentially a measure of the square of the nonlinear polarization $P_{SFG}^{(2)}$ generated at the surface by the visible and infrared optical fields :

$$I_{SFG} \propto |P_{SFG}^{(2)}|^2 \propto |\chi^{(2)}|^2 I_{IR} I_{vis} \quad (4.1)$$

where $\chi^{(2)}$ is the second-order nonlinear susceptibility and I_{IR} and I_{vis} are the intensities of the incident fields. $\chi^{(2)}$ is given by,

$$\chi^{(2)} = \chi_{NR}^{(2)} + \chi_R^{(2)} = A_0 e^{i\phi} + \sum_n \frac{A_n}{\omega_n - \omega_{IR} - i\Gamma_n} \quad (4.2)$$

So when the frequency of the incident infrared field is resonant with a vibrational mode, n , the SFG field is strongly enhanced. Here, A_0 is the real amplitude of the non-resonant susceptibility, ϕ its phase, A_n is the amplitude of the n^{th} vibrational mode, ω_n the resonant frequency, and Γ_n the linewidth of the transition.

Although the static spectral observables are useful (center frequencies and linewidths), it is clear that the structure of interfacial water and that of membrane bound water, is under-constrained by the few parameters that can be obtained from VSFG spectra. Irrespective of the type of interface, the SFG spectral linewidth of hydrogen-bonded water is very broad (~ 3100 to ~ 3500 cm^{-1}) and essentially featureless. This situation is analogous to studies of bulk water, where linear infrared absorbance and spontaneous Raman spectral lineshapes convolute homogenous, inhomogeneous and structural effects.

It has been shown in the past few decades that time-resolved vibrational pump-probe spectroscopies have the capability to provide experimental observables that further our understanding of the underlying dynamical molecular structure which is otherwise difficult to extract by a simple vibrational lineshape analysis. For instance, the IR absorption spectrum of bulk water is inhomogeneously broadened, which renders lineshape analyses practically meaningless for extracting relaxation and dephasing times of the O-H oscillator. However, by introducing a short-duration non-equilibrium vibrational perturbation to a sub-ensemble of O-H oscillators and subsequently monitoring the mechanism and rate of relaxation of this perturbation in time, one can obtain insights of the underlying H-bond networks at play. For bulk aqueous systems, pump-probe and multi-dimensional infrared spectroscopy have proven extremely useful in both describing the structure and time-dependent structural evolution of water itself as well as the manner in which water solvates small molecules [128, 129, 132, 135–139]. Such a pump-probe concept has recently been extended in our time-resolved SFG technique (TR-SFG) independently by the Shen group [87] and by us [93, 140], to study interfacial water. By using an intense IR pulse to excite O-H stretch vibrations at the interface and subsequently monitoring the dissipation of this excitation using VSFG, one can follow the relaxation of the non-equilibrium vibrational perturbation in real-time and thereby

increase our understanding of the influence of underlying molecular interactions and structure, on the macroscopic properties exhibited by biological membranes.

In this study, we have investigated water (H_2O) at the monolayer interfaces of four different lipids using frequency- and time-resolved SFG spectroscopy.

4.3 Experimental Section

Sample Preparation

All the lipids used in these experiments, 1,2-dipalmitoyl-3-trimethylammonium-propane (chloride salt) (DPTAP), 1,2-dimyristoyl-*sn*-glycero-3-phospho-L-serine (sodium salt) (DMPS), 1,2-dipalmitoyl-*sn*-glycero-3-phosphocholine (DPPC) and 1,2-dipalmitoyl-*sn*-glycero-3-phosphoethanolamine (DPPE) were all purchased from Avanti Polar Lipids. The chemical structures are shown in figure 4.1. For the time-resolved SFG experiments, the lipid monolayers were prepared at room temperature (22°C) in a commercial Langmuir trough (Kibron Inc, Finland) by spreading drops ($0.5\ \mu\text{l}/\text{drop}$) of $\sim 1.5\ \text{mM}$ lipid solution in chloroform/methanol (Sigma-Aldrich) onto an ultrapure water (H_2O) sub-phase (Millipore water, $18.2\ \text{M}\Omega\text{-cm}$ resistivity). For the frequency-resolved SFG experiments, D_2O was used as the sub-phase. Self-assembled monolayers of the corresponding lipid form on the sub-phase as the chloroform/methanol solution evaporates. The surface pressures were measured with a tensiometer using the Wilhelmy-plate method. Frequency- and time-resolved SFG measurements were both carried out at surface pressures corresponding to the liquid condensed phases of the different lipids ($\sim 30\text{-}40\ \text{mN m}^{-1}$).

The setups and experimental schemes for the frequency- and time-resolved SFG experiments have been described in detail in earlier chapters. Briefly, in a typical TR-SFG experiment, an intense mid-IR pump pulse, tuned to a vibrational resonance within the broad SFG spectrum of water at a lipid/water interface, vibrationally excites a sub-ensemble of O-H oscillators and the response of this excited system is monitored by observing the modulation in the SFG spectrum and intensity generated at the interface, as a function of the delay time between the IR pump and SFG probe pulses. A series of differential SFG transients ($I_{\text{pump-on}}^{\text{SFG}}/I_{\text{pump-off}}^{\text{SFG}}$) are recorded as a function of pump-probe delay time (usually varied from $-2\ \text{ps}$ to $100\ \text{ps}$), typically at four frequencies across the broad hydrogen-bonded SFG spectra for all the lipid monolayers: 3200 , 3300 , 3400 and $3500\ \text{cm}^{-1}$. In these experiments, the pump-on and pump-off SFG signals generated at the interface are spatially separated by a galvano mirror, synchronized to the 1-kHz laser repetition rate in a way that the galvano mirror has a certain position when an excitation pulse is blocked (pump-off) by a phase-locked chopper, and a certain other position when the pulse is unblocked (pump-on). Subsequently, these SFG signals are spectrally dispersed by a monochromator and finally recorded on an EM-CCD camera (discussed in chapter 2), whereby the accumulated pump-on and pump-off SFG spectra are read out from different regions on the CCD chip.

Note: The studies on DMPS/water interface were the first TR-SFG experiments done along with the neat water/air interface. These transients were recorded as a function of a pump-probe delay window

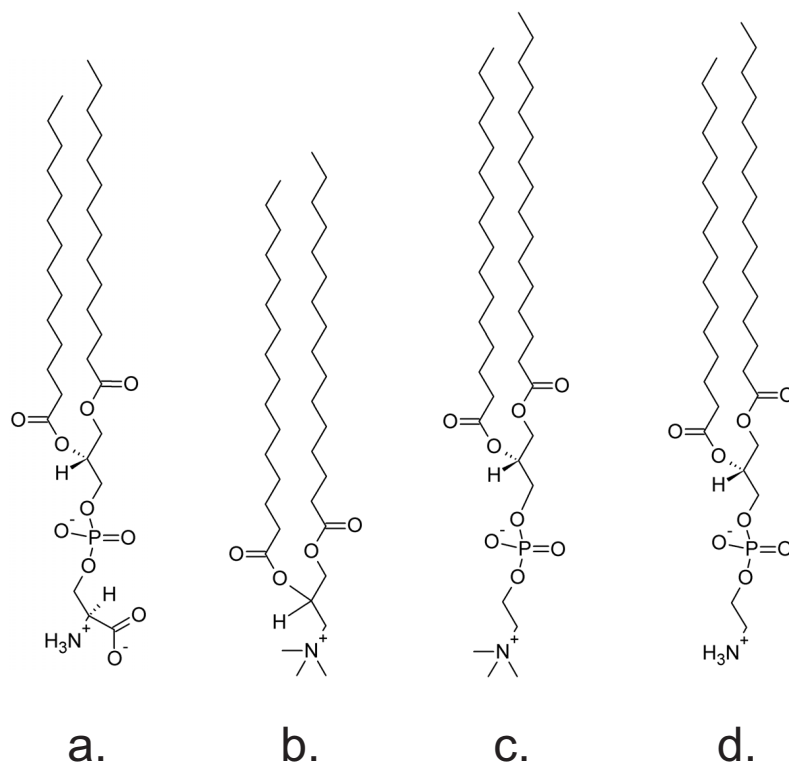


Figure 4.1. Chemical structures of the studied self-assembled monolayers on water: **(a)** 1,2-dimyristoyl-sn-glycero-3-phospho-L-serine (sodium salt) (DMPS), **(b)** 1,2-dipalmitoyl-3-trimethylammonium-propane (chloride salt) (DPTAP), **(c)** 1,2-dipalmitoyl-sn-glycero-3-phosphocholine (DPPC), **(d)** 1,2-dipalmitoyl-sn-glycero-3-phosphoethanolamine (DPPE). **(a)** has a net negative charge on the headgroup and **(b)** has a net positive charge. **(c)** and **(d)** are both zwitterionic (hence dipolar) and are chemically similar: **(c)** is the N-methylated form of **(d)**

of -500 fs up to 2 ps, in a spectrally integrated manner on a photomultiplier tube (instrumentation described in chapter 2). With further improvements of the detection technique and stability issues we were able to do experiments from -2 ps up to 100 ps pump-probe delays, using an EMCCD camera: the DPPC, DPPE and DPTAP monolayers on water were studied using this improved TR-SFG technique.

4.4 Results and Discussion

4.4.1 Frequency-resolved SFG experiments

The static frequency-resolved SFG spectra of the H-bonded water (D_2O) at various lipid/ D_2O monolayer systems are shown in figure 4.2. We observe that the static SFG spectra of the interfacial water at the chemically similar DPPC and DPPE monolayer systems are essentially identical. This is observed despite the fact that lipids with a bulkier headgroup (choline in DPPC) can pack less tightly

in the monolayer than the ones with a less bulky head group (ethanolamine in DPPE), thus causing a greater degree of hydration in the former (pp. 215 in [141]). The SFG spectral intensities of the interfacial water at charged lipid monolayers (DMPS and DPTAP) are much larger than the ones at the zwitterionic lipid/water interfaces, primarily due to two effects: (i) an extended orientation of water dipoles into the bulk due to a net electric field provided by the charged lipid headgroups and (ii) the second-order $P^{(2)}$ of the interfacial water is enhanced by a bulk $\chi^{(3)}$ response due to the additional DC-field (E_0), provided by the *sheet* of charged headgroups,

$$P_{\text{eff}}^{(2)} = \chi^{(2)} E_{\text{IR}} E_{\text{vis}} + \chi^{(3)} E_{\text{IR}} E_{\text{vis}} E_0 \quad (4.3)$$

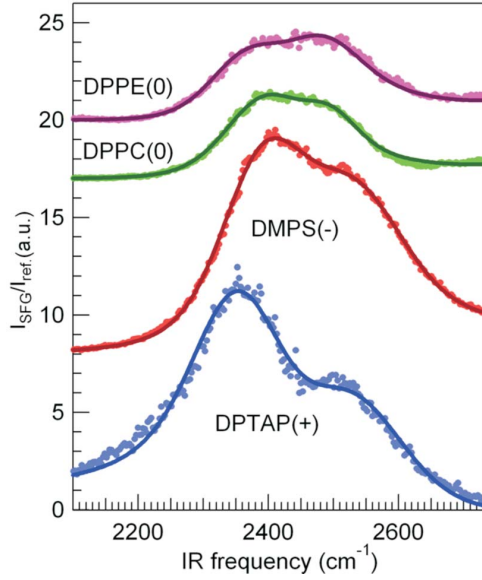


Figure 4.2. The static SFG spectra of the hydrogen-bonded O-D are shown for the four D_2O /lipid interfaces: DPTAP, DMPS, DPPC and DPPE. The respective lipid headgroup charges are also indicated in brackets.

As discussed in the previous chapter, the assignment of the double-peaked structure in the static SFG spectra of interfacial water has been the subject of intense debate. We follow here the reference [127]. Briefly, the SFG spectra of interfacial water is essentially from an inhomogeneously broadened symmetric stretch vibrational mode of the O-H (or O-D) oscillator, owing to a large distribution of hydrogen bond strengths in the interfacial water. Through recent findings in isotopic dilution experiments (HOD/ D_2O subphase) at both the air/water and lipid/water interfaces, it has been shown that a Fermi resonance coupling between the symmetric stretch and the isoenergetic overtone of the bending mode causes a lowering of the density of states around 3300 cm^{-1} which appears as a *dip* in an otherwise continuous and inhomogeneously broadened VSFG spectrum of H-bonded water [127]. Such coupling has been demonstrated to exist, using two-colour IR pump-probe experiments in bulk water [128, 129]. In these experiments, the O-H stretch modes are excited and a fast relaxation ($\sim 200 \text{ fs}$) process is observed to occur into the excited H-O-H bend mode. This is

consistent with the picture that the overtone of the bend mode, being iso-energetic with the O-H stretch fundamental, couples strongly with the excited O-H stretch mode, whereby the relaxation occurs through the bending mode.

4.4.2 Time-resolved SFG experiments

As we can see from the static SFG spectra (figure 4.2) of the four lipid monolayer systems, apart from the slightly varying double-peak structure, the spectra in the hydrogen-bonded region of water (D_2O) appear to be fairly similar in their center frequencies and broad line-widths. There seems to be a weak increase in hydrogen bonding strength going from DPPE-DPPC-DMPS to DPTAP, without any distinct spectral signature of prominent difference in the molecular structure or dynamics of the interfacial water molecules. As the headgroups are chemically fairly different, one might expect more pronounced differences in hydrogen-bonding properties. It is therefore interesting to study the spectrally broad rather featureless response with a non-equilibrium probe, the TR-SFG technique, and search for signatures of hydrogen-bonding heterogeneity in these model biological interfacial water molecules. TRSFG measurements were carried out at the water-model membrane interfaces, with the pump and probe IR pulses centered at 3200, 3300, 3400 and 3500 (± 10) cm^{-1} , using IR pulses with a spectral widths of ~ 120 cm^{-1} and pulse durations of ~ 140 fs. The TR-SFG transients from the various lipid/water interfaces are shown and discussed individually in the following sub-sections with figures 4.4, 4.6, 4.7 and 4.8. Preliminary inspection of the transients of the different systems, reveals that the response from the four interfaces can be classified into two groups:

(i) The charged lipid/water interface: DPTAP and DMPS

(a) Response at 3200 cm^{-1} : After the IR excitation, the decrease and initial recovery of the SFG intensity occur within the time resolution of the experiment (within ~ 100 fs). The maximum bleach signal occurs very quickly (at $t \leq 50$ fs) after $t=0$; there is very limited build-up of vibrational excitation during the pump pulse, indicative of a very short T_1 lifetime.

(b) Response at 3300, 3400 and 3500 cm^{-1} : The features of the transients at these frequencies look similar, where the bleaching occurs significantly delayed ($t > 50$ fs) compared to the traces observed at 3200 cm^{-1} . Also the initial recovery of the SFG intensity appears to be much slower at these frequencies than at 3200 cm^{-1} . After this initial relaxation process, a slow relaxation process is also evidently occurring, on timescales of tens of ps.

(ii) The zwitterionic lipid/water interface: DPPC and DPPE

(a) Response at 3200 and 3300 cm^{-1} : After the IR excitation, the SFG intensity decreases instantaneously (within ~ 50 fs), due to bleaching of the ground state. Subsequently, there is a partial recovery of the SFG signal, after which the signal decreases *again*, and finally continues to

recover to a level that is lower than its original value. The initial dynamics (bleach, partial recovery and second signal decrease) occur on sub-picosecond timescales, whereas the final slow rise occurs over tens of picoseconds.

(b) Response at 3400 and 3500 cm^{-1} : The transients look similar to the ones at the charged lipid/water interface - with an initial delayed bleach after excitation, subsequent relaxation of the bleach within 1 ps, followed by a slow rise in order of tens of ps. No additional signal decrease was observed at these frequencies.

The different long-time signal offsets in all the transients at delay times >100 ps can be readily attributed to the spectral shifts due to the IR pump-induced heating: it was verified that the SFG spectrum of the hydrogen-bonded O-H stretch mode shifts to *blue* frequencies owing to heat-induced weakening of H-bonds.

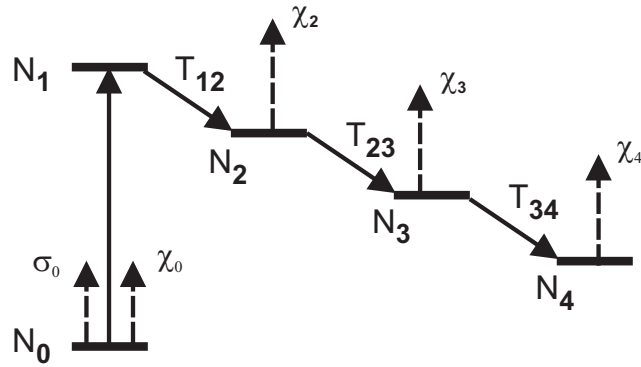


Figure 4.3. The 5-level kinetic model used in the TR-SFG data analysis. The population of the i^{th} state is denoted by N_i , the absorption cross-section for $0 \rightarrow 1$ transition is denoted by σ_0 , the relative susceptibility of state i is denoted by χ_i and the $i \rightarrow j$ time-constant is denoted by T_{ij} .

These transients can be described accurately by a 5-level kinetic model shown in figure 4.3: an extension to the 4-level system used to describe bulk water IR pump-probe transients [131, 136, 142, 143]. The relevant coupled differential equations describing the population kinetics in such a system can be written as,

$$\frac{dN_0(t)}{dt} = -I(t, \tau_{\text{fwhm}})\sigma_0(N_0(t) - N_1(t)) \quad (4.4)$$

$$\frac{dN_1(t)}{dt} = I(t, \tau_{\text{fwhm}})\sigma_0(N_0(t) - N_1(t)) - \frac{N_1(t)}{T_{12}} \quad (4.5)$$

$$\frac{dN_2(t)}{dt} = \frac{N_1(t)}{T_{12}} - \frac{N_2(t)}{T_{23}} \quad (4.6)$$

$$\frac{dN_3(t)}{dt} = \frac{N_2(t)}{T_{23}} - \frac{N_3(t)}{T_{34}} \quad (4.7)$$

$$\frac{dN_4(t)}{dt} = \frac{N_3(t)}{T_{34}} \quad (4.8)$$

where,

$$\begin{aligned} \frac{dN_x(t)}{dt} &= \text{the rate of population change in level } x \text{ at time, } t \\ I(t, \tau_{\text{fwhm}}) &= \text{the Gaussian pump pulse with a certain pulse duration, } \tau_{\text{fwhm}} \\ \sigma_0 &= \text{is the absorption cross-section for the } 0 \rightarrow 1 \text{ transition} \end{aligned}$$

As shown earlier in chapter 3, in our modeling of the TRSFG transient data, the susceptibilities and the relaxation times are kept as fit parameters and the normalized differential SFG signal, ΔI_{SFG} as a function of the pump-probe delay t , is then computed from the time-dependent state populations by,

$$\Delta I_{\text{SFG}}(t) = \frac{[(N_0(t) - N_1(t))\chi_0 + \chi_2 N_2(t) + \chi_3 N_3(t) + \chi_4 N_4(t)]^2}{[N_0(0)]^2} \quad (4.9)$$

This simple model provides an adequate description of the data as will be shown in the following sections for all the lipid/water systems. In contrast to the 4-level model used to describe the IR pump-probe measurements in bulk water [131, 136, 142, 143], the lipid/water TRSFG measurements require a 5-level model as shown in figure 4.3. The 5-level model can readily be interpreted as follows: infrared excitation of the molecules promotes population from the O-H stretch vibrational ground state v_0 , to the first vibrationally excited state v_1 . Subsequent vibrational relaxation occurs to a state v_2 on a timescale T_{12} , which can be identified as the vibrational lifetime T_1 . State v_2 corresponds to the system in which the energy has flowed out of the high-frequency vibrational O-H stretch, but has not yet equilibrated over all degrees of freedom. v_2 subsequently relaxes to v_3 with a timescale of T_{23} . v_3 corresponds to the situation where the excess energy is equilibrated over all degrees of freedom, following a reorganization of the hydrogen bond network. The timescale associated with the H-bond network rearrangement is T_{23} . Finally, the increase in temperature results in a change of the hydration state of the lipid monolayer: v_3 converts into the slightly different v_4 with a timescale of T_{34} , which is much larger (≥ 20 ps) than T_{12} and T_{23} . Its precise value depends on the monolayer composition. In the following, the different monolayer systems will be discussed one by one.

4.4.2.1 DPTAP/H₂O Interface

The TR-SFG transients for the DPTAP/water interface are shown in figure 4.4. As we can see, the data can be well described with the aforementioned 5-level kinetic model. Previous investigations of the vibrational dynamics of interfacial water at the water-air interface [93] and the water-silica

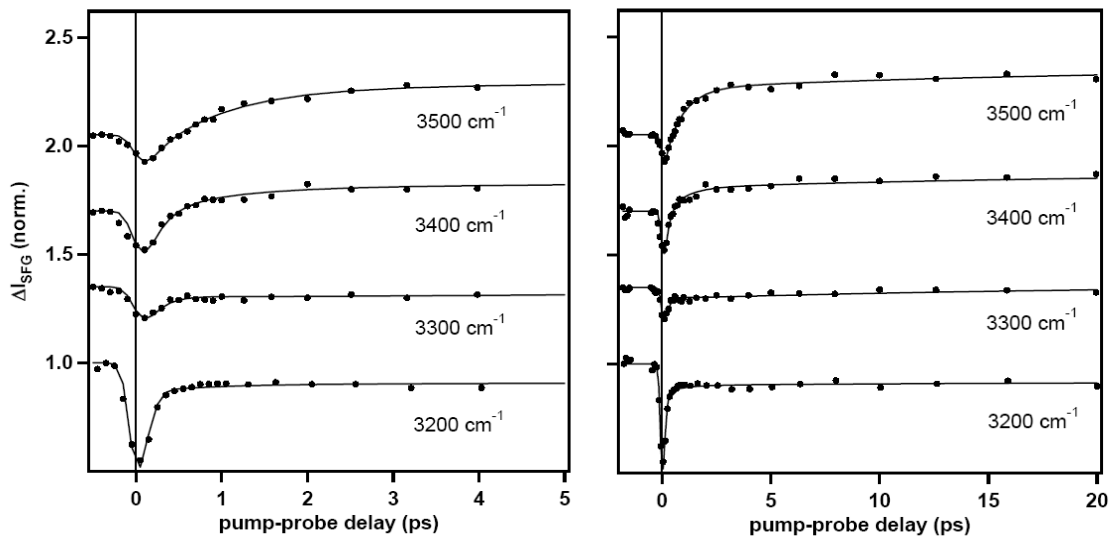


Figure 4.4. One-colour TR-SFG transients for the DPTAP/water interface recorded at four different IR frequencies indicated in the graph. The left panel depicts the dynamics up to 5 ps; the right up to 20 ps.

interface [87] have revealed very fast intermolecular energy transfer between water molecules. This very rapid (sub-50 fs) energy transfer leads to a homogeneous response of the different spectral components within the water band. When exciting a weakly hydrogen-bonded water molecule at high frequency (3500 cm^{-1}), the excitation can 'hop' rapidly to a strongly hydrogen-bonded water molecule at low frequency (3200 cm^{-1}). Moreover, the excitation is not restricted to the surface; the surface excitation can be transferred to and from the bulk. Therefore, although the intrinsic response may be different for interfacial water molecules with different hydrogen bonds, an averaged response was observed for both the water-air (as shown in chapter 3) and the water-silica [87] interfaces. It would therefore seem intuitive to attempt to apply a similar model of homogeneous response to water at the water-lipid interface. This implies that the three time constants that describe the transitions between the different states in the 5-level model would be the same for all frequencies.

Indeed, three out of four traces for DPTAP - and, as will be shown below, the same is true for the other lipids - can be described using one set of time constants. Remarkably, the 3200 cm^{-1} data are notably different: the vibrational relaxation time (T_{12} in the model) is appreciably shorter than that inferred for the other frequencies.

The following table 4.1 shows the various time constants extracted from the model:

Table 4.1.

DPTAP	T_{12} (fs)	T_{23} (fs)	T_{34} (ps)
3200 cm^{-1}	<50	840	20
3300 cm^{-1}	180	840	20
3400 cm^{-1}	180	840	20
3500 cm^{-1}	180	840	20

From table 4.1, we note that for the DPTAP/water interface, the lifetime of the O-H stretch excited state relaxes with a time constant of $T_{12} = 180$ fs, for the frequencies 3300, 3400 and 3500 cm^{-1} , whereas for 3200 cm^{-1} , the T_{12} appears to be extremely fast (< 50 fs). Figure 4.5 shows that although the 3300-3500 cm^{-1} transients can be described very well using a single $T_{12} = 180$ fs, this homogeneous model breaks down at 3200 cm^{-1} , where a T_{12} of 180 fs is evidently too large, and we must conclude that $T_{12} < 50$ fs.

The T_{12} time constants obtained for 3300 to 3500 cm^{-1} are found to be consistent with the scenario that a very fast Förster energy transfer causes the O-H excitation quanta to randomize amongst neighboring water molecules. The subsequent relaxation occurs into ν_2 - the anharmonically coupled states, presumably bending modes and finally of the excited O-H stretch mode and the excited low-frequency H-bond modes. This is consistent with the observations in bulk water [130,132] and the neat water-air interface [93]. However for the 3200 cm^{-1} mode, the T_{12} is extremely fast, < 50 fs, thus suggesting that vibrational relaxation is faster than intermolecular vibrational energy transfer.

These observations indicate a very fast spectral diffusion of the O-H excitation across the SFG spectrum of the DPTAP/water interface, between 3300 and 3500 cm^{-1} , that causes the T_{12} to be the same in this regime; at 3200 cm^{-1} , the extremely fast T_{12} can only suggest that the strongly H-bonded O-H oscillators relax faster than resonant energy transfer to neighbouring water molecules can occur. As a consequence, water molecules at the DPTAP/water interface exhibit homogeneous dynamics across the SFG spectrum beyond 3300 cm^{-1} , but display heterogeneity of the O-H oscillators associated with very strong hydrogen bonds (i.e., at 3200 cm^{-1}).

The T_{23} value of 840 fs observed for all the transients suggest that the energy flow out of the ν_2 state associated with of the adjustment of the hydrogen bond network to the local temperature increase due to vibrational relaxation - is comparable to the value obtained for bulk water, where the excitation flow out of ν_1 into the *hot* ground state takes $\sim 0.55 - 1$ ps [142, 143].

The relatively long T_{34} value of ~ 20 ps suggests a relaxation process which involves a collective rearrangement of water molecules associated with the change in hydration of the lipid head group region. This assignment is consistent with NMR studies of partially hydrated bilayers, which have shown that the timescale on which exchange occurs between bulk water and water associated with lipid head groups, is of the order of ≈ 100 ps [37].

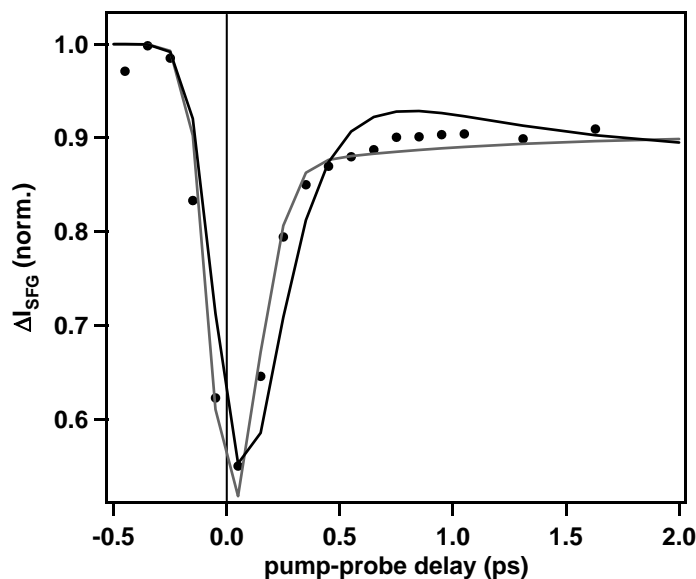


Figure 4.5. The one-colour TR-SFG transient for the DPTAP/water interface recorded at 3200 cm^{-1} . The solid grey line is a fit to the transient data using $T_{12} < 50\text{ fs}$ and the black line, using $T_{12} = 180\text{ fs}$. This shows that the homogeneous model where $T_{12} = 180\text{ fs}$ should describe the transients at all frequencies across the H-bonded O-H spectrum, breaks down at low O-H frequencies (i.e., 3200 cm^{-1}), where the hydrogen bonds are strong.

4.4.2.2 DMPS/H₂O Interface

The features of the TR-SFG transients for the DMPS/water interface, shown in figure 4.6 closely resemble those observed at the DPTAP/water interface and the time constants are indistinguishable: T_{12} for $3200\text{ cm}^{-1} \leq 50\text{ fs}$ whereas for $3300\text{--}3500\text{ cm}^{-1}$ is $\approx 180\text{ fs}$; T_{23} is $\approx 800\text{ fs}$ and $T_{34} \geq 20\text{ ps}$. This suggests a similar mechanism of energy flow dynamics being operative at the DMPS/water interface as at the DPTAP/water interface, showing signatures of strongly bound water molecules to the lipid head-group moieties (at 3200 cm^{-1}) and that of weakly bound water molecules whereby O-H excitations are randomized through a Förster type transfer mechanism to other neighbouring water molecules (at 3300 cm^{-1} and beyond).

Note: Before the TR-SFG technique had been improved to perform most of these lipid/water dynamics experiments, an earlier interpretation of the DMPS/water dynamics had been made based on the experiments performed up to 2 ps pump-probe delays. According to this interpretation, one distinct time-constant at each frequency could well describe the TR-SFG data. Such an interpretation indicates the existence of distinct sub-ensembles of water molecules across the SFG spectrum, energetically decoupled from the bulk of the system. The new interpretation presented here, concluded from improved experimental results, suggest a less heterogeneous behaviour: The response seems to be homogeneous for water molecules with vibrational frequencies in the range of $3300\text{--}3500\text{ cm}^{-1}$, whereas at 3200 cm^{-1} , a distinct sub-ensemble of strongly hydrogen-bonded water molecules

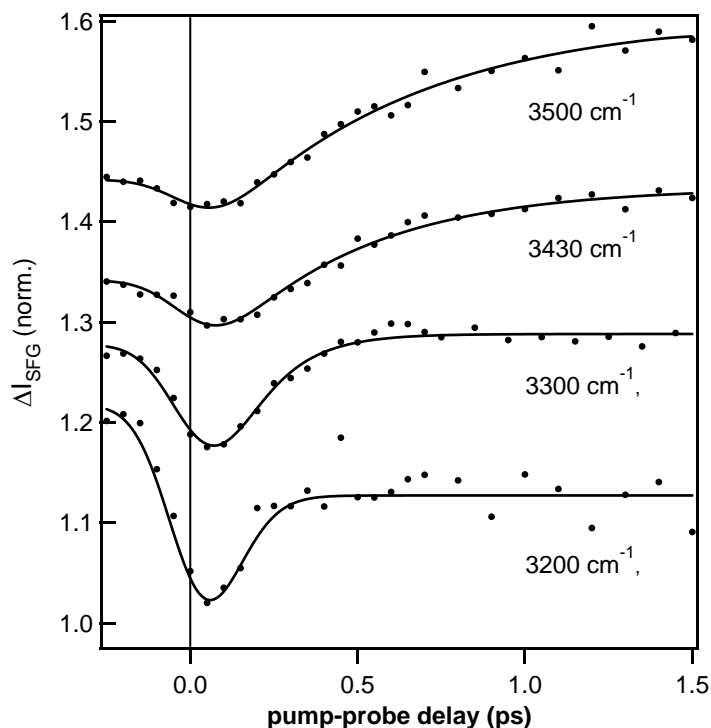


Figure 4.6. One-colour TR-SFG transients for the DMPS/water interface recorded across the H-bonded O-H SFG spectrum.

seem to be energetically decoupled from neighbouring water molecules.

4.4.2.3 DPPC/H₂O and DPPE/H₂O Interface

The TR-SFG transients for the DPPC/water and DPPE/water interfaces are shown in figures 4.7 and 4.8.

The data for both systems can be described well with the 5-level kinetic model and the time-constants of the O-H stretch mode excitation energy flow through the systems can be extracted as shown in tables 4.2 and 4.3:

Table 4.2. Time-constants for DPPC transients

DPPC	T ₁₂ (fs)	T ₂₃ (fs)	T ₃₄ (ps)
3200 cm ⁻¹	<50	950	40
3300 cm ⁻¹	180	950	40
3400 cm ⁻¹	180	950	40
3500 cm ⁻¹	180	950	40

Table 4.3. Time-constants for DPPE transients

DPPE	T ₁₂ (fs)	T ₂₃ (fs)	T ₃₄ (ps)
3200 cm ⁻¹	<50	680	70
3300 cm ⁻¹	180	680	70
3400 cm ⁻¹	180	680	70
3500 cm ⁻¹	180	680	70

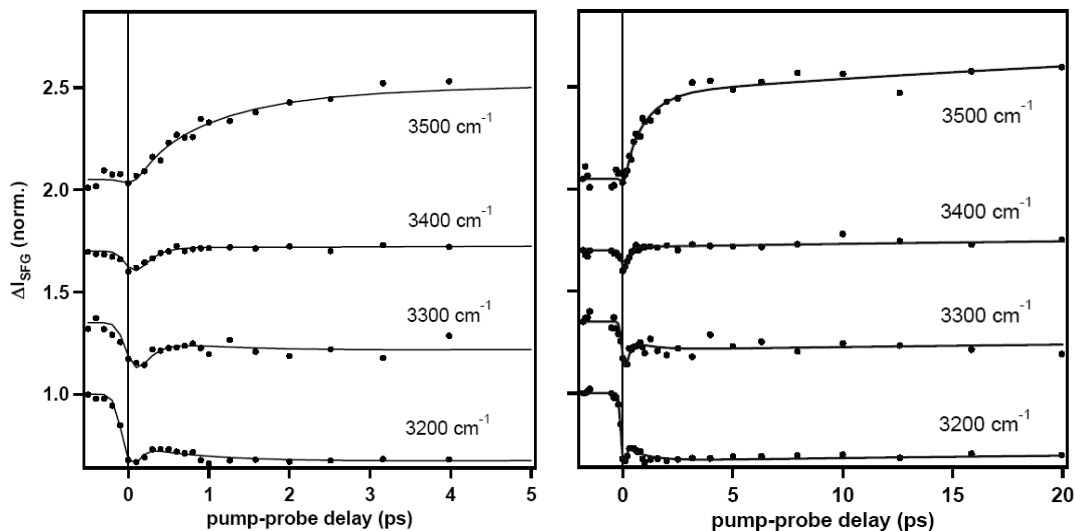


Figure 4.7. One-colour TR-SFG transients for the DPPC/water interface recorded at four different IR frequencies indicated in the graph. The left panel depicts the dynamics up to 5 ps; the right, up to 20 ps.

The initial relaxation dynamics (T_{12}) of H_2O across the DPPC/water and DPPE/water SFG spectrum are identical to those at the DPTAP/water and DMPS/water interfaces: $T_{12} < 50$ fs at 3200 cm^{-1} and is ~ 180 fs at 3300 cm^{-1} , 3400 cm^{-1} and 3500 cm^{-1} . Figure 4.9 demonstrates that $T_{12} = 180$ fs is incompatible with the transient data at 3200 cm^{-1} .

As we can see, although the initial dynamics of the TRSFG transients, from 3300 through 3500 cm^{-1} , can be described with a single T_{12} , the 3200 cm^{-1} lifetime is much shorter (>50 fs) than the lifetime at the blue side of the SFG spectra. This indicates a similar homogeneity of water molecules at zwitterionic interfaces as at the charged interfaces, for medium to weak hydrogen-bonded water (at 3300 cm^{-1} and up), where a Förster energy transfer of the excitation energy dominates the initial dynamics. The strongly hydrogen-bonded water molecules (at 3200 cm^{-1}) dissipate the excitation energy through IVR into the strong H-bond modes associated with the lipid headgroup moieties; thus energetically decoupled from the neighbouring bulk water.

This physical picture is schematically represented in figure 4.10, which shows the intrinsic T_1 lifetimes (in the absence of Förster energy transfer), along with the Förster energy transfer, as a function of frequency. The excitation of the O-H stretch vibration rapidly hops from one molecule to another. As a result, the excitation samples all the different types of local O-H oscillators, on a very short time scale. This timescale depends on the cross section of the O-H stretch vibration, which is also frequency dependent. As a result, the effective relaxation time is a weighted average of the T_1 values of all O-H oscillators near the interface - both bound to lipid headgroups and in the nearby bulk. Only at very low frequencies ($\sim 3200\text{ cm}^{-1}$, where hydrogen bonding is very strong and vibrational relaxation apparently is very fast, does the vibrational relaxation process outpace the energy transfer process, and IVR occurs quickly, without averaging over all possible

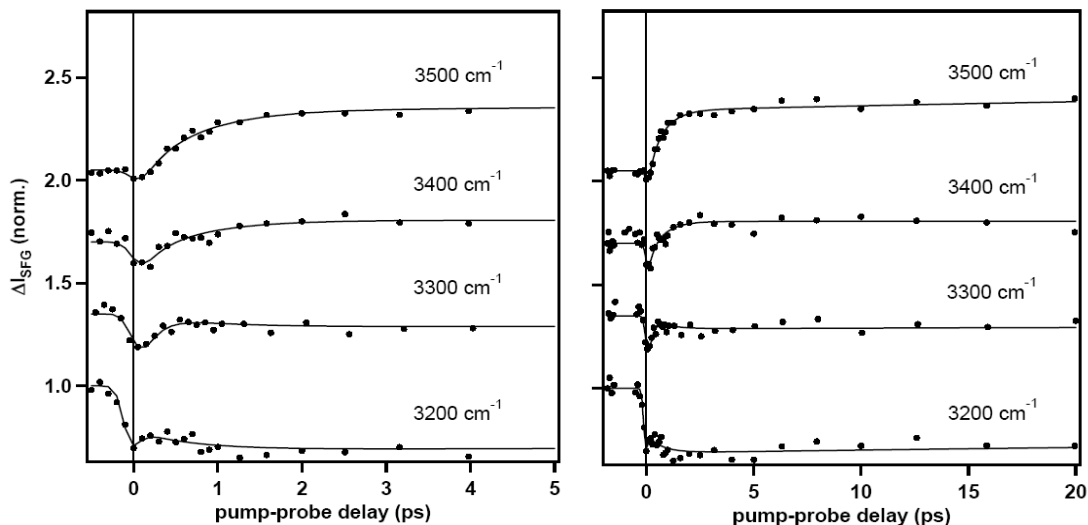


Figure 4.8. One-colour TR-SFG transients for the DPPE/water interface recorded at four different IR frequencies indicated in the graph. The left panel depicts the dynamics up to 5 ps; the right up to 20 ps.

hydrogen-bonded arrangements.

An additional interesting feature in the data is observed at ~ 500 fs for both the DPPC and DPPE transients, particularly at 3200 and 3300 cm^{-1} , where a clear *overshoot* in the transients is evident. This feature, apart from the different long time signal offsets, make the DPPC and DPPE interfacial TR-SFG transients distinct from the DMPS and DPTAP interfacial dynamics, where the overshoot at $t=500$ fs is clearly not present. The appearance of this feature demonstrates that the non-thermal intermediate state at the DPPC/water and DPPE/water interface has a quite different spectrum from that at the DMPS/water and DPTAP/water interface. This difference can be quantified through the difference in the relative SFG susceptibilities (χ) of the excited O-H oscillators at the zwitterionic interface, when compared to those at the charged interface. The following table shows the relative susceptibilities of the DPPC and DPTAP systems (extracted from the data fits), where the difference is most prominent.

Table 4.4. Relative susceptibilities of all the energy levels extracted from the TRSFG transients at 3200 cm^{-1} for DPPC/water and DPTAP/water interfaces

	χ_0	χ_2	χ_3	χ_4
DPTAP	1	0.914	0.939	0.949
DPPC	1	0.709	0.609	0.696

As is apparent from table 4.4, in the case of DPTAP/water interface, the susceptibility of every subsequent transient state is higher than the preceding one during the excitation energy flow after bleaching the ground state, i.e., $\chi_2 < \chi_3 < \chi_4$. However in the case of DPPC/water interface, the

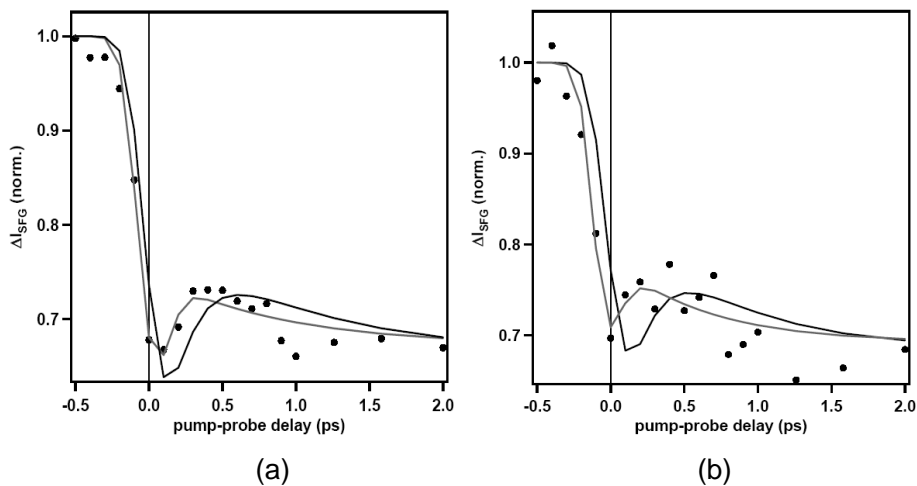


Figure 4.9. TRSFG transient data for 3200 cm^{-1} at (a) DPPC/water and at (b) DPPE/water interface. Also shown are the fits (grey solid lines) to the data with $T_{12} < 50$ fs and the attempts to fit the data (black solid lines) with $T_{12} = 180$ fs.

order of values of the relative susceptibilities is: $\chi_2 > \chi_3 < \chi_4$. This suggests that the transient structures of the strongly hydrogen-bonded water molecules at the DPPC interface are quite different from those at the DPTAP interface.

The T_{23} for DPPC and DPPE interfaces - timescales of equilibration of excitation energy over all the degrees of freedom of the *hot* water molecules - are ~ 950 and ~ 680 fs respectively, and are within the order of the bulk values of 0.55 - 1 ps, as discussed earlier. The T_{34} for DPPC and DPPE interfaces have been found to be ~ 40 and ~ 70 ps respectively, thus indicating a slow rearrangement of the hydration layers around the lipid head-groups.

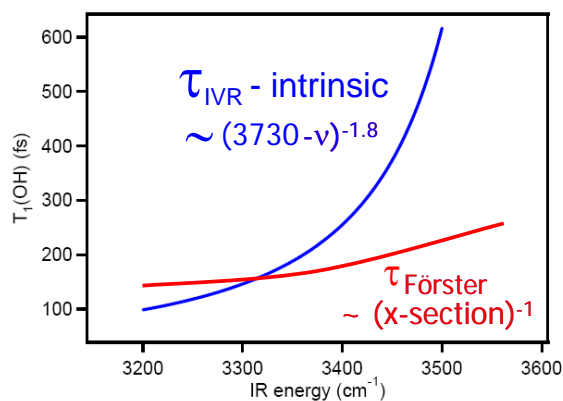


Figure 4.10. Schematic representation of the frequency dependence of the vibrational lifetime (τ_{IVR}) [144] and Förster energy transfer time [145], demonstrating that at low frequency the lifetime is shorter than the energy transfer time, and fast (sub-100 fs) vibrational relaxation can occur before energy transfer causes homogeneous response.

4.5 Conclusion

Four different model biological lipid/water interfaces were studied, namely monolayer's of DPTAP, DMPS, DPPC and DPPE on water, using our novel time-resolved SFG technique in order to elucidate the structural dynamics of the water molecules interfacing the lipid monolayers.

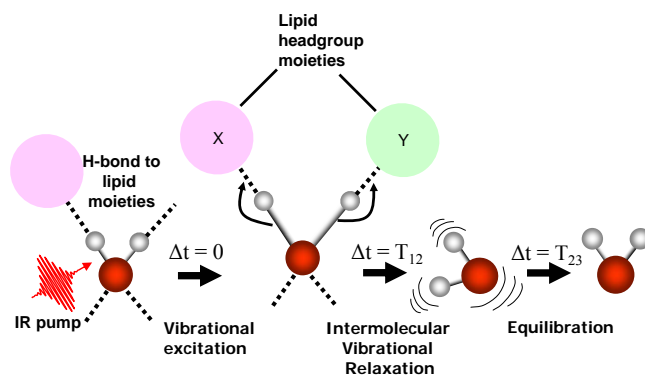


Figure 4.11. Cartoon depicting ultrafast vibrational relaxation. After excitation of the O-H oscillator, IVR occurs through the strong H-bond mode associated with the lipid headgroup moieties thus relaxing to an intermediate state and subsequently to a thermally equilibrated state. This mechanism of vibrational relaxation is concluded to be operative for strongly hydrogen bonded water molecules ($\tilde{\nu}=3200 \text{ cm}^{-1}$)

We find two predominant mechanisms of vibrational relaxation, irrespective of the details of the lipid monolayer system studied:

- (i) For the strongly bound water molecules (3200 cm^{-1} O-H stretch fundamental), vibrational re-

laxation occurs on timescales appreciably shorter than the pulse duration, presumably through the hydrogen bond modes associated with the lipid headgroup moieties (see figure 4.11). These water molecules relax so quickly, that they do not have time to exchange vibrational energy with neighbouring water molecules and the bulk.

(ii) For the medium and weakly bound water molecules ($3300\text{-}3500\text{ cm}^{-1}$, a Förster-type energy transfer amongst the neighbouring water molecules dominates the energy dissipation mechanism, which randomizes the excitation on very short timescales and subsequent relaxation occurs essentially with a time-constant of $\sim 200\text{ fs}$ - a phenomena also observed in bulk and neat water-air interfaces as we've seen in the previous chapter (see figure 3.7)

(iii) For the strongly bound water molecules (3200 cm^{-1}), transient features ("overshoot") were observed at the zwitterionic lipid/water systems that were absent for the charged lipid/water systems, which suggest differences in the way the interfacial water molecules couple to the zwitterionic headgroups than to the charged lipid headgroups. Shorter pulses and two-colour pump-probe SFG schemes need to be implemented, whereby exciting the water molecules and probing the headgroup moieties, one can conclusively make the distinction between the bonding mechanisms of the interfacial water molecules with the different lipid headgroups.

(iv) On inspection of the T_{23} - the time constant that reflects the rearrangement of the hydrogen-bonded network following relaxation of the O-H stretch excitation - we find that the values are within the range observed in bulk water. Therefore the vibrational energy redistribution among the low frequency H-bond modes at the interface is not so different from those in the bulk.

(v) Finally, a relatively long relaxation time has been identified (T_{34}), which has been assigned to a slow, collective reorganization of the hydration layers around the lipid headgroups - we find that it takes a factor of 2-3 longer for the zwitterionic headgroup water molecules than for those at the charged lipid headgroups. This might be suggestive of a more complex collective coupling of the hydration layers with the zwitterionic headgroups than with the charged lipid headgroups.

Structure and Dynamics of Water at Model Human Lung Surfactant interfaces

Abstract

We investigated the structure and dynamics of water in contact with a monolayer of artificial lung surfactant (LS), composed of four types of lipids and one protein. The interfacial water is investigated with frequency-domain and time-domain surface sum-frequency generation spectroscopy, in which the vibrational relaxation of specifically interfacial water molecules can be followed. We compare the response of water interfacing with three systems: a monolayer of the pure lipid that is dominant in the LS mixture, a monolayer of the four lipids, and a monolayer of the four lipids including the lung surfactant protein. We find remarkable differences in the vibrational energy relaxation mechanisms between the pure DPPC/water system and the mixtures - which essentially reveals the underlying differences in the associated interfacial water structure.

5.1 Introduction

This chapter reports on surface-specific experiments performed to directly probe the interfacial water at the water-model lung surfactant (LS) interface. Using steady state and time-resolved SFG we aim at elucidating the structure and dynamics of interfacial water, in order to increase our molecular-level understanding of the role of water in lung functioning. Human LS is a complex mixture of lipids and proteins that forms a monolayer at the air-alveoli interface of the lungs. This LS has some remarkable properties that make it crucial for the proper functioning of lungs, the deficiency and dysfunction of which leads to fatal respiratory disorders. In premature infants, deficiency of LS results in respiratory distress syndrome (RDS), which is one of the leading causes of infant deaths [146]. Dysfunction of LS is a condition associated with acute RDS (ARDS). ARDS is a result of lung injury and can affect patients of all ages¹. Current clinical treatment for RDS is through surfactant replacement therapy, namely, administration of exogenous model LS which mimic the natural LS. Thus a fundamental molecular understanding of LS structure and function can lead to improvements of the established treatments as well as invention of novel therapies. Prior studies have essentially focused on the LS lipid structure (with and without the LS protein/mimics) [147], however without much focus on the role of the interfacial water. With our frequency- and time-resolved SFG we have attempted to further our molecular understanding of the role of interfacial water at such biological membranes.

5.1.1 Lung Surfactants and Interfacial Water

The human LS monolayer at the air-alveoli interface of the lungs [146, 148, 149] is secreted by the alveolar type II cells into the hypophase in the form of lamellar bodies, which is then transformed into a unique surfactant assembly, tubular myelin (TM). With the aid of TM, the LS can adsorb rapidly onto the airalveolar hypophase interface during inhalation, forming a surfactant monolayer covering the alveolar hypophase. From a biophysical point of view this LS must satisfy three requirements for proper lung functioning: it must (i) reach ≈ 0 mN/m surface tension near the end of exhalation, (ii) have relatively high surface activity, and (iii) adsorb/desorb from the interface rapidly [147, 150]. The first requirement is met by monolayers of pure DPPC (1,2-Dipalmitoyl-sn-Glycero-3-Phosphocholine). Unfortunately, this system is neither sufficiently surface active, nor does it adsorb sufficiently rapidly, to be useful in-situ. Both requirements (ii) and (iii) are generally addressed by mixing lipids with DPPC that have either unsaturated bonds in their alkyl tails or tails that are particularly bulky. Pure DPPC monolayers have a relatively small lipid condensed (LC)/ lipid expanded (LE) phase coexistence that spans ~ 2 -5 mN/m. The addition of unsaturated or bulky lipids expands this coexistence region over a much larger range in surface pressure: where the LC phase is then dominated by DPPC and the LE by the bulky or unsaturated lipids [147]. The pressure range of this phase coexistence can be further enhanced by the addition of a component

¹Some celebrities victims and survivors of ARDS:

1. Patrick Bouvier Kennedy, son of President John F. Kennedy and First Lady Jacqueline Kennedy, died of RDS two days after his premature birth at 34 weeks gestation in 1963.
2. Freddie Highmore, a popular young British actor survived RDS after being born at 29 weeks.

that specifically interacts with DPPC in such a manner as to cause an increase in density; such a component might be thought of as a way of making LC domains more condensed [151]. LS films are thought to function in lungs by excluding components that form the LE domains at high pressure, leading to the "squeeze-out hypothesis" [147,152,153]. In the absence of any mechanism of retaining such material near the air/water interface one might expect that, over many expansion/compression cycles, loss of LS components through diffusion away from the film might be significant. Adding small amounts of a synthetic mimic of LS protein B helps overcome this problem by catalyzing the reversible formation of multi-layers at high compression: instead of being lost to diffusion LS components form multi-layers at high compression and reinsert into the monolayer at low compression [153–155]. Useful insights into such LS systems may be gained by studying mono-/multi-layers spread over an aqueous sub-phase. There is an extensive body of literature, and existing therapeutic products, that suggest LS function can be mimicked by a mixture of 3-4 well-defined synthetic lipids and a small, amphiphilic peptide that mimics the function of LS protein B [156,157]. Though such mixtures are known to be therapeutically effective, the role of interfacial water at membranes has not yet been clarified.

5.1.2 Frequency- and Time-Resolved SFG on model lung surfactant monolayers on water

In this study, we follow prior workers and use DOPG (1,2-Dioleoyl-sn-Glycero-3-[Phospho-*rac*-(1-glycerol)]) and tripalmitin (TP) as unsaturated and bulky components, add palmitic acid (PA) to drive further condensation of DPPC and employ the artificial protein KL₄ as an SP-B mimic [147,151]. We take VSFG spectra over the entire CH and O-H H-bonded region for first DPPC, then a 6:2:1:1 (by mass) mixture of DPPC:DOPG:PA:TP (called mixture) and finally a 6:2:1:1:1 mixture of DPPC:DOPG:PA:TP:KL₄ (called mixture + KL₄) at several molecular densities. The chemical structures for each of these LS components are shown in figure 5.1. In addition to the VSFG measurements, we also perform TRSFG measurements centered at 3200 cm⁻¹. Water in all three systems shows a new kind of dynamical response to vibrational excitation. The combined frequency resolved and pump-probe study of the LS system and its constituents sheds new light on the role of water in the molecular organization of the LS monolayer.

Sample preparation

1,2-Dipalmitoyl-sn-Glycero-3-Phosphocholine (DPPC) and 1,2-Dioleoyl-sn-Glycero-3-[Phospho-*rac*-(1-glycerol)] (sodium salt) (DOPG) were purchased from Avanti Polar Lipids. Palmitic Acid (PA) and Tripalmitin (TP) were purchased from Sigma-Aldrich. All were used as received. The structures of the lipids and surfactants are shown in figure 5.1. The 21 amino acid peptide KL₄ used in our experiment consists of 4 repeating units of Lys(K)-Leu(L)-Leu-Leu-Leu terminating with K. This short sequence peptide was custom made by AnaSpec, Inc. (San Jose). Stock solutions (≈ 2 mg/mL) of DPPC, PA and TP were prepared in HPLC grade chloroform while DOPG (≈ 2 mg/mL) and KL₄ (0.6 mg/mL) were prepared in 1:3 methanol/chloroform. The model lung surfactant lipid mixture

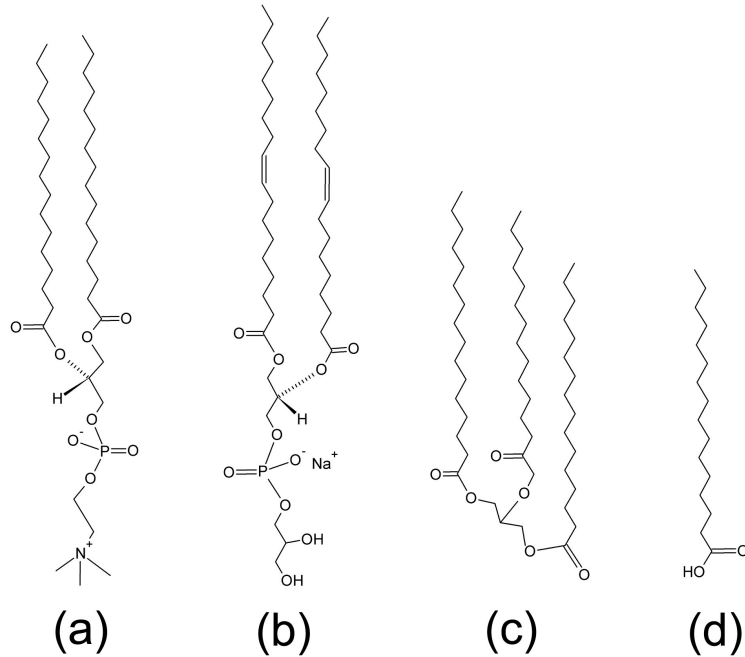


Figure 5.1. Chemical structures of the Lung Surfactant constituents: **(a)** 1,2-Dipalmitoyl-*sn*-Glycero-3-Phosphocholine (DPPC), **(b)** 1,2-Dioleoyl-*sn*-Glycero- 3-[Phospho-*rac*-(1-glycerol)] (DOPG), **(c)** tripalmitin (TP), **(d)** palmitic acid (PA).

without the KL_4 (i.e. mixture) was prepared by mixing DPPC/DOPG/PA/TP in a 6:2:1:1 mass ratio; and with the KL_4 (i.e. mixture + KL_4) with a mass ratio of (DPPC/DOPG/PA/TP/ KL_4) 6:2:1:1:1 [158].

For the VSFG experiments, Langmuir monolayers of DPPC and the model surfactant with and without KL_4 were prepared by drop wise addition of the stock solutions onto an ultrapure (Millipore) water sub-phase in a home-built teflon trough. A monolayer or multi-layer forms on top of the aqueous phase after rapid evaporation of the chloroform and methanol. As the time resolved measurements take several hours in our set up, a rotating trough was used in these experiments to prevent cumulative heating by the laser pulses. The surface pressures for the monolayers were monitored using a tensiometer (Kibron). Experiments were performed at two different surfactant densities for each sample type. For single component DPPC monolayers, experiments were performed at surface densities of 2.9 and 4.4×10^{-4} mg/cm² (corresponding to surface pressures of 15 and 35 mN/m respectively), for the mixture surface densities of 1.7 and 3.1×10^{-4} mg/cm² and for the mixture+ KL_4 , 2.1 and 3.1×10^{-4} mg/cm² (TRVSFG results are presented only for the high density mixture+ KL_4 sample). We observed large variability in the surface pressure for the mixture and mixture+ KL_4 systems as measured with our tensiometer. Prior fluorescence and scanning probe images of systems of similar composition to ours indicate lipid phase separation. It is therefore expected to be difficult to extrapolate point pressure measurements to entire monolayers in these systems [150, 158], as we observe for the mixture and mixture + KL_4 .

The experimental setups that have been used for frequency-resolved and time-resolved SFG experiments have been discussed in detail in chapter 2 (Experimental Technique).

5.2 Results and Analysis

Measurements were performed on 3 samples: pure DPPC, a 6:2:1:1 mixture of DPPC:DOPG:PA:TP (mixture) and a 6:2:1:1:1 mixture of DPPC:DOPG:PA:TP:KL₄ (mixture + KL₄). The frequency-resolved experiments were performed on a sub-phase of D₂O, rather than H₂O, as our frequency-resolved set-up is more suited to generate IR frequencies in the O-D stretching region than in the O-H. Without exception, experiments performed on an H₂O sub-phase reveal the same behavior for H₂O as for D₂O, allowing a straightforward comparison through a renormalization of the frequency axis. Time-resolved experiments were performed on an H₂O sub-phase. For the conventional VSFG measurements spectra were taken for each of the 3 systems at 2 distinct lipid densities corresponding to surface pressures of approximately ~ 15 and 30 mN/m for the lipids and ~ 7 and 15 mN/m for the lipid-protein mixture, giving a total of 6 measurements. For the TRSFG measurement no low density mixture + KL₄ traces were collected.

5.2.1 Frequency-resolved VSFG measurements

Frequency resolved VSFG measurements Figure 3 shows VSFG spectra for pure DPPC, the mixture and the mixture + KL₄, at two densities each. The spectra are characterized by broad O-D resonances in the $2200-2600$ cm⁻¹ range and narrow C-H resonances around 2900 cm⁻¹. The VSFG data is fitted using a Lorentzian model, as described in literature [159]. Briefly, the sum-frequency generation (SFG) intensity is proportional to the square of the nonlinear polarization P_{SFG} generated at the surface by the visible and infrared optical fields:

$$I_{SFG} \propto |P_{SFG}^2|^2 \propto |\chi^{(2)}|^2 I_{VIS} I_{IR} \quad (5.1)$$

where $\chi^{(2)}$ is the second-order nonlinear susceptibility and I_{VIS} and I_{IR} are the intensities of the incident fields. As discussed in earlier chapters, $\chi^{(2)}$ is given by,

$$\chi^{(2)} = \chi_{NR}^{(2)} + \chi_R^{(2)} = A_0 e^{i\phi} + \sum_n \frac{A_n}{\omega_n - \omega_{IR} - i\Gamma_n} \quad (5.2)$$

So when the frequency of the incident infrared field is resonant with a vibrational mode n , the SFG field is strongly enhanced. Here, A_0 is the real amplitude of the non-resonant susceptibility, ϕ its phase, A_n is the amplitude of the n^{th} vibrational mode, ω_n the resonant frequency, and Γ_n the linewidth of the transition. We substitute equation 5.2 into equation 5.1 and use the resulting expression to fit the frequency resolved VSFG spectra, the results are shown as black solid lines in figure 5.2.

The signal in the O-D stretch region is significantly larger for the lipid mixture - both with and without KL₄ - than for DPPC. The fits to the data reveal that the amplitudes of the susceptibility

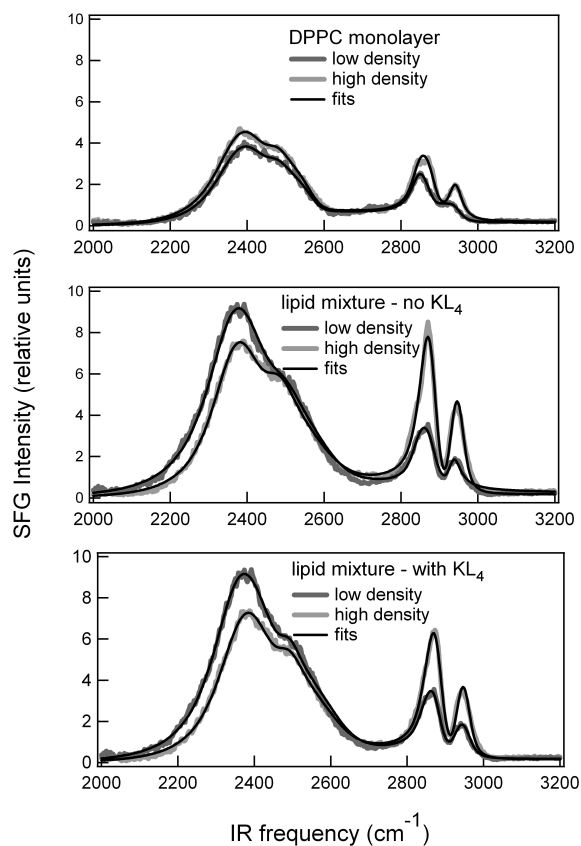


Figure 5.2. Frequency-resolved VSG spectra of the three monolayers at low (dark grey) and high (light grey) lipid densities each corresponding to surface pressures of ~ 15 and 30 mNm^{-1} . Lipid surface densities for low and high densities are: 2.9 and 4.4 mg cm^{-2} for DPPC, 1.7 and 3.1 for the mixture, and 2.1 and 3.1 for the mixture with KL_4 , all expressed in units of $10^{-4} \text{ mg cm}^{-2}$. Fits to the data (see text) are shown as black lines. Top panel shows data for the DPPC monolayer, centre panel shows data for the lipid mixture (no KL_4) and bottom panel shows data for the lipid mixture + KL_4 . All static SFG data were collected in SSP (SFG : VIS : IR) polarization configurations.

for the C-H stretch are very similar for all three systems; the lowered SFG intensity for DPPC in the C-H stretch region is caused by reduced interference with the O-D stretch. As expected, for all three systems the C-H resonances increase in intensity when the lipid density increases [160]. This is an effect of both an increase in the number of methyl (CH_3) and methylene (CH_2) groups contributing to the signal and the increased order among the CH_3 groups. There is, however, a remarkable difference between the behaviour of the water resonances as the lipid density is varied: for DPPC, the water SFG signal intensity *increases* weakly with increasing lipid density but for the mixture, with and without KL_4 , there is a significant *decrease* in the water signal as the lipid density is increased.

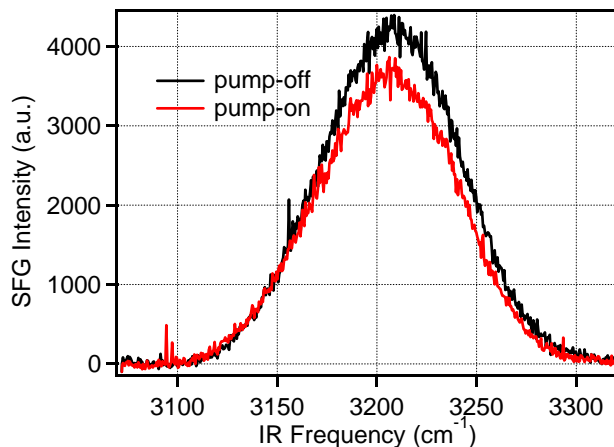


Figure 5.3. VSFG spectra of interfacial water with (*pump-on*) and without (*pump-off*) IR excitation, centered at $\approx 3200 \text{ cm}^{-1}$ and at a pump-probe delay of 50 fs.

5.2.2 Time-resolved SFG measurements

In addition to the VSFG measurements, TRSFG measurements were carried out at the water-membrane interfaces centered at $3200 \pm 10 \text{ cm}^{-1}$ (using pulses with a spectral width of $\sim 120 \text{ cm}^{-1}$). This frequency corresponds to the maximum in the SFG response in figure 5.2, for H_2O in the O-H stretch region. In all three systems, the dynamical response of water looks qualitatively similar. Immediately after excitation the SFG intensity decreases, due to bleaching of the ground state. The *pump-on* and *pump-off* SFG spectra of interfacial water at a pump-probe delay of 50 fs are shown in figure 5.3. The TRSFG dynamics transients for all the systems are shown in figure 5.4. For all cases, the look qualitatively similar: following the initial bleach, there is a partial recovery of the SFG signal, after which the signal decreases further, and finally levels off to a level that is significantly lower than its original value. The initial dynamics (bleach, partial recovery and second signal decrease) occur on sub-picosecond timescales, whereas the final slow rise occurs over tens of picoseconds. After this bleach, then, inspection of the data makes clear that it is characterized by three other distinct processes: partial rapid recovery, a second signal decrease and continued slow recovery.

Such a response is most simply described by a 5-level kinetic system, with three associated time constants as used in previous bulk studies (see chapter 4). The relevant coupled differential equations describing the population kinetics in such a system can be written as,

$$\frac{dN_0(t)}{dt} = -I(t, \tau_{fwhm})\sigma_0(N_0(t) - N_1(t)) \quad (5.3)$$

$$\frac{dN_1(t)}{dt} = I(t, \tau_{fwhm})\sigma_0(N_0(t) - N_1(t)) - \frac{N_1(t)}{T_{12}} \quad (5.4)$$

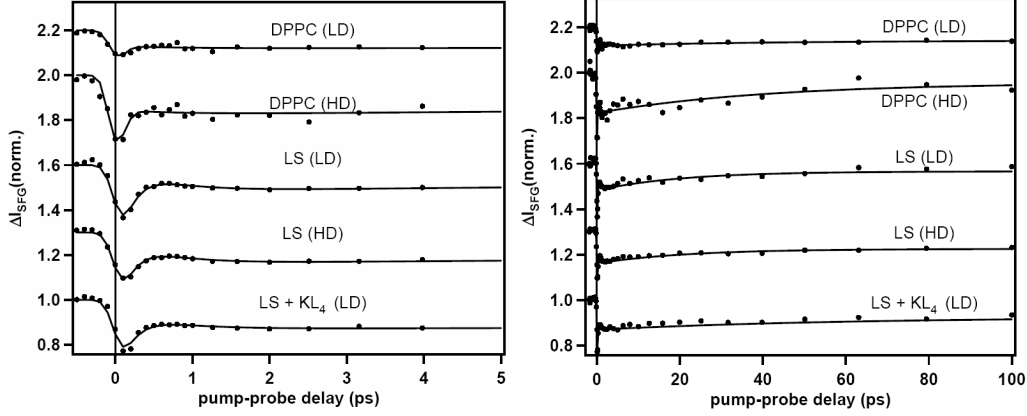


Figure 5.4. One-colour IR pump-SFG probe transients of water at various water/lung surfactant interface systems. Plots on left are the transients upto 5 ps pump-probe delay and the ones on right upto 100 ps. The systems studied are (i) DPPC at low density(LD), (ii) DPPC at high density (HD), (iii) LS without KL_4 at LD, (iv) LS without KL_4 at HD and (v) LS with KL_4 at LD. The transients are normalized by the *pump-off* reference SFG spectra, and have been offset for visual clarity. The 5-level model fits (explained in text) are also shown along with the data as solid lines.

$$\frac{dN_2(t)}{dt} = \frac{N_1(t)}{T_{12}} - \frac{N_2(t)}{T_{23}} \quad (5.5)$$

$$\frac{dN_3(t)}{dt} = \frac{N_2(t)}{T_{23}} - \frac{N_3(t)}{T_{34}} \quad (5.6)$$

$$\frac{dN_4(t)}{dt} = \frac{N_3(t)}{T_{34}} \quad (5.7)$$

where,

$$\begin{aligned} \frac{dN_x(t)}{dt} &= \text{the rate of population change in level } x \text{ at time, } t \\ I(t, \tau_{fwhm}) &= \text{the Gaussian pump pulse with a certain pulse duration, } \tau_{fwhm} \\ \sigma_0 &= \text{is the absorption cross-section for the } 0 \rightarrow 1 \text{ transition} \end{aligned}$$

In modelling of the data, the SFG susceptibilities and relaxation times are kept as fit parameters and the normalized differential SFG signal, ΔI_{SFG} as a function of the pump-probe delay t , is then computed from the time-dependent state populations by,

$$\Delta I_{SFG}(t) = \frac{[(N_0(t) - N_1(t))\chi_0 + \chi_2 N_2(t) + \chi_3 N_3(t) + \chi_4 N_4(t)]^2}{[N_0(0)]^2} \quad (5.8)$$

As is evident from inspection of figure 5.4, this simple model provides an adequate description of the data. The time constants that are inferred from the fit are shown in Table 5.1.

We interpret the relaxation times as follows: T_{12} represents the vibrational relaxation time T_1 ; T_{23}

Table 5.1. Relaxation times obtained from the fits^a to the data in figure 5.4 using the 5-level scheme.*LD = Low Density, †HD = High Density, ‡Mix = Mixture.

T_{xy}	DPPC(LD*)	DPPC(HD†)	Mix‡(LD)	Mix(HD)	Mix+KL ₄ (HD)	
T_{12} (fs)	<50	<50	190	190	200	^a Time
T_{23} (fs)	950	950	500	500	577	
T_{34} (fs)	40000	40000	20000	21450	60000	

constants obtained are within $\pm 15\%$ error, except for T_{23} for DPPC, for which the values are within $\pm 50\%$

represents the time associated with the adjustment of the hydrogen bonded network to the sudden temperature increase upon vibrational relaxation; T_{34} is associated with the equilibration over long timescales – its origin will be discussed below.

Several observations can be made. First of all, the values for T_{12} for the pure DPPC-water system (low and high density) are significantly smaller ($T_{12} < 50$ fs) than for both the mixtures - with and without KL₄. Very fast vibrational relaxation rates were also reported for all other pure lipid monolayer systems presented in chapter 4. Remarkably, the transients of the mixtures show a significant increase in the T_{12} (~ 200 fs). Figure 5.5 shows attempts to fit the transients for the LS mixture, with and without KL₄, with the same fast $T_{12} < 50$ that was observed for pure DPPC and other lipids at this IR frequency. It is apparent from this figure that fits with $T_{12} = 50$ fs and $T_{12} = 100$ fs do not adequately describe this data set.

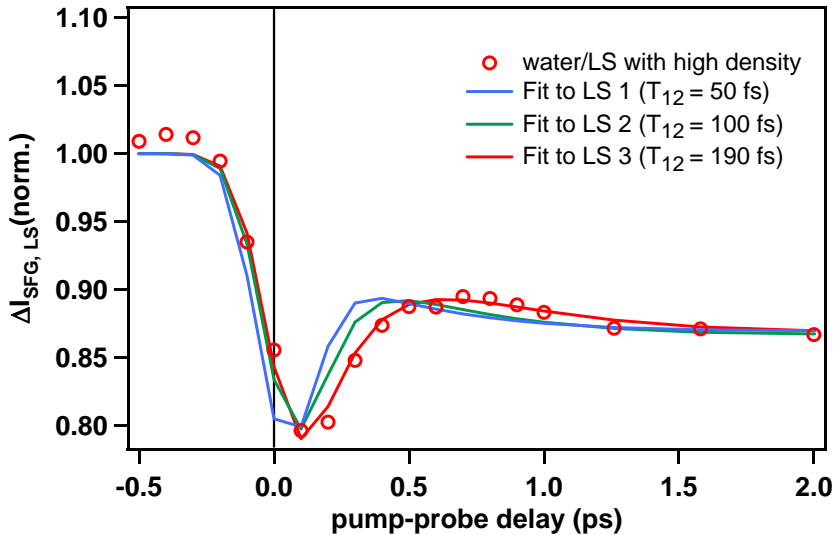


Figure 5.5. TRSFG transients (data in dots) of the water/Lung Surfactant (LS) mixture (without KL₄). Shown in bold red, is the best fit to the transient of LS/water using the 5-level kinetic model. The blue and green bold lines are fits to the LS/water transient data, using different time-constants indicated in the figure.

Secondly, the T_{23} of the DPPC-water system is ~ 950 fs, whereas for the mixtures, with or without KL_4 , the T_{23} s are ~ 500 fs. Thirdly, concerning the slow time constant T_{34} , although not an extremely sensitive parameter in the fitting procedure for the given signal-to-noise of the transient data, there is a significant dependence on the monolayer composition and ranges between ~ 20 to ~ 60 ps - depending on the monolayer system and their densities on the subphase.

5.3 Discussion

5.3.1 Frequency-resolved SFG measurements

The generic VSFG spectra of interfacial liquid water all have in common a broad, double peaked feature from $\sim 3100\text{-}3550\text{ cm}^{-1}$ originating from the O-H stretch vibrations of interfacial water (see figure 5.2). The much-debated assignment of this broad double-peaked feature has already been discussed in chapter 3. Despite the complications arising in quantitative structural interpretation of the O-H stretch spectrum owing to intermolecular coupling and intramolecular couplings, a number of qualitative observations can be made from the O-H SFG spectra studied in this chapter, for instance, (i) the SFG intensity in the O-D stretch region is significantly larger for the lipid mixture - with and without KL_4 - than for DPPC, and (ii) for DPPC, the water signal *increases* weakly with increasing lipid density but for the mixture with and without KL_4 , it *decreases* with increasing lipid density.

The VSFG amplitude of the O-H (O-D) stretch vibrations of interfacial water is known to increase at nominally charged interfaces (see, for example, the study by Gragson and coworkers of monolayers of differently charged surfactants at the air/water interface [161]). As indicated in figure 5.1, the headgroup of DOPG is negatively charged. With this information, observation (i) can thus be rationalized by noting that both the mixture and the mixture + KL_4 contain significant amounts of negative charge in the monolayer and thus the amplitude of the O-H (O-D) stretch in these systems might be expected to be larger than that near the pure DPPC (zwitterionic) monolayer. Rationalizing observation (ii.) requires noting that mixtures of DPPC, DOPG, PA and TP are known to phase separate (under a wide range of pressures) into relatively more condensed domains (enriched in DPPC and PA) and relatively more liquid domains (enriched in DOPG, TP and, if applicable, KL_4) [162, 163]. The relatively liquid domains are thought to preferentially *squeeze out* as the monolayer is compressed [147, 153].

5.3.2 Time-resolved SFG measurements

As discussed above, it is challenging to extract details of structural dynamics of interfacial water from the static SFG spectra. Although differences in lineshape are clearly evident, interpreting the structural significance of these observations is not straightforward; the dynamical response can however, shed additional light on local water organization. As shown in previous chapters, we have applied TRSFG to both the air/water [93] and 1,2-dimyristoyl-sn-glycero-3-[phospho-L-

serine](DMPS)/water interfaces [94] while others have applied it to water at the silica/water interface [87].

The TRSFG transient data could be described by the mentioned 5-level kinetic model shown in chapter 4 (figure 4.3), as discussed earlier in this chapter and also in chapter 2. First, from the O-H stretch vibrational ground state N_0 , excitation is taken into state N_1 , almost instantaneously, in which the stretch mode is excited. Subsequently vibrational relaxation occurs to a state N_2 in T_{12} timescales: a non-equilibrium state arising out of efficient anharmonic coupling of the excited O-H stretch mode with the excited low-frequency H-bond modes in response to the quasi-instantaneous temperature increase due to the excitation pulse. N_2 subsequently relaxes to N_3 with a timescale of T_{23} : a *hot* ground state where the excess energy is equilibrated over all degrees of freedom of the H-bond modes and thereby reorganizing the hydrogen bond network. Finally, the excitation energy flows out of N_3 into N_4 with a timescale of T_{34} much larger (≥ 20 ps) than T_{12} and T_{23} , depending on the monolayer composition. The N_4 state can be interpreted as a state arising out of a collective reorganization of the hydrogen bond network due to exchange of water molecules across the lipid hydration shell.

Keeping this scenario in mind we can attribute the obtained time constants to the structural dynamics of the interfacial water at the various monolayers in our study. We observe that the T_{12} of the DPPC/water system at 3200 cm^{-1} is < 50 fs and is comparable to those observed at 3200 cm^{-1} for the DPTAP/water (see figure 4.5, chapter 4) and DMPS/water systems. On the other hand, the mixtures with and without KL_4 exhibit a T_{12} of ≈ 200 fs. This relatively slower T_{12} for the mixture/water systems is however, reminiscent of the bulk water population dynamics, where it has been argued that the initial O-H stretch excitation is randomized via a Förster-type energy transfer between neighbouring water molecules [93, 130, 132], whereby the subsequent relaxation occurs in ≈ 200 fs. Thus, the water molecules at the interface of LS mixtures are more bulk-like, in the sense that Förster-type energy transfer dominates the relaxation dynamics of this type of interfacial water. However, at the DPPC/water interface, the vibrational relaxation is almost 4 times faster than at the LS mixture/water interface - faster than (or at least as fast as) the rate at which a Förster-type transfer can randomize the excitation on the O-H oscillators. Such a fast relaxation process may arise due to efficient coupling between the O-H oscillators of the interfacial water and the head-groups moieties, for instance the phosphocholine moiety.

T_{23} , which is interpreted as the vibrational energy redistribution (VER) timescale for the excitation quanta over all degrees of freedom of the reorganized H-bond network in response to the quasi-instantaneous *thermalization*, ranges between ≈ 500 and ≈ 950 fs for all the interfaces: consistent with previously reported timescales in bulk water [142, 143].

For DPPC, T_{34} is ≈ 40 ps, ≈ 20 ps for the mixture without KL_4 and ≈ 60 ps for the mixture with KL_4 . NMR studies of partially hydrated bilayers suggest this to be a significant fraction of the timescale on which exchange of individual water molecules between those strongly associated with lipid head groups and the bulk occur (typical exchange times (τ_{exch}) reported to be ≈ 100 ps) [37].

As described above, the addition of KL_4 to the mixture has relatively little effect on vibrational relaxation (T_{12} and T_{23}) but does have a significant influence on relatively slow structural relaxation

processes (i.e. T_{34}). Interestingly, the addition of KL_4 to the lipid mixture does have a significant effect on the pressure isotherm [162,164]: at high surface pressures, the lipid density (normalized to the monolayer interfacial area) is lower in the presence of KL_4 . This observation, in combination with scanning probe studies of model LS films, is most simply understood as the result of formation of multi-layers in the lipid mixture with KL_4 present [150]. The formation of multi-layers also explains the slowing down of structural rearrangement: multi-layer formation is expected to slow down the exchange of water with the bulk. From the spectrally resolved data we have already concluded that at high pressures in both the mixture and mixture + KL_4 interfacial water contact with DOPG is likely decreased.

5.4 Conclusions

In the current study, we investigated the structure and dynamics of interfacial water in contact with a monolayer of model lung surfactant, composed of four types of lipids (referred to as mixture) and one 21-amino acid peptide (KL_4), at various surface densities. Using frequency- and time-resolved SFG spectroscopies, we followed the rate and mechanism of vibrational relaxation of interfacial water molecules in real-time, after being excited with an intense IR pump pulse. This essentially revealed the vibrational dynamics of interfacial water molecules which is a sensitive probe of the interactions between the water and the membrane moieties - a primary event in defining the macroscopic functionalities of the membrane itself.

In our static SFG studies, we have addressed the differential hydration (by D2O) of each lung surfactant (LS) component by examining three systems: a monolayer of the pure lipid that is dominant in the lung surfactant mixture (DPPC), a monolayer of the four lipids (mixture), and a monolayer of the four lipids including the protein (mixture + KL_4). The lineshapes of the O-D stretch observed in the static SFG spectra for each experimental system are similar. However qualitative differences in SFG spectral amplitudes as a function of monolayer density and composition are clearly present:

1. The O-D stretch SFG amplitude is larger for the mixture and the mixture + KL_4 than for DPPC, regardless of the surface pressure and,
2. the amplitude of the O-D stretch increases in the DPPC monolayer as a function of pressure but decreases with pressure for the mixture and the mixture + KL_4

These differences are consistent with prior VSFG studies which have shown that the presence of DOPG in the LS film gives it a large O-D stretch amplitude relative to DPPC and this amplitude decreases with pressure as DOPG is preferentially excluded from the film into relatively less ordered multi-layers.

In the TR-SFG experiments at the 3200 cm^{-1} pump and probe frequencies - synonymous with strong hydrogen-bonding of the O-H - some remarkable observations have been made:

1. The initial relaxation process defined by T_{12} of the mixture/water system, with and without KL_4 , is ≈ 200 fs - which is reminiscent of the bulk water population dynamics, where it has been argued that the initial O-H stretch excitation is randomized via a Förster-type energy transfer between closely lying neighbouring water molecules (within 2.8 \AA). This is consistent with the *squeeze-out* model, where the water molecules are more dense in the headgroup region of the LS mixture (with and without KL_4). Remarkably however, at the DPPC/water interface, the T_{12} of the water molecules is < 50 fs, suggesting an alternative mechanism of energy flow rather than randomization of the excitation through Förster transfer. This is consistent with a scenario where the density of interfacial water molecules is much sparse at the DPPC/water interface than at the LS mixture/water interface - thus water molecules efficiently coupling to the H-bond modes associated with the phosphocholine headgroups rather than the surrounding fewer water molecules.
2. The vibrational energy redistribution of the excitation energy over all the degrees of freedom of the thermally excited H-bond modes, defined by T_{23} is essentially the same for all the systems and is consistent with time constants observed in bulk, which ranges from 0.5 to 1 ps.
3. A very long T_{34} is observed for all the lipids in the order of 10s of picoseconds and the values range from 20 to 60 ps, depending on the lipid details. Such slow processes can be attributed to collective rearrangements of water molecules or exchange of water molecules across hydration layers.

Ultrafast energy flow in model biological membranes

Abstract

We report on the energy flow dynamics in model membranes, investigated by surface-specific time-resolved (femtosecond) sum frequency generation spectroscopy. This recently developed technique allows us to probe energy dynamics selectively at the water/lipid interface. We report vibrational relaxation dynamics of C–H stretch modes in the lipid alkyl chains, and reveal that incoherent energy transfer occurs from excited CH₂ groups to the terminal CH₃ groups. We also find evidence for strong anharmonic coupling between different CH₂ and CH₃ modes. Relaxation and energy transfer processes within the lipid alkyl chain occurs on (sub-)picosecond timescales. Studies of the dynamics on different lipid phases (gel or liquid crystalline phase) reveal a marked independence of the dynamics on the precise molecular conformation of the lipids. In addition, we report the energy transfer dynamics between membrane-bound water and lipids, and find that the transfer of heat between water and lipids occurs remarkably fast: heat is transferred across the monolayer, from the polar head group region of the lipid to the end of the alkyl chain, within 1 ps. These results demonstrate the potential of using ultrafast surface-specific spectroscopies to elucidate biomolecular dynamics at membrane surfaces.

6.1 Introduction

The dynamics of excitation transfer and energy flow in biological systems have been studied extensively the past decade [165, 166], for several reasons. First of all, a number of important biological processes relies on fast energy transfer processes. In photosynthesis, for example, the events that occur when photons impinge on a light harvesting complex, involve the excitation going through several intermediate states before reaching the reaction center; the initial steps in this energy migration process occurs on femtosecond timescales. [167] It is evident that a complete understanding of photosynthesis requires insights on all relevant timescales.

Moreover, it has become apparent that even for biofunctionality that does not rely on large-scale, dynamical energy transfer processes, dynamical studies can provide important insights into biomolecular processes and functions: it is becoming increasingly clear that insights into the static structure of biomolecules is not always sufficient to completely understand their function. [168, 169] For instance, conformational fluctuations that may occur over many timescales have been shown to play an important role in protein action. [168, 170–172]

This realization is prompting increasing efforts to elucidate dynamical aspects of biomolecular structure and functioning. Indeed, femtosecond, time-resolved studies of biomolecules which probe the energy dynamics in biomolecules is providing important information about the function of those biomolecules, which cannot be obtained from static experiments. [171–175] Although biomolecular dynamics are being studied extensively in bulk biological systems (see e.g. [166, 171–177] and refs therein), this is less so for biological surfaces, most notably membranes [54, 175, 178–180]. This is remarkable, considering that up to 40% of all cellular proteins - the micro-machines of life - are embedded in membranes. Our understanding of this intricate surface is essential to comprehend - and ultimately control - the many biochemical and biomedical processes that occur at, or even within, the membrane surface, including viral infection and targeted drug delivery. The reason for this lag in our knowledge is therefore clearly not the lack of relevant questions, but the limited number of techniques that are sufficiently sensitive and surface specific to probe molecular dynamics in a membrane. Indeed, much of our knowledge of membrane protein and lipid dynamics originates from molecular dynamics (MD) simulations (see, e.g. Refs. [181]).

The reports mentioned above [54, 166, 171–177] are based on femtosecond laser spectroscopy. This approach is uniquely suited to provide direct access to biomolecular dynamics, by investigating the temporal evolution of the biomolecular system in real-time. As such, the approach complements techniques that infer biomolecular dynamics in membrane systems from steady-state measurements, such as time-domain fluorescence (upconversion [72] or correlation [41]) spectroscopies, ESR/EPR [42, 43] and NMR (see, e.g. Refs. [45, 46] studies of membrane dynamics, neutron [48, 49] and x-ray scattering [51, 182].

Indeed, there have been several femtosecond laser-based studies addressing the dynamics of biological membrane model systems, notably water-lipid interactions. [178–180] and trans-membrane proteins [54, 175]. We present here the first surface-specific study of vibrational energy relaxation and energy transfer in such a model membrane system. The technique presented here – time-resolved

sumfrequency generation (TR-SFG) – has the advantage of being surface specific. The experiments reported here were performed on lipid monolayers prepared on an ultrapure water subphase, which allows for detailed control of the membrane parameters, e.g. the surface pressure and lipid phase.

Our method relies on exciting specific vibrational modes within, or at, the membrane surface and monitoring the subsequent energy relaxation and transfer processes with femtosecond time resolution. The cell membrane consists of two leaflets of lipids where the hydrophobic chains of the lipid form the interior of the membrane and the hydrophilic headgroups face the aqueous environment. [183] Our model membrane is a self-assembled lipid monolayer on water. Monolayers are considered excellent model systems for membrane biophysics, since a biological membrane can be considered as two weakly coupled monolayers. [184] We study monolayer vibrational dynamics using the surface-specific vibrational spectroscopy of second order nonlinear sum frequency generation (SFG) spectroscopy. [26, 30, 185] A limited number of time-resolved studies of specifically surface properties have been reported [83, 84, 87, 93, 103, 116, 186–188], but this is, to the best of our knowledge, the first application of this technique to lipid systems.

Lipid layers can be in different thermodynamic phases, depending on lipid composition, temperature and lateral pressure. [189] Different lipid phases exhibit different properties, e.g. in terms of the mobility of constituents. Thus, the phase behavior of lipids is very important for the functioning of a membrane. Owing to its relevance, the study of (model) membrane phase behavior has therefore received much attention. [190] Fluorescence studies (e.g. [191–193]) have revealed domain formation in biological and model systems, and have provided important information about the mobility of membrane components, i.e. membrane fluidity. The lipid phase can be traced directly to the order / disorder state of the lipid hydrocarbon chain. For a highly compressed, saturated lipid, the alkyl chain will be in an ordered all-trans configuration (figure 6.3). Lipids with a lower degree of saturation may be in the more fluid crystalline liquid state at room temperature. This state is characterized by gauche defects in the alkyl chain, to which SFG is extremely sensitive

Indeed, steady-state SFG spectroscopy has been applied extensively to study lipid and surfactant interfaces. [60, 64, 75, 194, 195] This paper reports the first time-resolved SFG measurements of the energy flow in model membranes. We report on the vibrational relaxation of the C–H modes in lipids in different thermodynamic phases (the ordered gel and disordered liquid crystalline phase), as well as the dynamics of energy transfer between the water and the lipid.

The outline of the paper is as follows: first, the basic principles of the surface specific SFG technique are discussed in section 6.2. Here, it is also explained how an infrared pump field can be added to the SFG scheme to measure the dynamics of vibrational energy relaxation and energy transfer processes. In section 6.3, schematics of the experiment, the detection technique and sample preparation methods are provided. The results for the measurements of the vibrational relaxation and energy transfer are presented in section 6.4, as well as the analysis to obtain the lifetimes and transfer rates from the experimental data. Finally, the findings are compared to previous bulk studies in section 6.5, which reveals the specifics of the role of the interface in the relaxation dynamics.

6.2 Time-resolved Surface Spectroscopy

Our experimental approach relies on pump-probe spectroscopy. An ultrashort (femtosecond) infrared pump pulse excites a specific vibration within the model membrane (e.g. a C-H stretch vibration within the lipid alkyl chain or the O-H stretch vibration of membrane-bound water). The relaxation and energy transfer dynamics are interrogated by a second, delayed probe pulse pair, using femtosecond Time Resolved Sum Frequency Generation (TR-SFG) spectroscopy. This technique provides direct, non-invasive access to membrane lipids and membrane-bound water, through their molecular vibrations. TR-SFG relies on the resonant enhancement of frequency mixing when an infrared pulse is resonant with a surface vibration. It is inherently surface sensitive (owing to broken inversion symmetry at the surface [26]), and therefore only probes ~ 1 monolayer deep. The time resolution is determined by the duration of the laser pulses (~ 120 fs); the time delay between the excitation and probing pulses can be varied in a controlled manner by increasing the optical path length traveled by the probe pulses. As the laser probes an area of typically ~ 0.1 mm², it interacts with a large number of molecules (typically $\sim 10^{11}$). Molecular scale information is obtained through the molecular vibrations, and the synchronized response of the individual molecules in the membrane ensemble following the excitation process.

Before discussing the time resolved technique in detail, the main features of the SFG probe are briefly discussed first. Subsequently, the technique of TR-SFG is detailed, in particular the similarities and differences with common time resolved techniques like transient IR spectroscopy.

6.2.1 Steady-state Sum Frequency Generation

In the TR-SFG scheme presented here, the second-order non-linear technique of SFG is applied as a probe. As illustrated in figure 6.1, SFG relies on the resonant enhancement of the process of generating the sum frequency of an infrared and a visible photon when the former is resonant with a vibrational transition. This process is governed by the second order non-linear susceptibility $\chi^{(2)}$ of the system. Due to symmetry considerations, $\chi^{(2)}$ vanishes in isotropic, centro-symmetric bulk media, such as water. At the interface, the symmetry is necessarily broken and second order nonlinear processes are allowed.

In the experiment, an infrared (IR) and a visible (VIS) laser beam are spatially and temporally overlapped at the surface, inducing a nonlinear polarization at a frequency which is the sum of the frequencies of the two incoming fields: $\omega_{SFG} = \omega_{IR} + \omega_{VIS}$. In figure 6.1, a schematic representation of the water-lipid interface is shown with the IR and VIS probe beams (the pump IR beam will be discussed later). The generated SFG signal is emitted both in transmission (not shown) and reflection, conserving the phase-matching of the in-plane components of the wavevectors. The SFG intensity I_{SFG} is proportional to the nonlinear Fresnel factors L , [196] the nonlinear susceptibility tensor $\chi^{(2)}$ and the intensities of the incoming fields I_{VIS} and I_{IR} :

$$I_{SFG} = L \left| \chi^{(2)} \right|^2 I_{VIS} I_{IR} \quad (6.1)$$

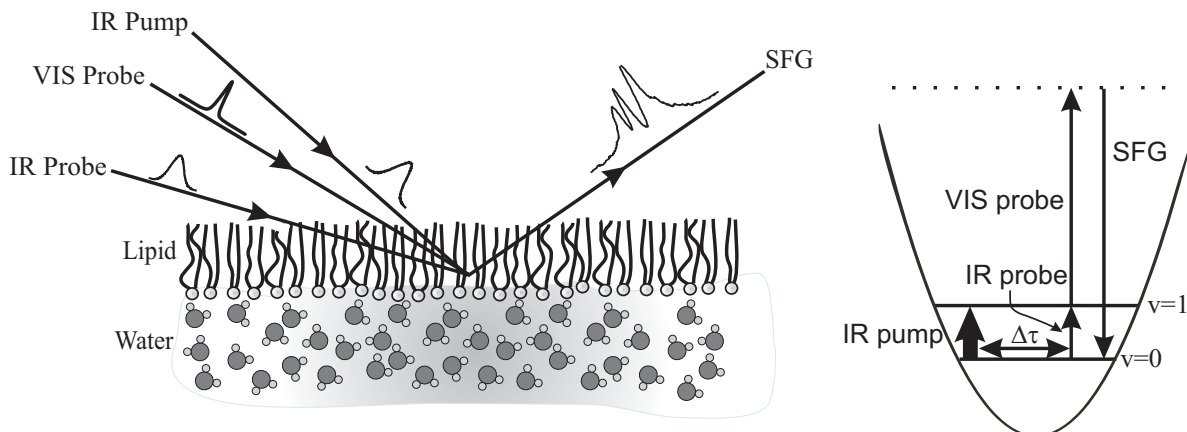


Figure 6.1. The experimental geometry of (TR-)SFG spectroscopy is shown in the left panel for a water-lipid interface. The IR probe and VIS probe are overlapped in space and time at the surface to generate an SFG signal. In a TR-SFG experiment, an additional IR pump beam is overlapped with the probe beams, which induces a change in the SFG signal. In the right panel, an energy diagram of the TR-SFG scheme is presented. The IR pump field transfers population from the ground ($v=0$) to the first excited vibrational level ($v=1$), decreasing the SFG signal. Vibrational relaxation will repopulate the ground state and the original SFG signal will be recovered. SFG generated from the IR pump and VIS probe can be spatially filtered out.

For a nonresonant VIS and SFG field, the nonlinear susceptibility tensor can be described as:

$$\chi^{(2)} = A_{NR} \exp(i\phi) + \sum_n \frac{A_n(N_{0,n} - N_{1,n})}{\omega_{IR} - \omega_n + i\Gamma_n} \quad (6.2)$$

Here, the vibrational resonance n is characterized by amplitude A_n , frequency ω_n and width Γ_n . A relatively small amount of SFG can also be generated away from the resonance; this process is characterized by A_{NR} and ϕ representing the nonresonant amplitude and phase. When the IR field is resonant with a vibrational transition, the SFG signal is enhanced and a vibrational spectrum of surface molecules is obtained. The resonant amplitude A_n depends on the population difference between the excited and ground states $\Delta n = N_{0,n} - N_{1,n}$. The probe IR field is sufficiently weak that Δn remains unchanged; at room temperature $\Delta n / (N_{0,n} + N_{1,n})$ is close to unity for high-frequency vibrations, such as the C-H and O-H stretch.

Femtosecond laser pulses inherently support a large bandwidth ($\sim 200 \text{ cm}^{-1}$, in our case). We therefore make use of a multiplex SFG scheme as described elsewhere. [197–199] Using a broadband IR field several spectrally narrow vibrations can be addressed resonantly at once, and a full spectrum is recorded without the necessity of tuning the IR wavelength. The spectral resolution is governed by the narrowband ($\sim 10 \text{ cm}^{-1}$) visible upconversion field.

6.2.2 Time-resolved Sum Frequency Generation

The principles behind the TR-SFG technique are explained in detail in chapter 1-3. As shown in Equation 6.2, the effective non-linear susceptibility tensor is proportional to the population difference

between the first excited and the ground state: $\chi^{(2)} \sim \Delta n$. In the TR-SFG scheme, a vibrational transition is excited with a resonant IR pump, changing Δn and the subsequent relaxation dynamics (the decay back from the vibrationally excited state $v=1$ to the vibrational ground state $v=0$) can be followed by probing the nonlinear susceptibility after a variable delay time τ using the SFG probe pair. The geometry of the different beams is depicted in figure 6.1, and the energy-level diagram of the technique is shown in the right panel. Due to the pump-induced population transfer from the ground to the excited state, the population difference Δn becomes smaller temporarily, and the SFG signal decreases accordingly. In other words, after the arrival of the pump pulse, a transient decrease of the signal ('bleach') is observed. The population distribution will subsequently evolve back to equilibrium by vibrational relaxation and the original SFG level will be recovered. This technique has been implemented previously in the picosecond regime. [83, 84, 103, 116, 186, 187] Recently this technique has been applied with femtosecond time resolution, so far only to probe adsorbates on metal surfaces [188] and interfacial water. [87, 93]

In conventional time-resolved IR spectroscopy, when different vibrational resonances are present in the steady-state spectrum, the (transient) spectrum can be described by a linear combination of, e.g., Lorentzian line-shapes. For SFG, the coherent nature of the process dictates that the vibrational resonances can interfere with one another. This means that changes in one resonance due to vibrational excitation will affect the spectral shape of other resonances in the proximity. To correctly infer the dynamics from the transient spectra, it is therefore necessary to fit the peaks of each vibration using equation 6.2 to obtain the amplitudes A_n for every mode at each delay time. The time-dependent differential TR-SFG signal for a specific amplitude A'_n is therefore computed in terms of the fitted amplitude $A_n(\tau)$ at pump delay τ and the fitted amplitude A_{n0} of the reference with the pump off

$$A'_n = \frac{A_n(\tau)}{A_{n0}}. \quad (6.3)$$

In our data analysis, we fit the two SFG spectra with pump on and pump off to expressions 6.2 and 6.1 for each delay time, varying only the amplitudes A_n between the spectra. The ratio A'_n then provides a direct measure of the temporal evolution of the vibrational population.

6.3 Experiment

The study of ultrafast surface dynamics with TR-SFG, requires an intense IR pump, an IR probe and narrowband visible field. The pump-induced decrease in the SFG signal is detected by alternating the pump field on/off, and computing the ratio of the SFG signals. The lipid monolayers were prepared using the Langmuir-Blodgett method on a H₂O or D₂O subphase. Details of the laser setup are described in Chapter 2 while the sample preparation methods are presented below.

6.3.1 Sample preparation

The lipids 1,2-Dipalmitoyl-sn-Glycero-3-Phosphocholine (DPPC), 1,2-Dioleoyl-sn-Glycero-3-Phosphocholine (DOPC) and 1,2-dipalmitoyl-3-trimethylammonium-propane (DPTAP) were purchased from Avanti

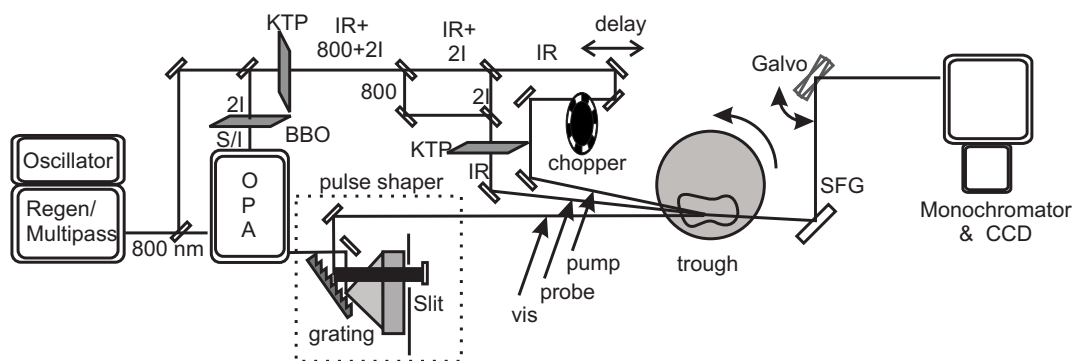


Figure 6.2. Schematic representation of the experimental setup. The output of a 1 kHz amplified femtosecond laser system is used to generate IR pump and probe pulses in a two-step process; narrowband VIS pulses are generated in a pulse shaper with an adjustable slit to select the wavelength. The pump IR beam can be variably delayed using an optical delay line, is mechanically chopped to 500 Hz and all beams are intersected at the interface. The SFG generated at the interface from the IR probe and the VIS beams is dispersed by a monochromator and imaged onto a CCD array. On the CCD, the SFG signal with the pump on is displaced vertically with a galvano mirror from the signal with pump off at 500 Hz

Polar Lipids and were used without further purification. The chemical structures are depicted in figure 6.3. Solutions of the lipids were made in chloroform. The lipid monolayer was spread using a drop cast method in a home-built Teflon trough while monitoring the surface pressure with a Wilhelmy plate tensiometer (Kibron). All measurements were carried out at surface pressures of $\Pi \approx 25$ mN/m, where at room temperature DPPC and DPTAP are in the highly ordered gel phase, but DOPC is in the disordered liquid crystalline phase. Hence, the tails of DPPC and DPTAP are all straight up in a all-trans (zig-zag) configuration, whereas in the case of DOPC, the tails are much more randomly oriented and have gauche defects with cis-trans configurations (see cartoons in figure 6.3). For the subphase, either distilled Millipore filtered H₂O (18 M Ω cm resistivity) of pH 7, or commercially obtained D₂O (Cambridge Isotopes, 99.96% D) was used.

For the temperature dependent measurements of H₂O-DPTAP, the trough was heated or cooled with four Peltier elements from 10° up to 60°. The temperature was measured using a thermocouple. To prevent the formation of bubbles upon heating, the water was degassed prior to the experiment.

To avoid the effect of laser damage of the sample due to repeated laser shots, the trough was rotated to completely refresh the sample every 5 laser shots. New samples were prepared after every three hours of data acquisition, if necessary.

6.4 Results

6.4.1 Static SFG Spectra

In figure 6.3, the steady-state spectra for monolayers of DPPC (a), DOPC (b), both on D₂O and DPTAP on H₂O (c) at room temperature and surface pressures of $\Pi \approx 25$ mN/m are shown as gray lines in the C-H stretch region from 2800-3000 cm⁻¹ (for H₂O-DPTAP up to 3300 cm⁻¹). The

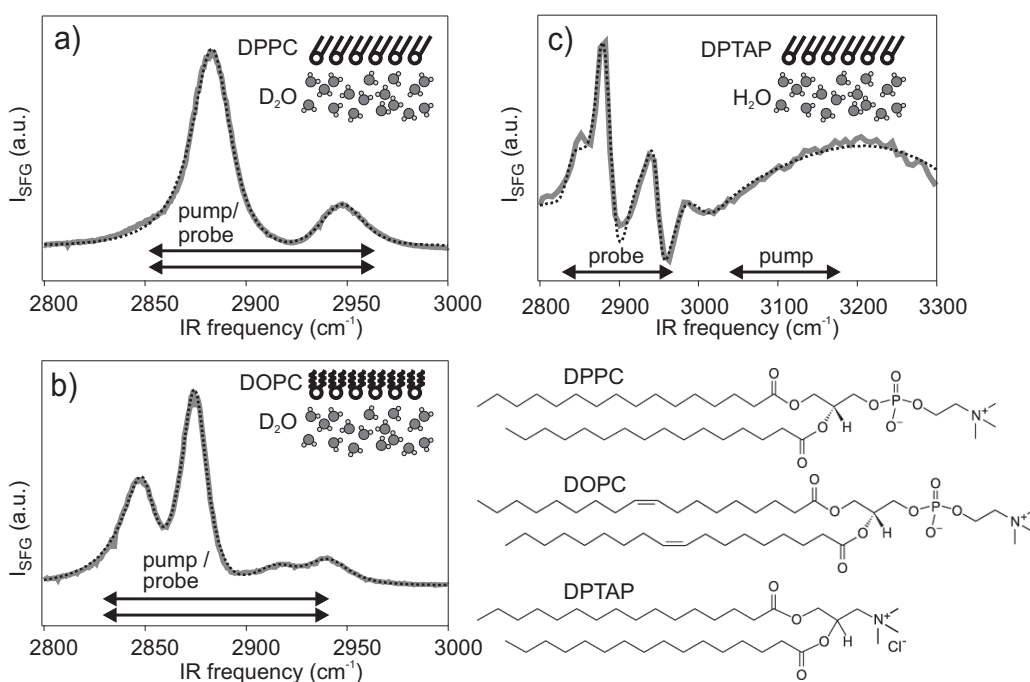


Figure 6.3. The steady-state SFG spectra (solid gray line) are shown for D₂O-DPPC (a), D₂O-DOPC (b) and H₂O-DPTAP (c) at room temperature and surface pressures of $\Pi \sim 25$ mN/m. For DPTAP, additional spectra at 30°C, 40°C and 50°C are shown. The dashed black line is a fit to the experimental data. For the assignment of the peaks, see text. The chemical structures of the lipids are shown for convenience and the phase of the lipids is indicated by the cartoon next to the spectrum.

spectra are not corrected for the Gaussian shaped IR power spectrum. The spectra for DPPC and DOPC are recorded during the time resolved measurements on a D₂O subphase as the average of all the spectra recorded with the pump field off. The DPTAP on H₂O is recorded in a separate setup where the IR wavelength was scanned to include the O-H stretch region of water. The spectrum shows the wing of the water spectrum that interferes with the C-H stretch bands. The assignment of the peaks are well-known from literature. All spectra show the CH₃ vibrations: symmetric stretch ν_{s,CH_3} at 2870 cm⁻¹, Fermi resonance (ν_{FR,CH_3}) at 2940 cm⁻¹ and antisymmetric stretch vibration ν_{as,CH_3} at 2955 cm⁻¹. For DPPC and DPTAP, the CH₂ resonances are almost invisible, due to the high degree of order within the lipid alkyl chain: In the ordered all-trans configuration, the chain has inversion symmetry and, as a result, the CH₂ resonances are SFG inactive. For DPTAP a slight CH₂ (at 2847 cm⁻¹) contribution can be observed due to laser heating of the sample. Since DOPC is in the disordered liquid crystalline phase at room temperature, the alkyl chains have many gauche defects and the CH₂ vibrations are clearly observed: the symmetric CH₂ stretch at 2847 cm⁻¹ (ν_{s,CH_2}), antisymmetric stretch at 2911 cm⁻¹ (ν_{as,CH_2}) and Fermi resonance (ν_{FR,CH_2}) at 2893 cm⁻¹. For the case of DOPC, where the resolution has to be sufficient to distinguish the CH₂ and CH₃ peaks, the VIS pulse shaper is operated in high-resolution mode at the expense of intensity

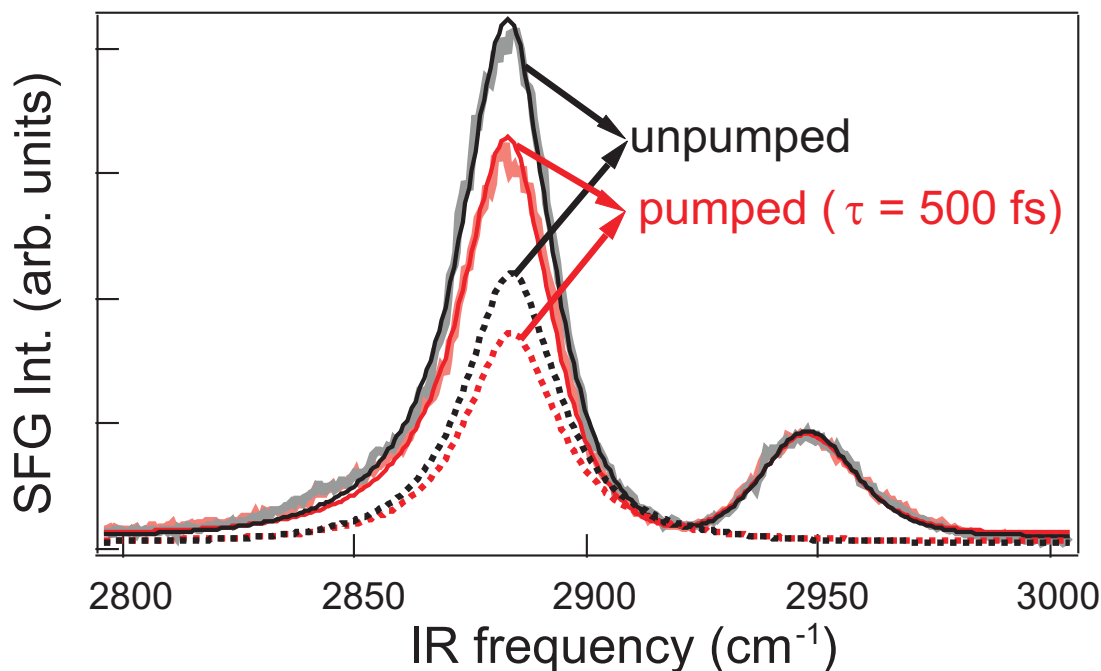


Figure 6.4. Pumped and unpumped SFG spectra at a pump-probe delay of 500 fs for DPPC. The thin solid lines are fits to the experimental data using models as detailed in section 6.2; the dotted lines show the fitted amplitudes of the ν_{s,CH_3} -mode, which are used to determine the vibrational relaxation time for this mode.

and signal-to-noise. The dashed black lines in figure 6.3 are fits of the data using equation 6.2 and the literature values for the resonance frequencies.

The SFG peak around 2950 cm^{-1} contains contributions from both ν_{as,CH_3} and ν_{FR,CH_3} , with a four times larger contribution from the former. In the analysis of the time-resolved spectra, the influence of the much smaller ν_{FR,CH_3} is neglected in this study.

6.4.2 Time Resolved SFG Spectra

For the dynamical studies, the average spectra of $\sim 125,000$ laser pulses, the IR pump being alternately switched on and off, are obtained at typically 40 time points. Next, each of these spectra are fit individually to account for the interference effects as discussed in section 6.2.2 and to obtain the amplitudes A in equation 2 that are proportional to the population differences between different vibrational levels. And finally, the ratio between the amplitudes with the IR pump on/off as a function of time delay are computed for each vibration. Data is collected up to 100 ps to accurately obtain the final signal level.

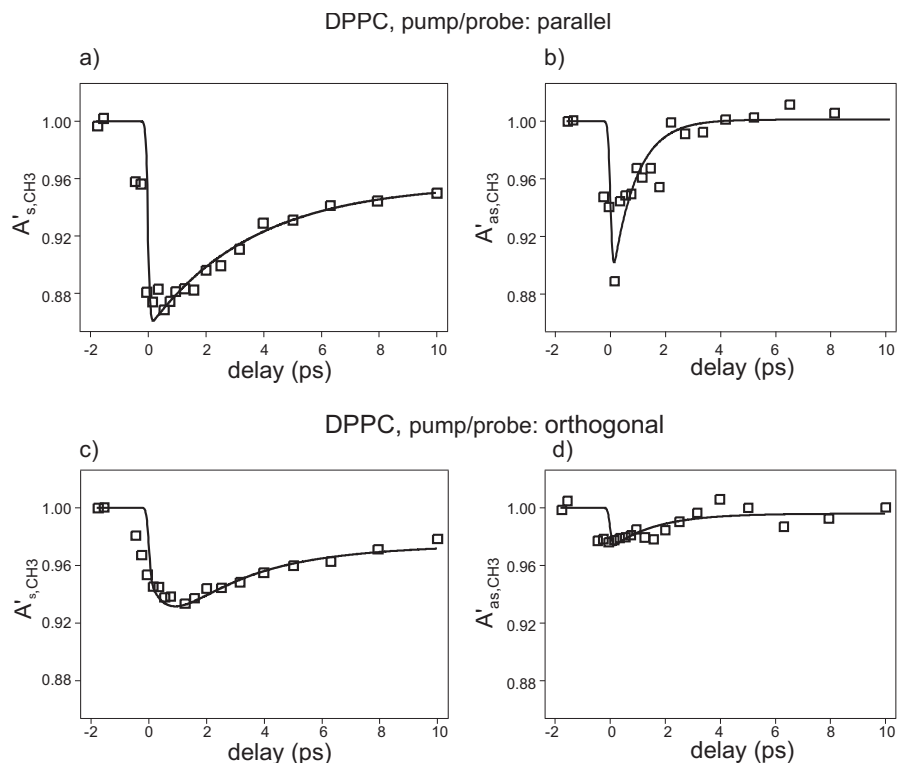


Figure 6.5. Time traces (open squares) are shown for DPPC for the following vibrations and polarization combinations: SSP (pump: P-polarized), ν_{s,CH_3} (a); SSP (pump: P-polarized) ν_{as,CH_3} (b); SSP (pump: S-polarized), ν_{s,CH_3} (c); and SSP (pump: S-polarized), ν_{as,CH_3} (d). The solid lines are fits to the experimental data models as detailed in section 6.5.

6.4.2.1 DPPC

In a first set of experiments, the vibrational relaxation of lipid monolayers was investigated using a one-colour experiment with pump and probe IR wavelength centered at $\sim 2900 \text{ cm}^{-1}$. Owing to the large bandwidth of the IR pulses, all CH_2 and CH_3 vibrations in the lipid alkyl chain are excited simultaneously. The relaxation of the different modes can be followed independently using the amplitudes of the different SFG resonances, as explained in section 6.2.2. A D_2O -subphase was used to avoid the heating of the subphase by the IR pump pulse. Heating by the IR pump pulse is suppressed in D_2O , since the O-D vibrations are far off from the IR pump frequency. The polarizations of the SFG, VIS and probe IR fields were respectively S, S and P.

A typical experimental result is shown in figure 6.4, which reveals a decrease in SFG intensity for all frequencies within the bandwidth (most evident for the symmetric CH_3 stretch around 2880 cm^{-1}). Fits to the data are also shown, with the individual amplitude for the symmetric CH_3 stretch shown as dotted lines. These amplitudes are used to infer the vibrational dynamics for the different modes.

In figure 6.5 the time traces for the inferred amplitudes of the susceptibility for the terminal CH_3 vibration are shown as open squares for ν_{s,CH_3} (a) and ν_{as,CH_3} (b) for the parallel pump and probe

IR fields (P-polarized). For the orthogonal pump and probe IR field (pump: S-polarized), the data for ν_{s,CH_3} is shown in panel (c) and for ν_{as,CH_3} in panel (d).

The main features are the bleach due to excitation to the first vibrational level and recovery of the signal by vibrational relaxation. It is apparent that relaxation occurs significantly quicker for the ν_{as,CH_3} mode than for the ν_{s,CH_3} mode. The relaxation rates will be quantified in the next section. The bleach for the case of parallel polarized pump and probe IR fields is significantly larger than for the orthogonal case: for ν_{s,CH_3} the bleach is respectively $\sim 15\%$ and $\sim 5\%$, and for ν_{as,CH_3} respectively $\sim 10\%$ and $\sim 2\%$. For the symmetric CH_3 stretch vibration, the transition dipole has an angle of 30° with respect to the surface normal which implies that the bleach for the P-polarized pump is indeed expected to be larger than for the S-polarized pump. The overall signal-to-noise ratio is better for the symmetric vibration than for the asymmetric, because the SFG intensity is much larger.

In most of the time traces, in particular panel (a) and (c) of figure 6.5, a decrease of the SFG signal is observed before the pump arrival. This can be explained by the perturbed Free Induction Decay: [200] the probe IR field induces a coherent polarization that decays with the decoherence time constant T_2 . As long as this coherent polarization exists and the visible pulse is present, an SFG signal will be generated. At small negative delay, the pump pulse arrives at the sample after the probe pulse has interacted with the sample, but before the coherent polarization has completely decayed. As a result, the pump can change the signal already at negative delay. This process only affects the data before time $t = 0$ fs, does not affect our conclusions and is not included in the analysis of the data.

Surprisingly, for orthogonal polarizations of pump and probe, the signal is not only smaller (panel (c) of figure 6.5), but there is clearly a second, much slower, contribution to the bleach of (ν_{s,CH_3}). This process cannot be attributed to a bleach due to laser excitation, because the FWHM pulse duration of the IR field is < 120 fs. Since the slow component cannot be attributed to direct laser excitation of ν_{s,CH_3} , this process must be caused by energy transfer from a different mode.

Because this component is only observed in the data with the pump IR field S-polarized, the energy transfer is most likely from the CH_2 vibrations whose transition dipole moments are parallel to the interface. The pump field excites the in-plane CH_2 vibrations more efficiently when the pump field is polarized parallel to the surface (i.e. S-polarized). The observed line-shape effects on the CH_3 group is due to the excitation of the CH_2 . There can be two ways by which $CH_2 \rightarrow CH_3$ energy transfer happens. (i) In a coherent process, vibrational excitation transfer occurs directly from the CH_2 - to the CH_3 -groups. (ii) The CH_2 - CH_3 energy coupling can be attributed to incoherent processes: the excitation energy on the CH_2 -groups is transferred to the surrounding low frequency bath modes that are, in turn, anharmonically coupled to the CH_3 group, thereby exciting the CH_3 modes. It will be shown below that we have strong indications that the latter, incoherent process is responsible for the delayed signal in-growth.

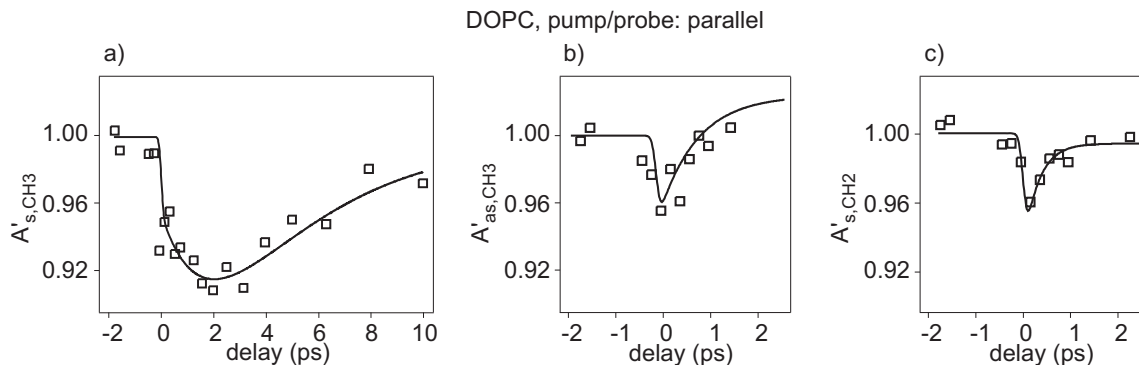


Figure 6.6. Time traces (open squares) are shown for DOPC for the parallel SSP (pump: P-polarized) polarization combination for ν_{s,CH_3} , ν_{as,CH_3} and ν_{s,CH_2} . DOPC is in the liquid crystalline phase at room temperature. The solid lines are fits to the experimental data.

6.4.2.2 DOPC

To investigate whether the lipid vibrational dynamics are dependent on the lipid phase, i.e. the molecular conformation of the lipid, we also investigated the molecularly disordered DOPC lipid monolayer. The DOPC SFG spectrum (figure 6.3b) shows CH_2 vibrations in addition to the CH_3 resonances, due to the presence of gauche defects in the alkyl chain that break the symmetry. This is due to the gel-to-liquid crystalline phase transition point of DOPC being well below room temperature (see cartoons next to the spectra in figure 6.3).

The results are shown in figure 6.6. Due to the disorder in the liquid expanded phase, both the SFG intensity and the bleach are much lower than those observed for DPPC. Furthermore, to disentangle all peaks the VIS bandwidth is reduced at the cost of intensity. In figure 6.6 the time traces are shown (open squares) for ν_{s,CH_3} (a), ν_{as,CH_3} (b) and ν_{s,CH_2} (c) for the parallel pump and probe polarizations.

Although the energy transfer process from CH_2 - to CH_3 -groups was observed in DPPC only for the perpendicular pump and probe polarizations, in the case of DOPC this process is clearly present for parallel polarizations as well. The reason is that in the case of DPPC the transition dipole moments of the CH_2 groups are largely restricted to the horizontal plane and cannot be excited efficiently with P-polarized pump field. In the liquid expanded phase of DOPC, many CH_2 groups have a component in the vertical plane and can be excited with the P-polarized pump field.

It is evident from figure 6.6 that the dynamics are remarkably similar for the two different lipids in different phases. A qualitative comparison with the results for DPPC (figure 6.5) reveals fast relaxation of the ν_{as,CH_3} mode and slower relaxation for the ν_{s,CH_3} mode in both cases. The ν_{s,CH_2} symmetric CH_2 stretching mode also exhibits very fast decay.

6.4.2.3 Heat transfer across the monolayer

The incoherent energy transfer or heat transfer from bulk water phase across the lipid monolayer was investigated by exciting the water near the interface and monitoring the terminal CH_3 signal

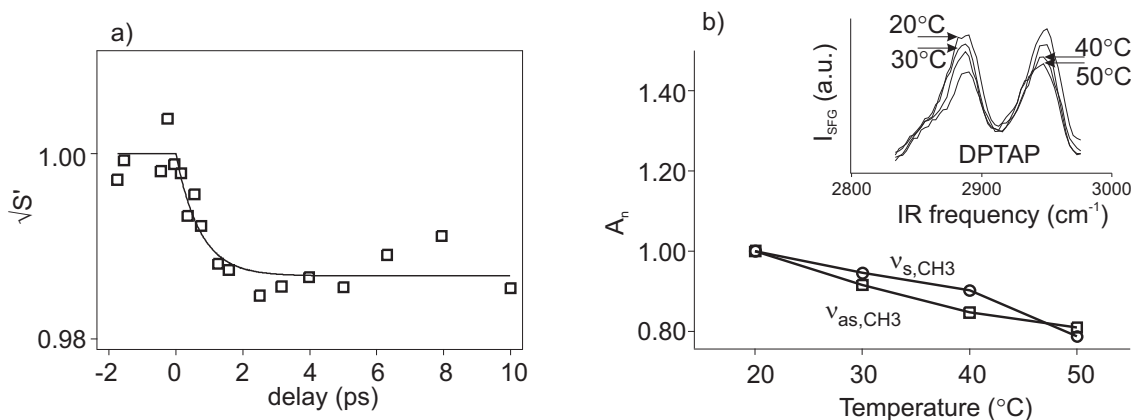


Figure 6.7. The time trace (open squares) is shown for heat transfer from water to DPTAP with the SSP (P-polarized pump) polarization combination (a). The contribution from CH₃ symmetric and the combination band of the antisymmetric stretch and Fermi resonance are summed together. The solid line is a fit to the experimental data. Data points between 10–100 ps (not shown) reveal that the signal remains at the value indicated by the fit at long delay times. In panel (b) the temperature dependent amplitudes of ν_{s,CH_3} and ν_{as,CH_3} are shown from 20 to 50°C, obtained from temperature dependent DPTAP SFG spectra, as shown in the inset.

of DPTAP. For reference purposes, the influence of a change in temperature on the C-H region of the lipid spectrum was studied under steady-state conditions as shown in the inset in figure 6.7b. For the temperature interval from 20°C to 50°C, a small decrease in the overall signal is observed. Because the IR wavelength is centered further to the blue side, the spectral shape is slightly different from 6.3c.

For the time-resolved studies, a two-color scheme was employed with the IR pump wavelength at the wing of the O-H-stretch region at $\sim 3100 \text{ cm}^{-1}$ and the IR probe centered at the C-H-stretch region at $\sim 2900 \text{ cm}^{-1}$. Since the effect on the signal intensity of the CH₃ vibrations due to a temperature change is very limited, the SFG spectrum over the entire C-H stretch region (symmetric, asymmetric and Fermi-resonance) was integrated to obtain an acceptable signal-to-noise ratio. The time trace for the heat transfer process is shown in figure 6.7 as open squares. The change in the steady-state amplitudes due to a change in temperature is shown in figure 6.7b) and was computed from the temperature-dependent spectra as shown in the inset. From the dynamical studies, a decrease of the signal level of $\sim 1.5 \%$ is found, corresponding to a change in temperature of ~ 2 degrees. To rule out any energy transfer process that does not originate from pumping the surface water molecules, the experiment was repeated with D₂O instead of H₂O. In this case, no dynamics were observed (data not shown), showing that the dynamics originate only from excitation of the water molecules, from which heat is transferred into the lipids on sub-picosecond timescales.

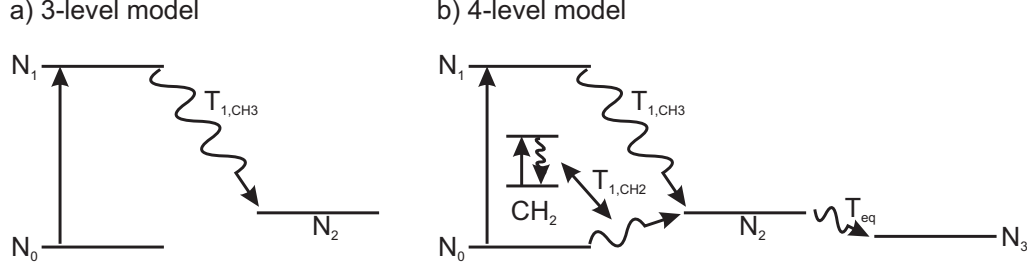


Figure 6.8. To describe and quantify the vibrational relaxation in lipids, 3-level (a) and 4-level (b) models are employed. In the 3-level model, after excitation the system relaxes directly to a final “hot” ground state. In the 4-level model, both CH₃ and CH₂ vibrations are excited: the relaxation of the CH₃ decays to an intermediate state and the relaxation of the CH₂ results in an energy transfer from the ground state to the intermediate state. Finally, the system equilibrates to a “hot” ground state.

6.4.3 Data Analysis

To quantify the time scales of the vibrational relaxation and energy transfer processes from the data, we calculate the population distribution in the ground and excited states. The experimental data can be modeled according to this model and time scales can be extracted.

The simplest model to describe the features of the vibrational relaxation as observed in figure 6.5a and 6.5b for the SSP (P-polarized pump) polarization combination, is a three level model as shown figure 6.8a. Besides the ground state N_0 and the excited state N_1 , a hot ground state N_2 is necessary to account for the slight offset of the final SFG level at long delay times. The physical meaning of the hot ground state N_2 is that after vibrational relaxation, the temperature has increased locally. The hot ground state is populated by vibrational relaxation at a rate T_1 . The differential equations that describe the time-dependent population distribution read:

$$\begin{aligned}
 \frac{dN_0}{dt} &= -\sigma G(t)(N_0 - N_1) \\
 \frac{dN_1}{dt} &= \sigma G(t)(N_0 - N_1) - \frac{N_1}{T_1} \\
 \frac{dN_2}{dt} &= \frac{N_1}{T_1}
 \end{aligned} \tag{6.4}$$

Here, σ is a measure of the IR cross section, which determines the efficiency of the population transfer and $G(t)$ describes the Gaussian pulse profile of the excitation (pump) pulse. The generated SFG signal from state N_0 and N_2 is then proportional to

$$I_{SFG} \propto (N_0 - N_1 + cN_2)^2 \tag{6.5}$$

where c accounts for a smaller/larger SFG signal from state N_2 than from the ground state N_0 , caused by the heating. To fit the amplitudes for a specific vibration the square root of equation 6.5

is used.

It is apparent that the three level model cannot account for the observations of ν_{s,CH_3} in panel c) of figure 6.5 for the orthogonal pump and probe polarization, as it cannot account for the delayed ingrowth of the signal. Clearly, a second process in addition to direct vibrational excitation results in a decrease of the SFG intensity. Given its strong dependence on the pump polarization, it is evident that this process must be attributed to excitation of CH_2 modes in the lipid chain. The fact that the additional ingrowth of the signal occurs on precisely the same ~ 1 ps timescale on which the CH_2 modes decay (see Fig. 6.6c) demonstrates that this energy transfer from CH_2 to CH_3 modes must be due to incoherent energy transfer, i.e. heating of the CH_3 groups due to relaxation of the CH_2 groups. The complete process can thus be modeled with the 4-level energy diagram of figure 6.8b: the pump field excites the ν_{s,CH_3} by inducing population transfer from the ground state N_0 to the excited N_1 of this mode. At the same time the ν_{s,CH_2} is excited to its first vibrational level. The sub-picosecond relaxation of the CH_2 groups (figure 6.6 c) results in the lipid heating up considerably, bringing the lipid and its CH_3 groups to a hot, intermediate state N_2 . Relaxation of CH_3 groups themselves will also lead to a population of this state. Thermal equilibration with the water bath - i.e. heat flow out of the monolayer into the water subsystem - is reflected in the model by a transition from N_2 to the final new ground state (at elevated temperature) N_3 at a rate $1/T_{eq}$. The corresponding differential equations read:

$$\begin{aligned}
\frac{dN_0^{CH_2}}{dt} &= -\sigma_{CH_2} G(t)(N_0^{CH_2} - N_1^{CH_2}) \\
\frac{dN_1^{CH_2}}{dt} &= \sigma_{CH_2} G(t)(N_0^{CH_2} - N_1^{CH_2}) - \frac{N_1^{CH_2}}{T_{1,CH_2}} \\
\frac{dN_0}{dt} &= -\sigma_{CH_3} G(t)(N_0 - N_1) \\
\frac{dN_1}{dt} &= \sigma_{CH_3} G(t)(N_0 - N_1) - \frac{N_1}{T_{1,CH_3}} \\
\frac{dN_2}{dt} &= \frac{N_1}{T_{1,CH_3}} + \Delta \frac{N_1^{CH_2}}{T_{1,CH_2}} - \frac{N_2}{T_{eq}} \\
\frac{dN_3}{dt} &= \frac{N_2}{T_{eq}}
\end{aligned} \tag{6.6}$$

Here, σ_{CH_3} and σ_{CH_2} are IR cross sections determining of the population transfers to respectively ν_{s,CH_3} and ν_{s,CH_2} , and Δ is a measure for the strength of the effect of the relaxed CH_2 mode on the CH_3 mode. The signal is then given by

$$I_{SFG} \propto (N_0 - N_1 + cN_2 + c'N_3)^2 \tag{6.7}$$

where c and c' account for the SFG signal strengths from the intermediate and final level.

Finally, for the model to describe the heat transfer from the water to the lipids (experiments shown in figure 6.7), we assume a single exponential process. We have previously established that vibrational relaxation of water molecules at low O-H stretch frequencies occurs very quickly (sub-

50 fs) [94], so that heat is deposited quasi-instantaneously at the lipid interface. Its flow into the lipid layer is assumed to follow simple exponential behavior. Hence, due to the heating from initial temperature T_0 to final temperature T_f , the nonlinear susceptibility $\chi(t)$ evolves in time from $\chi(T_0)$ to $\chi(T_f)$ at an exponential rate $1/T_t$ as (see figure 6.8)

$$\chi(t) \propto (\chi(T_0) - \chi(T_f)) \exp(-t/T_t) + \chi(T_f), \quad (6.8)$$

with the SFG signal proportional to $\chi(t)^2$.

The data for DPPC in figure 6.5a, 6.5b and 6.5d is fitted using the 3-level model as CH_2 excitation is minimal for the P-polarized pump pulse. The time constant for the vibrational relaxation of ν_{s,CH_3} in the parallel pump and probe polarization is found to be $T_1 = 3.6 \pm 0.5$ ps. For ν_{as,CH_3} the time constant is fitted globally for the parallel and orthogonal pump/probe data and is found to be $T_1 = 1.0 \pm 0.3$ ps. The data for DOPC in figure 6.6b and 6.6c is also fitted with the 3-level model and yields time constants of $T_1 = 0.8 \pm 0.3$ ps for the ν_{as,CH_3} and $T_1 = 0.8 \pm 0.3$ ps for the ν_{s,CH_2} . The heat transfer rate for the H_2O -DPTAP system is modeled with equation 6.8 and yields a time constant of $T_t = 0.95 \pm 0.4$ ps. Finally, the ν_{s,CH_3} data with CH_2 energy transfer for DPPC (figure 6.5c) and DOPC (figure 6.6a) are both reproduced with the 4-level model. All time constants are fixed, as they have been determined independently in the other measurements, *i.e.* $T_{1,\text{CH}_3} = 3.6$ ps, $T_{1,\text{CH}_2} = 0.8$ ps and $T_{eq} = 0.95$ ps. For T_{eq} , it is assumed that the energy transfer from the lipid to the subphase (*i.e.* the equilibration process) occurs at the same rate at which the transfer from the subphase to the lipid occurs.

6.5 Discussion

The vibrational relaxation of the C-H stretching mode has been investigated in numerous studies in bulk liquids. [201, 202] It has been shown that the pathway of relaxation of all C-H stretching vibrations occurs via the same intermediate level and therefore the different vibrations show similar dynamics. [201] The vibrational lifetime $\tau = 3.6$ ps for ν_{s,CH_3} in the terminal methyl groups of DPPC and DOPC is comparable to the bulk values. It is also similar to the ν_{s,CH_3} lifetime of acetonitrile at the acetonitrile-air interface and the ν_{s,CH_3} lifetime within a Cd stearate monolayer on silver. [116, 203] The lifetime $\tau = 1.2$ ps for the asymmetric ν_{as,CH_3} is significantly faster than the observed lifetimes of ν_{s,CH_3} , indicating that unlike in bulk liquid, the vibrational pathway is distinctly different for the two modes.

The much faster relaxation of ν_{as,CH_3} can be explained by strong coupling of the ν_{as,CH_3} to the CH_2 vibration. For these two modes, the transition dipoles lie in the same plane, and dipole-dipole coupling is expected to play an important role. The CH_2 vibrations are highly delocalized in the all-trans chains, which may account for the faster relaxation than in bulk where the chains have more random conformations, and the CH_2 vibrations are expected to be localized. Another possible effect that may play a role in the apparent fast relaxation is the rotational motion of the terminal methyl group around the C-C bond. [204–206] This reorientation does not affect the ν_{s,CH_3} , since

its transition moment is parallel to the axis of rotation. For the in-plane ν_{as,CH_3} vibration, the rotational motion leads to dephasing of the ν_{as,CH_3} vibration on the timescale of $T_2=0.8$ ps. [205] It is clear that the relatively high degree of order within the lipid alkyl chain - even for the crystalline liquid DOPC - facilitates vibrational relaxation and energy transfer.

Energy transfer across membranes and cooling has been studied previously in reverse micelles. [178, 207] It has been shown, using micelles of different sizes, that the cooling within the interior water, can be well described using classical thermodynamics. [207] The energy transfer across a surfactant layer can actually follow different pathways. [178] The timescale of $\tau = 0.95$ ps obtained here, is in good agreement with the value found for the energy transfer from the interior water to the polar headgroup of the surfactant in the reverse micelles. [178]

To summarize, the energy flow in model lipid membranes after vibrational excitation can be described with three time constants. The ν_{s,CH_3} relaxes with a time constant of $T=3.6$ ps, comparable to findings in bulk studies. Unlike in bulk, in lipid membranes with the chains an all-trans conformation, the ν_{as,CH_3} is strongly coupled to the CH_2 vibration and shows a much faster relaxation time of $T=0.8$ ps. The fast relaxation of CH_2 mode is tentatively attributed to delocalization of CH_2 modes. In principle, one would expect the CH_2 relaxation to slow down for the DOPC monolayer, due to the presence of gauche defects in the alkyl chain that will reduce the delocalization of the CH_2 vibrations. Apparently, the number of gauche defects is insufficient to reduce the vibrational relaxation rates. Finally, the energy transfer between the subphase and lipid membranes or equivalently the equilibration to a “hot” ground state takes place on a timescale of $T_{eq}=0.95$ ps.

6.6 Conclusions and Outlook

We have reported the dynamics of energy flow in a biomimetic lipid monolayer using surface-specific, femtosecond time-resolved vibrational spectroscopy. We find that relaxation of C-H stretching modes occur on very short timescales, with marked variations for different modes, in contrast to observations for bulk alkanes. The technique also allows us to elucidate energy transfer times across the lipid monolayer, providing insights into the dynamics of water-membrane interactions. The successful application of this technique to the study of model membranes, as presented here, paves the way for a novel class of experiments to study biomolecular dynamics in membrane systems, including the dynamics of conformational fluctuations and transformations of specifically membrane proteins.

Bibliography

- [1] IKEDA, S., J. HAYAKAWA, Y. ASHIZAWA, Y. M. LEE, K. MIURA, H. HASEGAWA, M. TSUNODA, F. MATSUKURA, and H. OHNO (2008) "Tunnel magnetoresistance of 604% at 300 K by suppression of Ta diffusion in CoFeB/MgO/CoFeB pseudo-spin-valves annealed at high temperature," *APPLIED PHYSICS LETTERS*, **93**(8).
- [2] SIGLE, W. (2005) "Analytical transmission electron microscopy," *Ann. Rev. Mater. Res.*, **35**, pp. 239–314.
- [3] PETFORD-LONG, A. K. and A. N. CHIARAMONTI (2008) "Transmission Electron Microscopy of Multilayer Thin Films," *Ann. Rev. Mater. Res.*, **38**(1).
- [4] CHESTERS, M. A. and G. A. SOMORJAI (1975) "The Structure of Surfaces," *Ann. Rev. Mater. Sci.*, **5**(1), pp. 99–113.
- [5] JONA, F. (1978) "LEED Crystallography," *J. Phys. C-Solid State Phys.*, **11**(21), pp. 4271–4306.
- [6] GIANCARLO, L. C. and G. W. FLYNN (1998) "Scanning tunneling and atomic force microscopy probes of self-assembled, physisorbed monolayers: Peeking at the peaks," *Ann. Rev. Phys. Chem.*, **49**, p. 297.
- [7] CYR, D. M., B. VENKATARAMAN, and G. W. FLYNN (1996) "STM investigations of organic molecules physisorbed at the liquid-solid interface," *Chem. Mater.*, **8**(8), pp. 1600–1615.
- [8] HAMERS, R. J. (1989) "Atomic-Resolution Surface Spectroscopy with the Scanning Tunneling Microscope," *Ann. Rev. Phys. Chem.*, **40**(1), pp. 531–559.
- [9] HANSMA, H. G. (2001) "Surface biology of DNA by atomic force microscopy," *Ann. Rev. Phys. Chem.*, **52**, pp. 71–92, surface biology of DNA by atomic force microscopy.
- [10] THOMAS, R. K. (2004) "Neutron Reflection from Liquid Interfaces," *Ann. Rev. Phys. Chem.*, **55**(1), pp. 391–426.
- [11] TROUW, F. R. and D. L. PRICE (1999) "Chemical Applications of Neutron Scattering," *Ann. Rev. Phys. Chem.*, **50**(1), pp. 571–601.
- [12] SCHLOSSMAN, M. L. and A. M. TIKHONOV (2008) "Molecular Ordering and Phase Behavior of Surfactants at Water-Oil Interfaces as Probed by X-Ray Surface Scattering," *Ann. Rev. Phys. Chem.*, **59**(1), pp. 153–177.

- [13] PETRACHE, H., N. GOULIAEV, S. TRISTRAM-NAGLE, R. ZHANG, R. SUTER, and J. NAGLE (1998) "Interbilayer interactions from high-resolution x-ray scattering," *Phys. Rev. E - Statistical Physics, Plasmas, Fluids, and Related Interdisciplinary Topics*, **57**(6), pp. 7014–7024.
- [14] JUNGWIRTH, P. and D. TOBIAS (2001) "Molecular structure of salt solutions: A new view of the interface with implications for heterogeneous atmospheric chemistry," *J. Phys. Chem. B*, **105**(43), pp. 10468–10472.
- [15] BOERO, M., M. PARRINELLO, and K. TERAKURA (1999) "Ziegler-Natta heterogeneous catalysis by first principles computer experiments," *Surf. Sci.*, **438**(1-3), pp. 1–8.
- [16] LIU, H. and A. CHAKRABARTI (1999) "Molecular dynamics study of adsorption and spreading of a polymer chain onto a flat surface," *Polymer*, **40**(26), pp. 7285–7293.
- [17] TANIZAKI, S. and M. FEIG (2005) "A generalized Born formalism for heterogeneous dielectric environments: Application to the implicit modeling of biological membranes," *J. Chem. Phys.*, **122**(12).
- [18] POHORILLE, A. and M. WILSON (1995) "Molecular-dynamics studies of simple membrane water interfaces - structure and functions in the beginnings of cellular life," *Orig. Life And Evol. Bios.*, **25**(1-3), pp. 21–46.
- [19] BENJAMIN, I. (1997) "Molecular structure and dynamics at liquid-liquid interfaces," *Ann. Rev. Phys. Chem.*, **48**, pp. 407–451.
- [20] BERKOWITZ, M. L., D. L. BOSTICK, and S. PANDIT (2006) "Aqueous Solutions next to Phospholipid Membrane Surfaces: Insights from Simulations," *Chem. Rev.*, **106**(4), pp. 1527–1539.
- [21] MCGURK, S. L., R. J. GREEN, G. H. W. SANDERS, M. C. DAVIES, C. J. ROBERTS, S. J. B. TENDLER, and P. M. WILLIAMS (1999) "Molecular interactions of biomolecules with surface-engineered interfaces using atomic force microscopy and surface plasmon resonance," *Langmuir*, **15**(15), pp. 5136–5140.
- [22] WILLETS, K. A. and R. P. VAN DUYN (2007) "Localized surface plasmon resonance spectroscopy and sensing," *Ann. Rev. Phys. Chem.*, **58**, pp. 267–297.
- [23] TRENARY, M. (2000) "Reflection Absorption Infrared Spectroscopy And The Structure Of Molecular Adsorbates On Metal Surfaces," *Ann. Rev. Phys. Chem.*, **51**(1), pp. 381–403.
- [24] ITOH, K. and H. OGURI (2006) "Structures of palmitoyl-L and DL-lysine monolayers at the air-water interface Polarization modulation infrared reflection absorption spectroscopic study," *Langmuir*, **22**(22), pp. 9208–9213.
- [25] ESTRELA-LOPIS, I., G. BREZESINSKI, and H. MOHWALD (2001) "Dipalmitoyl-phosphatidylcholine/phospholipase D interactions investigated with polarization-modulated infrared reflection absorption spectroscopy," *Biophys. J.*, **80**(2), pp. 749–754.
- [26] SHEN, Y. R. (1989) "Surface-properties probed by second harmonic and sum-frequency generation," *Nature*, **337**(6207), pp. 519–525.
- [27] ——— (1989) "Optical Second Harmonic Generation at Interfaces," *Ann. Rev. Phys. Chem.*, **40**(1), pp. 327–350.
- [28] HEINZ, T. F. and G. A. REIDER (1989) "Surface studies with optical second-harmonic generation," *Trends Anal. Chem.*, **8**(6), pp. 235–242.

- [29] EISENTHAL, K. B. (1992) "Equilibrium and dynamic processes at interfaces by second harmonic and sum frequency generation," *Ann. Rev. Phys. Chem.*, **43**, pp. 627–661.
- [30] ——— (1996) "Liquid interfaces probed by second-harmonic and sum-frequency spectroscopy," *Chem. Rev.*, **96**(4), pp. 1343–1360.
- [31] MILHAUD, J. (2004) "New insights into water-phospholipid model membrane interactions," *Biochim. Biophys. Acta - Biomembranes*, **1663**(1-2), pp. 19–51.
- [32] BURSING, H., S. KUNDU, and P. VOHRINGER (2003) "Solvation dynamics at aqueous lipid-membrane interfaces explored by temperature-dependent 3-pulse-echo peak shifts: Influence of the lipid polymorphism," *J. Phys. Chem. B*, **107**(10), pp. 2404–2414.
- [33] JENDRASIAK, G. L. and R. L. SMITH (2000) *Cell. Mol. Biol. Lett.*, **5**, pp. 35–49.
- [34] POOLMAN, B., J. J. SPITZER, and J. A. WOOD (2004) "Bacterial osmosensing: roles of membrane structure and electrostatics in lipid-protein and protein-protein interactions," *Biochim. Biophys. Acta - Biomembranes*, **1666**(1-2), pp. 88–104.
- [35] ZHOU, Z., B. G. SAYER, D. W. HUGHES, R. E. STARK, and R. M. EPAND (1999) "Studies of phospholipid hydration by high-resolution magic-angle spinning nuclear magnetic resonance," *Biophys. J.*, **76**(1), pp. 387–399.
- [36] KURZE, V., B. STEINBAUER, T. HUBER, and K. BEYER (2000) "A H-2 NMR study of macroscopically aligned bilayer membranes containing interfacial hydroxyl residues," *Biophys. J.*, **78**(5), pp. 2441–2451.
- [37] GAWRISCH, K., H. C. GAEDE, M. MIHAILESCU, and S. H. WHITE (2007) "Hydration of POPC bilayers studied by H-1-PFG-MAS-NOESY and neutron diffraction," *Eur. Biophys. J. Biophys. Lett.*, **36**(4-5), pp. 281–291.
- [38] FREITES, J. A., D. J. TOBIAS, G. VON HEIJNE, and S. H. WHITE (2005) "Interface connections of a transmembrane voltage sensor," *Proc. Natl. Acad. Sci USA*, **102**(42), pp. 15059–15064.
- [39] SANDS, Z. A. and M. S. P. SANSOM (2007) "How does a voltage sensor interact with a lipid bilayer? Simulations of a potassium channel domain," *Structure*, **15**(2), pp. 235–244.
- [40] LU, W., J. KIM, W. QIU, and D. ZHONG (2004) "Femtosecond studies of tryptophan solvation: correlation function and water dynamics at lipid surfaces," *Chem. Phys. Lett.*, **388**(1-3), pp. 120–126.
- [41] BACIA, K., S. KIM, and P. SCHWILLE (2006) "Fluorescence cross-correlation spectroscopy in living cells," *Nature Methods*, **3**(2), pp. 83–89.
- [42] BORBAT, P., A. COSTA-FILHO, K. EARLE, J. MOSCICKI, and J. FREED (2001) "Electron spin resonance in studies of membranes and proteins," *Science*, **291**(5502), pp. 266–269.
- [43] MARSH, D. and L. HORVATH (1998) "Structure, dynamics and composition of the lipid-protein interface. Perspectives from spin-labelling," *Biochim. Biophys. Acta - Reviews on Biomembranes*, **1376**(3), pp. 267–296.
- [44] MCCARNEY, E. R., B. D. ARMSTRONG, R. KAUSIK, and S. HAN (2008) "Dynamic nuclear polarization enhanced nuclear magnetic resonance and electron spin resonance studies of hydration and local water dynamics in micelle and vesicle assemblies," *Langmuir*, **24**(18), pp. 10062–10072.

- [45] NEVZOROV, A. and M. BROWN (1997) “Dynamics of lipid bilayers from comparative analysis of H-2 and C-13 nuclear magnetic resonance relaxation data as a function of frequency and temperature,” *J. Chem. Phys.*, **107**(23), pp. 10288–10310.
- [46] MCCONNELL, H. and A. RADHAKRISHNAN (2006) “Theory of the deuterium NMR of sterol-phospholipid membranes,” *Proc. Natl. Acad. Sci. USA*, **103**(5), pp. 1184–1189.
- [47] HOLLAND, G. P. and T. M. ALAM (2008) “Unique backbone-water interaction detected in sphingomyelin bilayers with H-1/P-31 and H-1/C-13 HETCOR MAS NMR spectroscopy,” *Biophys. J.*, **95**(3), pp. 1189–1198.
- [48] RHEINSTADTER, M., C. OLLINGER, G. FRAGNETO, F. DEMMEL, and T. SALDITT (2004) “Collective dynamics of lipid membranes studied by inelastic neutron scattering,” *Phys. Rev. Lett.*, **93**(10).
- [49] RHEINSTADTER, M. C., T. SEYDEL, and T. SALDITT (2007) “Nanosecond molecular relaxations in lipid bilayers studied by high energy-resolution neutron scattering and in situ diffraction,” *Phys. Rev. E*, **75**(1, Part 1).
- [50] TRISTRAM-NAGLE, S. and J. NAGLE (2004) “Lipid bilayers: thermodynamics, structure, fluctuations, and interactions,” *Chem. Phys. Lipids*, **127**(1), pp. 3–14.
- [51] SALDITT, T., C. LI, and A. SPAAR (2006) “Structure of antimicrobial peptides and lipid membranes probed by interface-sensitive X-ray scattering,” *Biochim. Biophys. Acta - Biomembranes*, **1758**(9), pp. 1483–1498.
- [52] HRISTOVA, K. and S. WHITE (1998) “Determination of the hydrocarbon core structure of fluid dioleoylphosphocholine (DOPC) bilayers by x-ray diffraction using specific bromination of the double-bonds: Effect of hydration,” *Biophys. J.*, **74**(5), pp. 2419–2433.
- [53] GORDON, L., P. MOBLEY, R. PILPA, M. SHERMAN, and A. WARING (2002) “Conformational mapping of the N-terminal peptide of HIV-1 gp41 in membrane environments using C-13-enhanced Fourier transform infrared spectroscopy,” *Biochim. Biophys. Acta - Biomembranes*, **1559**(2), pp. 96–120.
- [54] MUKHERJEE, P., I. KASS, I. ARKIN, and M. ZANNI (2006) “Picosecond dynamics of a membrane protein revealed by 2D IR,” *Proc. Natl. Acad. of Sci. USA*, **103**(10), pp. 3528–3533.
- [55] SEANTIER, B., M.-C. GIOCONDI, C. LE GRIMELLE, and P.-E. MILHIET (2008) “Probing supported model and native membranes using AFM,” *Curr. Opin. Coll. Interface Sci.*, **13**(5), pp. 326–337.
- [56] BOYD, R. W. (2003) *Nonlinear Optics, Second Edition*, Academic Press, Elsevier.
- [57] SHEN, Y. R. (1984) *The Principles of Nonlinear Optics*, John Wiley & Sons, Inc.
- [58] LAMBERT, A. G. (2001) *Sum Frequency Spectroscopy of Adsorption on Hydrophilic Mica Substrates*, Ph.D. thesis.
- [59] EKSPALA, “Picosecond SFG Spectrometer,” [http://www.ingcrys.com/Website PDF files/SFG.pdf](http://www.ingcrys.com/Website%20PDF%20files/SFG.pdf).
- [60] CONBOY, J. C., M. C. MESSMER, and G. L. RICHMOND (1996) “Investigation of surfactant conformation and order at the liquid-liquid interface by total internal reflection sum-frequency vibrational spectroscopy,” *J. Phys. Chem.*, **100**(18), pp. 7617–7622.

- [61] RICHMOND, G. L. (2001) "Structure and bonding of molecules at aqueous surfaces," *Ann. Rev. Phys. Chem.*, **52**, pp. 357–389.
- [62] DU, Q., R. SUPERFINE, E. FREYSZ, and Y. R. SHEN (1993) "Vibrational Spectroscopy of Water at the Vapor Water Interface," *Phys. Rev. Lett.*, **70**(15), pp. 2313–2316.
- [63] SCATENA, L. F., M. G. BROWN, and G. L. RICHMOND (2001) "Water at hydrophobic surfaces: Weak hydrogen bonding and strong orientation effects," *Science*, **292**(5518), pp. 908–912.
- [64] WATRY, M. R., T. L. TARBUCK, and G. L. RICHMOND (2003) "Vibrational sum-frequency studies of a series of phospholipid monolayers and the associated water structure at the vapor/water interface," *J. Phys. Chem. B*, **107**(2), pp. 512–518.
- [65] BONN, M., C. HESS, and M. WOLF (2001) "The dynamics of vibrational excitations on surfaces: CO on Ru(001)," *J. Chem. Phys.*, **115**(16), pp. 7725–7735.
- [66] GRAGSON, D. E., B. M. MCCARTY, and G. L. RICHMOND (1996) "Surfactant/water interactions at the air/water interface probed by vibrational sum frequency generation," *J. Phys. Chem.*, **100**(34), pp. 14272–14275, 0022-3654.
- [67] WALKER, R. A., D. E. GRAGSON, and G. L. RICHMOND (1999) "Induced changes in solvent structure by phospholipid monolayer formation at a liquid-liquid interface," *Coll. Surf. A-Physicochemical And Engineering Aspects*, **154**(1-2), pp. 175–185.
- [68] BROWN, M. G., D. S. WALKER, E. A. RAYMOND, and G. L. RICHMOND (2003) "Vibrational sum-frequency spectroscopy of alkane/water interfaces: Experiment and theoretical simulation," *J. Phys. Chem. B*, **107**(1), pp. 237–244.
- [69] ZHAO, X. L., S. W. ONG, and K. B. EISENTHAL (1993) "Polarization Of Water-Molecules At A Charged Interface second Harmonic Studies Of Charged Monolayers At The Air-Water-Interface," *Chem. Phys. Lett.*, **202**(6), pp. 513–520.
- [70] ZHANG, D., J. GUTOW, and K. B. EISENTHAL (1994) "Vibrational Spectra, Orientations, and Phase Transitions in Long-Chain Amphiphiles at the Air/Water Interface: Probing the Head and Tail Groups by Sum Frequency Generation," *J. Phys. Chem.*, **98**, p. 13729.
- [71] KIM, J. and P. S. CREMER (2000) "IR-Visible SFG investigations of interfacial water structure upon polyelectrolyte adsorption at the solid/liquid interface," *J. Am. Chem. Soc.*, **122**(49), pp. 12371–12372.
- [72] LU, R., W. GAN, B. H. WU, H. CHEN, and H. F. WANG (2004) "Vibrational polarization spectroscopy of CH stretching modes of the methylene group at the vapor/liquid interfaces with sum frequency generation," *J. Phys. Chem. B*, **108**(22), pp. 7297–7306.
- [73] TYRODE, E., C. M. JOHNSON, A. KUMPULAINEN, M. W. RUTLAND, and P. M. CLAEISSON (2005) "Hydration state of nonionic surfactant monolayers at the liquid/vapor interface: Structure determination by vibrational sum frequency spectroscopy," *J. Am. Chem. Soc.*, **127**(48), pp. 16848–16859.
- [74] CHEN, H., W. GAN, B. WU, Z. Z. WU, and H. WANG (2005) "Determination of the two methyl group orientations at vapor/acetone interface with polarization null angle method in SFG vibrational spectroscopy," *Chem. Phys. Lett.*, **408**, p. 284.
- [75] CHEN, X. Y., M. L. CLARKE, J. WANG, and Z. CHEN (2005) "Sum frequency generation vibrational spectroscopy studies on molecular conformation and orientation of biological molecules at interfaces," *Int. J. Mod. Phys. B*, **19**(4), pp. 691–713.

- [76] WANG, J., X. Y. CHEN, M. L. CLARKE, and Z. CHEN (2005) “Detection of chiral sum frequency generation vibrational spectra of proteins and peptides at interfaces in situ,” *Proc. Nat. Ac. Sci. USA*, **102**(14), pp. 4978–4983.
- [77] ROKE, S., J. SCHINS, M. MULLER, and M. BONN (2003) *Phys. Rev. Lett.*, **90**(12), p. 128101.
- [78] BONN, M., S. ROKE, O. BERG, L. B. F. JUURLINK, A. STAMOULI, and M. MULLER (2004) “A molecular view of cholesterol-induced condensation in a lipid monolayer,” *J. Phys. Chem. B*, **108**(50), pp. 19083–19085.
- [79] NIBBERING, E. T. J., H. FIDDER, and E. PINES (2005) “Ultrafast chemistry: Using Time-Resolved Vibrational Spectroscopy for Interrogation of Structural Dynamics,” *Ann. Rev. Phys. Chem.*, **56**(1), pp. 337–367.
- [80] OWRUTSKY, J. C., D. RAFTERY, and R. M. HOCHSTRASSER (1994) “Vibrational Relaxation Dynamics in Solutions,” *Ann. Rev. Phys. Chem.*, **45**(1), pp. 519–555.
- [81] JONAS, D. M. (2003) “Two-dimensional Femtosecond Spectroscopy,” *Ann. Rev. Phys. Chem.*, **54**(1), pp. 425–463.
- [82] HAMM, P., J. HELBING, and J. BREDENBECK (2008) “Two-Dimensional Infrared Spectroscopy of Photoswitchable Peptides,” *Ann. Rev. Phys. Chem.*, **59**(1), pp. 291–317.
- [83] GUYOT-SIONNEST, P., P. DUMAS, Y. J. CHABAL, and G. S. HIGASHI (1990) “Lifetime of an adsorbate-substrate vibration: H on Si(111),” *Phys. Rev. Lett.*, **64**(18), pp. 2156–2159.
- [84] HARRIS, A. L., L. ROTHBERG, L. H. DUBOIS, N. J. LEVINOS, and L. DHAR (1990) “Molecular vibrational energy relaxation at a metal surface: Methyl thiolate on Ag(111),” *Phys. Rev. Lett.*, **64**(17), pp. 2086–2089.
- [85] BACKUS, E. H. G., A. EICHLER, A. W. KLEYN, and M. BONN (2005) “Real-time observation of molecular motion on a surface,” *Science*, **310**(5755), pp. 1790–1793.
- [86] SEKIGUCHI, K., S. YAMAGUCHI, and T. TAHARA (2008) “Femtosecond time-resolved electronic sum-frequency generation spectroscopy: A new method to investigate ultrafast dynamics at liquid interfaces,” *J. Chem. Phys.*, **128**(11), sekiguchi, Kentaro Yamaguchi, Shoichi Tahara, Tahei.
- [87] MCGUIRE, J. A. and Y. R. SHEN (2006) “Ultrafast vibrational dynamics at water interfaces,” *Science*, **313**(5795), pp. 1945–1948.
- [88] EMMERICHS, U., S. WOUTERSEN, and H. J. BAKKER (1997) “Generation of intense femtosecond optical pulses near 3 μ m with a kilohertz repetition rate,” *J. Opt. Soc. Am. B - Opt. Phys.*, **14**(6), pp. 1480–1483.
- [89] BIERLEIN, J. D. and H. VANHERZEELE (1989) “Potassium titanyl phosphate: properties and new applications,” *J. Opt. Soc. Am. B*, **6**(4), pp. 622–633.
- [90] SMITS, M., A. GHOSH, J. BREDENBECK, S. YAMAMOTO, M. MULLER, and M. BONN (2007) “Ultrafast energy flow in model biological membranes,” *New J. Phys.*, **9**, p. 20.
- [91] BREDENBECK, J., A. GHOSH, M. SMITS, and M. BONN (2008) “Ultrafast two dimensional-infrared spectroscopy of a molecular monolayer,” *J. Am. Chem. Soc.*, **130**(7), pp. 2152–2153.

- [92] BONN, M., C. HESS, J. H. MINERS, T. F. HEINZ, H. J. BAKKER, and M. CHO (2001) “Novel surface vibrational spectroscopy: Infrared-infrared-visible sum-frequency generation,” *Phys. Rev. Lett.*, **86**(8), pp. 1566–1569.
- [93] SMITS, M., A. GHOSH, M. STERRER, M. MULLER, and M. BONN (2007) “Ultrafast vibrational energy transfer between surface and bulk water at the air-water interface,” *Phys. Rev. Lett.*, **98**(98302), p. 4.
- [94] GHOSH, A., M. SMITS, J. BREDEBECK, M. MULLER, and M. BONN (2007) “Membrane-bound water is energetically decoupled from the bulk: an ultrafast surface vibrational study,” *J. Am. Chem. Soc.*, **129**, pp. 9608–9609.
- [95] MCCONNELL, H. M. (1991) “Structures and transitions in lipid monolayers at the air-water-interface,” *Ann. Rev. Phys. Chem.*, **42**, pp. 171–195.
- [96] BENJAMIN, I. (1996) “Chemical reactions and solvation at liquid interfaces: A microscopic perspective,” *Chem. Rev.*, **96**(4), pp. 1449–1475.
- [97] CHANDLER, D. (2005) “Interfaces and the driving force of hydrophobic assembly,” *Nature*, **437**(7059), pp. 640–647.
- [98] GARRETT, B. C. (2004) “Ions at the air/water interface,” *Science*, **303**(5661), pp. 1146–1147.
- [99] AYOTTE, P., S. B. NIELSEN, G. H. WEDDLE, M. A. JOHNSON, and S. S. XANTHEAS (1999) “Spectroscopic Observation of Ion-Induced Water Dimer Dissociation in the $X^-(H_2O)_2$ ($X = F, Cl, Br, I$) Clusters,” *J. Phys. Chem. A*, **103**(50), pp. 10665–10669, <http://pubs.acs.org/doi/pdf/10.1021/jp991963r>.
URL <http://pubs.acs.org/doi/abs/10.1021/jp991963r>
- [100] HU, J. H., Q. SHI, P. DAVIDOVITS, D. R. WORSNOP, M. S. ZAHNISER, and C. E. KOLB (1995) “Reactive Uptake of $Cl_2(g)$ and $Br_2(g)$ by Aqueous Surfaces as a Function of Br- and I- Ion Concentration: The Effect of Chemical Reaction at the Interface,” *J. Phys. Chem.*, **99**(21), pp. 8768–8776, <http://pubs.acs.org/doi/pdf/10.1021/j100021a050>.
URL <http://pubs.acs.org/doi/abs/10.1021/j100021a050>
- [101] DOUARCHE, C., J. L. SIKORAV, and A. GOLDAR (2008) “Aggregation and Adsorption at the Air-Water Interface of Bacteriophage OX174 Single-Stranded DNA,” **94**(1), pp. 134–146.
- [102] (1972) *Water, A Comprehensive Treatise*, edited by F. Franks, (Plenum, New York).
- [103] BENDERSKII, A. V. and K. B. EISENTHAL (2002) “Dynamical time scales of aqueous solvation at negatively charged lipid/water interfaces,” *J. Phys. Chem. A*, **106**(33), pp. 7482–7490.
- [104] MORITA, A. and J. T. HYNES (2000) “A theoretical analysis of the sum frequency generation spectrum of the water surface,” *Chem. Phys.*, **258**(2-3), pp. 371–390.
- [105] ——— (2002) “A theoretical analysis of the sum frequency generation spectrum of the water surface. II. Time-dependent approach,” *J. Phys. Chem. B*, **106**(3), pp. 673–685.
- [106] PERRY, A., H. AHLBORN, B. SPACE, and P. B. MOORE (2003) “A combined time correlation function and instantaneous normal mode study of the sum frequency generation spectroscopy of the water/vapor interface,” *J. Chem. Phys.*, **118**(18), pp. 8411–8419.

- [107] SHEN, Y. R. and V. OSTROVERKHOV (2006) "Sum-frequency vibrational spectroscopy on water interfaces: Polar orientation of water molecules at interfaces," *Chem. Rev.*, **106**(4), pp. 1140–1154.
- [108] ASBURY, J. B., T. STEINEL, K. KWAK, S. A. CORCELLI, C. P. LAWRENCE, J. L. SKINNER, and M. D. FAYER (2004) "Dynamics of water probed with vibrational echo correlation spectroscopy," *J. Chem. Phys.*, **121**(24), pp. 12431–12446.
- [109] FECKO, C. J., J. J. LOPARO, S. T. ROBERTS, and A. TOKMAKOFF (2005) "Local hydrogen bonding dynamics and collective reorganization in water: Ultrafast infrared spectroscopy of HOD/D₂O," *J. Chem. Phys.*, **122**(5), p. 054506.
- [110] WANG, Z. H., A. PAKOULEV, Y. PANG, and D. D. DLOTT (2004) "Vibrational substructure in the OH stretching transition of water and HOD," *J. Phys. Chem. A*, **108**(42), pp. 9054–9063.
- [111] LINDNER, J., P. VOHRINGER, M. S. PSHENICHNIKOV, D. CRINGUS, D. A. WIERSMA, and M. MOSTOVOY (2006) "Vibrational relaxation of pure liquid water," *Chem. Phys. Lett.*, **421**(4-6), pp. 329–333.
- [112] LAENEN, R., K. SIMEONIDIS, and A. LAUBEREAU (2002) "Subpicosecond spectroscopy of liquid water in the infrared: Effect of deuteration on the structural and vibrational dynamics," *J. Phys. Chem. B*, **106**(2), pp. 408–417.
- [113] TAN, H. S., I. R. PILETIC, R. E. RITER, N. E. LEVINGER, and M. D. FAYER (2005) "Dynamics of water confined on a nanometer length scale in reverse micelles: Ultrafast infrared vibrational echo spectroscopy," *Phys. Rev. Lett.*, **94**(5), p. 057405.
- [114] DOKTER, A. M., S. WOUTERSEN, and H. J. BAKKER (2005) "Anomalous slowing down of the vibrational relaxation of liquid water upon nanoscale confinement," *Phys. Rev. Lett.*, **94**, p. 178301.
- [115] GILIJAMSE, J. J., A. J. LOCK, and H. J. BAKKER (2005) "Dynamics of confined water molecules," *Proc. Natl. Acad. Sci. USA*, **102**(9), pp. 3202–3207.
- [116] SASS, M., M. LETTENBERGER, and A. LAUBEREAU (2002) "Orientation and vibrational relaxation of acetonitrile at a liquid : solid interface, observed by sum-frequency spectroscopy," *Chem. Phys. Lett.*, **356**(3-4), pp. 284–290.
- [117] DU, Q., E. FREYSZ, and Y. R. SHEN (1994) "Surface Vibrational Spectroscopic Studies of Hydrogen-Bonding and Hydrophobicity," *Science*, **264**(5160), pp. 826–828.
- [118] ——— (1994) "Vibrational-Spectra of Water-Molecules at Quartz Water Interfaces," *Phys. Rev. Lett.*, **72**(2), pp. 238–241.
- [119] GRAGSON, D. E. and G. L. RICHMOND (1998) "Investigations of the Structure and Hydrogen Bonding of Water Molecules at Liquid Surfaces by Vibrational Sum Frequency Spectroscopy," *J. Phys. Chem. B*, **102**(20), pp. 3847–3861.
- [120] RAYMOND, E. A., T. L. TARBUCK, M. G. BROWN, and G. L. RICHMOND (2003) "Hydrogen-bonding interactions at the vapor/water interface investigated by vibrational sum-frequency spectroscopy of HOD/H₂O/D₂O mixtures and molecular dynamics simulations," *J. Phys. Chem. B*, **107**(2), pp. 546–556.
- [121] RAYMOND, E. A. and G. L. RICHMOND (2004) "Probing the molecular structure and bonding of the surface of aqueous salt solutions," *J. Phys. Chem. B*, **108**(16), pp. 5051–5059.

- [122] SHULTZ, M. J., S. BALDELLI, C. SCHNITZER, and D. SIMONELLI (2002) "Aqueous solution/air interfaces probed with sum frequency generation spectroscopy," *J. Phys. Chem. B*, **106**(21), pp. 5313–5324.
- [123] BUCH, V. (2005) "Molecular structure and OH-stretch spectra of liquid water surface," *J. Phys. Chem. B*, **109**(38), pp. 17771–17774.
- [124] WALKER, D. S., D. K. HORE, and G. L. RICHMOND (2006) "Understanding the population, coordination, and orientation of water species contributing to the nonlinear optical spectroscopy of the vapor-water interface through molecular dynamics simulations," *J. Phys. Chem. B*, **110**(41), pp. 20451–20459.
- [125] LIU, D. F., G. MA, L. M. LEVERING, and H. C. ALLEN (2004) "Vibrational Spectroscopy of aqueous sodium halide solutions and air-liquid interfaces: Observation of increased interfacial depth," *J. Phys. Chem. B*, **108**(7), pp. 2252–2260.
- [126] GAN, W., D. WU, Z. ZHANG, R. FENG, and H. WANG (2006) "Polarization and experimental configuration analyses of sum frequency generation vibrational spectra, structure, and orientational motion of the air/water interface," *J. Chem. Phys.*, **124**, p. 114705.
- [127] SOVAGO, M., R. K. CAMPEN, G. W. H. WURPEL, M. MÜLLER, H. J. BAKKER, and M. BONN (2008) "The vibrational response of hydrogen bonded interfacial water is dominated by intramolecular coupling," *Phys. Rev. Lett.*, **100**, p. 173901.
- [128] ASHIHARA, S., N. HUSE, A. ESPAGNE, E. T. J. NIBBERING, and T. ELSAESSER (2006) "Vibrational couplings and ultrafast relaxation of the O-H bending mode in liquid H₂O," *Chem. Phys. Lett.*, **424**, pp. 66–70.
- [129] ——— (2007) "Ultrafast structural dynamics of water induced by dissipation of vibrational energy," *J. Phys. Chem. A*, **111**(5), pp. 743–746.
- [130] COWAN, M. L., B. D. BRUNER, N. HUSE, J. R. DWYER, B. CHUGH, E. T. J. NIBBERING, T. ELSAESSER, and R. J. D. MILLER (2005) "Ultrafast memory loss and energy redistribution in the hydrogen bond network of liquid H₂O," *Nature*, **434**(7030), pp. 199–202.
- [131] NIENHUYS, H. K., S. WOUTERSEN, R. A. VAN SANTEN, and H. J. BAKKER (1999) "Mechanism for vibrational relaxation in water investigated by femtosecond infrared spectroscopy," *J. Chem. Phys.*, **111**(4), pp. 1494–1500.
- [132] WOUTERSEN, S. and H. J. BAKKER (1999) "Resonant intermolecular transfer of vibrational energy in liquid water," *Nature*, **402**(6761), pp. 507–509.
- [133] HARRIS, A. L. and L. ROTHBERG (1991) "Surface vibrational-energy relaxation by sum frequency generation - 5-wave mixing and coherent transients," *J. Chem. Phys.*, **94**(4), pp. 2449–2457.
- [134] STEINER, T. (2002) "The hydrogen bond in the solid state," *Angew. Chem.-Int. Ed.*, **41**(1), pp. 48–76.
- [135] WOUTERSEN, S., U. EMMERICHS, and H. J. BAKKER (1997) "Femtosecond mid-IR pump-probe spectroscopy of liquid water: Evidence for a two-component structure," *Science*, **278**(5338), pp. 658–660.
- [136] NIBBERING, E. T. J. and T. ELSAESSER (2004) "Ultrafast vibrational dynamics of hydrogen bonds in the condensed phase," *Chem. Rev.*, **104**(4), pp. 1887–1914.

- [137] PARK, S. and M. D. FAYER (2007) "Hydrogen bond dynamics in aqueous NaBr solutions," *Proc. Natl. Acad. Sci USA*, **104**(43), pp. 16731–16738.
- [138] HUSE, N., S. ASHIHARA, E. T. J. NIBBERING, and T. ELSAESSER (2005) "Ultrafast vibrational relaxation of O-H bending and librational excitations in liquid H₂O," *Chem. Phys. Lett.*, **404**(4-6), pp. 389–393.
- [139] BAKKER, H. J. (2008) "Structural Dynamics of Aqueous Salt Solutions," *Chem. Rev.*, **108**, pp. 1456–1473.
- [140] GHOSH, A., M. SMITS, J. BREDENBECK, N. DIJKHUIZEN, and M. BONN (2008) "Femtosecond time-resolved and two-dimensional vibrational sum frequency spectroscopic instrumentation to study structural dynamics at interfaces," *Rev. Sci. Instru.*, **79**(9), p. 093907.
- [141] YEAGLE, P. L. (2005) *The Structure of Biological Membranes, Second Edition*, CRC Press.
- [142] LOCK, A. J., S. WOUTERSEN, and H. J. BAKKER (2001) "Ultrafast energy equilibration in hydrogen-bonded liquids," *J. Phys. Chem. A*, **105**(8), pp. 1238–1243.
- [143] LOCK, A. J. and H. J. BAKKER (2002) "Temperature dependence of vibrational relaxation in liquid H₂O," *J. Chem. Phys.*, **117**(4), pp. 1708–1713.
- [144] STAIB, A. and J. T. HYNES (1993) "Vibrational predissociation in hydrogen-bonded O-H...O complexes via OH stretch O-O stretch energy-transfer," *Chem. Phys. Lett.*, **204**(1-2), pp. 197–205.
- [145] (2007) "Variation of the transition dipole moment across the OH stretching band of water," *Chem. Phys.*, **341**(1-3), pp. 218 – 229.
- [146] NOTTER, R. H. (2000) *Lung Surfactants: Basic Science and Clinical Applications*, New York: Marcel Dekker.
- [147] MA, G. and H. C. ALLEN (2006) "New insights into lung surfactant monolayers using vibrational sum frequency generation spectroscopy," *Photochem. Photobiol.*, **82**(6), pp. 1517–1529.
- [148] GOERKE, J. and J. A. CLEMENTS. (1986) *Alveolar surface tension and lung surfactant, in Handbook of Physiology: The Respiratory System, Vol. III (Edited by P. T. Mackelm and J. Mead), pp. 247261.*, American Physiology Society, Washington.
- [149] GOERKE, J. (1998) "Pulmonary surfactant: functions and molecular composition," *Biochim. Biophys. Acta*, **1408**(2-3), pp. 79–89.
- [150] ZASADZINSKI, J. A., J. DING, H. E. WARRINER, F. BRINGEZU, and A. J. WARING (2001) "The physics and physiology of lung surfactants," *Curr. Opin. Coll. Int. Sci.*, **6**(5-6), pp. 506–513.
- [151] MA, G. and H. C. ALLEN (2007) "Condensing effect of palmitic acid on DPPC in mixed Langmuir monolayers," *Langmuir*, **23**(2), pp. 589–597.
- [152] GOPAL, A. and K. Y. LEE (2006) "Headgroup Percolation and Collapse of Condensed Langmuir Monolayers," *J. Phys. Chem. B*, **110**(44), pp. 22079–22087.
- [153] MAO, G., J. DESAI, C. R. FLACH, and R. MENDELSON (2008) "Structural characterization of the monolayer-multilayer transition in a pulmonary surfactant model: IR studies of films transferred at continuously varying surface pressures," *Langmuir*, **24**(5), pp. 2025–2034.

- [154] CAI, P., C. R. FLACH, and R. MENDELSON (2003) "An infrared reflection-absorption spectroscopy study of the secondary structure in (KL4)(4)K, a therapeutic agent for respiratory distress syndrome, in aqueous monolayers with phospholipids," *Biochem.*, **42**(31), pp. 9446–9452.
- [155] WANG, H. F., W. GAN, R. LU, Y. RAO, and B. H. WU (2005) "Quantitative spectral and orientational analysis in surface sum frequency generation vibrational spectroscopy (SFG-VS)," *Int. Rev. Phys. Chem.*, **24**(2), pp. 191–256.
- [156] COCHRANE, C. G. and S. D. REVAK (1991) "Pulmonary Surfactant Protein-B (Sp-B) - Structure-Function-Relationships," *Science*, **254**(5031), pp. 566–568.
- [157] FRERKING, I., A. GUNTHER, W. SEEGER, and U. PISON (2001) "Pulmonary surfactant: functions, abnormalities and therapeutic options," *Intensive Care Medicine*, **27**(11), pp. 1699–1717.
- [158] SAENZ, A., O. CANADAS, L. A. BAGATOLLI, M. E. JOHNSON, and C. CASALS (2006) "Physical properties and surface activity of surfactant-like membranes containing the cationic and hydrophobic peptide KL4," *Febs J.*, **273**(11), pp. 2515–2527.
- [159] BAIN, C. D., P. B. DAVIES, T. H. ONG, R. N. WARD, and M. A. BROWN (1991) "Quantitative-analysis of monolayer composition by sum-frequency vibrational spectroscopy," *Langmuir*, **7**(8), pp. 1563–1566.
- [160] CHEN, X. Y. and Z. CHEN (2006) "SFG studies on interactions between antimicrobial peptides and supported lipid bilayers," *Biochim. Biophys. Acta - Biomembranes*, **1758**(9), pp. 1257–1273.
- [161] GRAGSON, D. E., B. M. MCCARTY, and G. L. RICHMOND (1997) "Ordering of interfacial water molecules at the charged air/water interface observed by vibrational sum frequency generation," *J. Am. Chem. Soc.*, **119**(26), pp. 6144–6152.
- [162] BRINGEZU, F., J. DING, G. BREZESINSKI, and J. ZASADZINSKI (2001) "Changes in model lung surfactant monolayers induced by palmitic acid," *Langmuir*, **17**(15), pp. 4641–4648.
- [163] DISCHER, B. M., W. R. SCHIEF, V. VOGEL, and S. B. HALL "Phase Separation in Monolayers of Pulmonary Surfactant Phospholipids at the Air Water Interface: Composition and Structure," *Biophys. J.*
- [164] BRINGEZU, F., J. DING, G. BREZESINSKI, A. WARING, and J. ZASADZINSKI (2002) "Influence of pulmonary surfactant protein B on model lung surfactant monolayers," *Langmuir*, **18**(6), pp. 2319–2325.
- [165] MARTIN, M. M. and J. T. HYNES (eds.) (2004) *Femtochemistry and Femtobiology: Ultrafast Events in Molecular Science*, Elsevier, Amsterdam.
- [166] KIMBLE, M. and W. CASTLEMAN JR. (eds.) (2006) *Femtochemistry VII: Fundamental Ultrafast Processes in Chemistry*, Elsevier, Amsterdam.
- [167] BRIXNER, T., J. STENGER, H. M. VASWANI, M. CHO, R. E. BLANKENSHIP, and G. R. FLEMING (2005) *Nature*, **434**, p. 625.
- [168] LU, H. P., L. Y. XUN, and X. S. XIE (1998) *Science*, **282**, p. 1877.
- [169] SACHS, J. N. and D. M. ENGELMAN (2006) *Ann. Rev. Biochem.*, **75**, p. 707.

- [170] FRAUENFELDER, H., B. H. MCMAHON, R. H. AUSTIN, K. CHU, and J. T. GROVES (2001) *Proc. Natl. Acad. Sci. USA*, **98**, p. 2370.
- [171] WANG, H. F. (2004) "A simplified formulation of linear and nonlinear spectroscopy of ordered molecular systems," *Chin. J. Chem. Phys.*, **17**(3), pp. 362–368.
- [172] FINKELSTEIN, I. J., H. ISHIKAWA, S. KIM, A. M. MASSARI, and M. D. FAYER (2007) *Proc. Natl. Acad. Sci. USA*, **104**, p. 2637.
- [173] AUSTIN, R. H., A. H. XIE, L. VAN DER MEER, B. REDLICH, P. A. LINDGARD, H. FRAUENFELDER, and D. FU (2005) *Phys. Rev. Lett.*, **94**, p. 128101.
- [174] LIM, M. H., P. HAMM, and R. M. HOCHSTRASSER (1998) *Proc. Nat. Ac. Sci. USA*, **95**, p. 15315.
- [175] FANG, C., A. SENES, L. CRISTIAN, W. F. DEGRADO, and R. M. HOCHSTRASSER (2006) *Proc. Natl. Acad. Sci. USA*, **103**, p. 16740.
- [176] (2002) *Femtochemistry and Femtobiology, Ultrafast Dynamics in Molecular Science*. Imperial College Press: London, Elsevier, Amsterdam.
- [177] (2004) *Femtochemistry and Femtobiology: Ultrafast Events in Molecular Science*, Elsevier, Amsterdam.
- [178] DEAK, J. C., Y. S. PANG, T. D. SECHLER, Z. H. WANG, and D. D. DLOTTT (2004) "Vibrational energy transfer across a reverse micelle surfactant layer," *Science*, **306**(5695), pp. 473–476.
- [179] VOLKOV, V. V., F. NUTI, Y. TAKAOKA, R. CHELLI, A. M. PAPINI, and R. RIGHINI (2006) *J. Am. Chem. Soc.*, **128**, p. 9466.
- [180] VOLKOV, V. V., D. J. PALMER, and R. RIGHINI (2007) "Heterogeneity of water at the phospholipid membrane interface," *J. Phys. Chem. B*, **111**(6), pp. 1377–1383.
- [181] GUMBART, J., Y. WANG, A. AKSIMENTIEV, E. TAJKHORSHID, and K. SCHULTEN (2005) *Curr. Opin. Struct. Biol.*, **15**, p. 423.
- [182] TRISTRAM-NAGLE, S. and J. F. NAGLE (2004) *Chem. Phys. Lipids*, **127**, p. 3.
- [183] NAGLE, J. F. and S. TRISTRAM-NAGLE (2000) "Structure of lipid bilayers," *Biochim. Biophys. Acta-Reviews on Biomembranes*, **1469**(3), pp. 159–195.
- [184] KAGANER, V. M., H. MOHWALD, and P. DUTTA (1999) *Rev. Mod. Phys.*, **71**, p. 779.
- [185] MOAD, A. J. and G. J. SIMPSON (2004) *J. Phys. Chem. B*, **108**, p. 3548.
- [186] NGUYEN, K. T., X. M. SHANG, and K. B. EISENTHAL (2006) "Molecular rotation at negatively charged surfactant/aqueous interfaces," *J. Phys. Chem. B*, **110**(40), pp. 19788–19792.
- [187] KUBOTA, J. and K. DOMEN (2007) "Study of the dynamics of surface molecules by time-resolved sum-frequency generation spectroscopy," *Anal. Bioanal. Chem.*, **388**(1), pp. 17–27.
- [188] LANE, I., D. KING, and H. ARNOLDS (2007) *J. Chem. Phys.*, **126**, p. 024707.
- [189] YEAGLE, P. L. (ed.) (2005) *The structure of biological membranes*, CRC Press, Washington D.C.

- [190] KOYNOVA, R. and M. CAFFREY (2002) *Chem. Phys. Lipids*, **115**, p. 107.
- [191] FUJIWARA, T., K. RITCHIE, H. MURAKOSHI, K. JACOBSON, and A. KUSUMI (2002) *J. Cell Biol.*, **157**, p. 1071.
- [192] KORLACH, J., P. SCHWILLE, W. W. WEBB, and G. W. FEIGENSON (1999) *Proc. Natl. Acad. Sci. USA*, **96**, p. 8461.
- [193] LAGERHOLM, B. C., G. E. WEINREB, K. JACOBSON, and N. L. THOMPSON (2005) *Ann. Rev. Phys. Chem.*, **56**, p. 309.
- [194] MA, G. and H. C. ALLEN (2006) "DPPC Langmuir monolayer at the air-water interface: Probing the tail and head groups by vibrational sum frequency generation spectroscopy," *Langmuir*, **22**(12), pp. 5341–5349.
- [195] GURAU, M. C., E. T. CASTELLANA, F. ALBERTORIO, S. KATAOKA, S. M. LIM, R. D. YANG, and P. S. CREMER (2003) "Thermodynamics of phase transitions in Langmuir monolayers observed by vibrational sum frequency spectroscopy," *J. Am. Chem. Soc.*, **125**(37), pp. 11166–11167.
- [196] SHEN, Y. R. (1994) "Frontiers in Laser Spectroscopy, Proceedings of the International School of Physics "Enrico Fermi", Course CXX, 23 June-3 July 1992," .
- [197] VAN DER HAM, E. W. M., Q. H. F. VREHEN, and E. R. ELIEL (1996) *Opt. Lett.*, **21**, p. 1448.
- [198] RICHTER, L. J., T. P. PETRALLI-MALLOW, and J. C. STEPHENSON (1998) "Vibrationally resolved sum-frequency generation with broad-bandwidth inf rared pulses," *Opt. Lett.*, **23**, pp. 1594–1596.
- [199] SMITS, M., M. SOVAGO, G. W. H. WURPEL, D. KIM, M. MULLER, and M. BONN (2007) *J. Phys. Chem. C*, **111**, p. 8878.
- [200] BONN, M., C. HESS, S. FUNK, J. H. MINERS, B. N. J. PERSSON, M. WOLF, and G. ERTL (2000) *Phys. Rev. Lett.*, **84**(20), p. 4653.
- [201] GRAENER, H. and A. LAUBEREAU (1982) *Appl. Phys. B*, **29**, p. 213.
- [202] DEAK, J. C., L. K. IWAKI, and D. D. DLOTT (1998) *Chem. Phys. Lett.*, **293**, p. 405.
- [203] HARRIS, A. L. and N. J. LEVINOS (1989) "Vibrational-energy relaxation in a molecular monolayer at a metal-surface," *J. Chem. Phys.*, **90**(7), pp. 3878–3879.
- [204] WEI, X., P. B. MIRANDA, and Y. R. SHEN (2001) "Surface vibrational spectroscopic study of surface melting of ice," *Phys. Rev. Lett.*, **86**(8), pp. 1554–1557.
- [205] SUNG, J. H. and D. KIM (2007) "Fast motion of the surface alcohol molecules deduced from sum-frequency vibrational spectroscopy," *J. Phys. Chem. C*, **111**(4), pp. 1783–1787.
- [206] FOURKAS, J. T., R. A. WALKER, S. Z. CAN, and E. GERSHGORIN (2007) *J. Phys. Chem. C*, **111**, p. 8902.
- [207] SEIFERT, G., T. PATZLAFF, and H. GRAENER (2002) "Size dependent ultrafast cooling of water droplets in microemulsions by picosecond infrared spectroscopy," *Phys. Rev. Lett.*, **88**(14), p. 147402.

Summary

Biological membranes which define the external boundaries of living cells, are mostly composed of self-assembled bilayers of phospholipid molecules. Phospholipids are amphiphilic in nature, where the hydrophilic *head* consists of either dipolar or charged moieties and the hydrophobic *tail* is an apolar alkyl chain. These molecules self-assemble into bilayers as soon as they come in contact with water, with the polar heads solvated by the water molecules and the apolar tails trying to stay away from the water. However, a real biological membrane is not just the bilayer by itself. The lipid bilayer also provides the essential scaffolding for a variety of transmembrane and integral proteins. Together, they chaperone and organize a variety of complex reactions that control the cellular mass-energy balance and signaling across the cell, thus giving life to a cell. The complex membrane structure and function relies on subtle interactions with the surrounding interfacial water plays. The role of water in membrane functioning has been somewhat overlooked, and is often approximated as merely an effective dielectric medium in which the cell resides and functions. However, the properties of the membrane change dramatically as the degree of hydration varies; lipid hydration process has important structural and functional consequences for the membrane. For instance, hydration dynamics and water-lipid interaction strengths are closely related to the membrane fluidity and the molecular organization of the lipids. Thus the cellular membrane structure and function is essentially dependent on the interplay of interactions between the lipids, proteins and the interfacial water molecules. However, the interfacial water layer around the membranes is only a few molecules thick ($\sim 5 \text{ \AA}$). It is therefore technically very challenging to directly observe the interfacial water molecules in order to get a clearer picture of the contribution of water to membrane structure and function.

In this thesis, the nonlinear optical technique of vibrational sum frequency generation (VSFG) spectroscopy is used to directly probe the structure of interfacial water and lipid molecules in a model biological membrane, with surface-specificity. Since the focus of this study lies on the interaction between interfacial water and lipids, a lipid monolayer system provides a good membrane model, rather than the actual lipid bilayer system. The surface-specificity of the technique relies on the intrinsic breaking of symmetry at interfaces, where the 2nd order nonlinear optical process of sum frequency generation (SFG) is allowed. By overlapping two focused laser beams in space

and time, and intersecting those at the water-lipid or the water-air interface, one can generate the sum frequency (SF) spectrum originating only from the interfacial molecules. When the frequency of one of the laser beams is tuned (in the mid-infrared range) to a vibrational resonance of interfacial molecules, the SF signal is greatly enhanced, thus providing the essential IR spectrum of the interfacial species.

As we know from IR absorption spectroscopy, a wealth of structural information can be extracted about a molecule by monitoring the IR spectrum under different conditions of, say, temperature, solvents, pH, etc. Similarly VSFG provides us with surface molecular information. However, since both IR and VSFG spectroscopies are time-averaged techniques, the spectra reflect only the time-averaged molecular structure, thereby washing out any dynamic structural process that maybe hidden beneath the spectra. This is also true for VSFG experiments performed on water-air and water-lipid interfaces. The static VSFG spectra of water at these interfaces is generally broad ($\sim 500 \text{ cm}^{-1}$) and rather featureless. The different interfaces that are studied in this thesis vary from a simple neat water-air interface to as complex an interface as a model lung surfactant comprising of 4 different kinds of lipids and a 21-amino acid polypeptide; and for all of these interfaces, the VSFG spectra of the interfacial water appear quite similar.

This situation is reminiscent of IR studies of bulk water, where the broad and featureless spectra have been interrogated with ultrafast IR pump-probe laser techniques. Using these techniques, much information on the structural dynamics of water could be gathered. In a typical IR pump-probe experiment, a highly intense ultrashort IR pump pulse ($\sim 100 \text{ fs}$ pulse duration) with its frequency tuned to the O-H stretch vibration of water, locally excites the molecular vibration and subsequently an IR probe pulse monitors the relaxation of the vibrational excitation at different delay times after the excitation process. In this way, transient spectra can be collected on time-scales as short as $\sim 100 \text{ fs}$. The ultrafast spectral changes reflect the dynamic structural evolution in real-time. Taking cues from these IR pump-probe technique on *bulk* water, a novel IR pump-VSFG probe has been developed to probe *interfacial* water. In this thesis, VSFG spectra from the interfacial molecules are collected at various delay times following an IR excitation. In this technique, in addition to the two SF generating laser beams, a high intensity ultrashort ($\sim 100 \text{ fs}$) pulsed IR laser beam is also overlapped at the interface and is variably delayed with respect to the probe SF generating laser beam. A number of model biological interfaces have been studied using this IR pump-VSFG probe (or time-resolved SFG, TRSFG).

In the first study, the neat water-air interface was investigated with the TRSFG technique, keeping the IR pump and probe frequencies the same. The static VSFG spectrum of the hydrogen-bonded O-H oscillators at the neat water-air interface is broad ($3200\text{-}3500 \text{ cm}^{-1}$) and might be expected to be inhomogeneously broadened: at 3200 cm^{-1} the sub-ensemble of O-H oscillators is strongly H-bonded whereas at 3500 cm^{-1} it is weakly H-bonded. However, the TRSFG relaxation dynamics across the spectrum was demonstrated to be independent of the sub-ensemble of water molecules being excited and probed. The relaxation dynamics of these two widely different sub-ensembles being the same, is very much like the behavior exhibited by bulk water. In the bulk, an ultrafast Förster-type vibrational energy transfer ($\sim 50 \text{ fs}$) between neighboring water molecules, dominates

the vibrational relaxation dynamics. As a result of the fast vibrational energy transfer between different water molecules, the excitation samples various sub-ensembles on ultrafast timescales and also randomizes the excitation polarization information. The same mechanism was found to be operative at the water interface. Indeed, the bulk relaxation timescales could well describe our TRSFG transient data, with $T_1=200$ fs and $T_{thermalization}=500$ fs. Furthermore, polarization-resolved TRSFG show that the excitation is scrambled very quickly, consistent with the scenario of bulk-like relaxation. Thus we demonstrated that the surface and bulk water are indistinguishable as a result of an efficient Förster-type vibrational energy transfer between the surface and bulk water molecules.

In our second study, a lipid monolayer-water interface was investigated using TRSFG in order to distinguish between effects due to water-lipid headgroup interactions and effects due to mere termination of the bulk, as at the neat water-air interface. The lipid used here was 1,2 Dimyristoyl Glycero-3-Phospho-L-Serine (DMPS, Sodium salt), which has a net negative charge on the headgroup. We demonstrated that the TRSFG dynamics at the lipid-water interface was indeed different from those at the air-water interface. Although the sub-ensembles of medium to weakly hydrogen-bonded water molecules ($3300-3500\text{ cm}^{-1}$) showed similar T_1 dynamics as the neat water-air interface, the sub-ensemble of strongly hydrogen-bonded water molecules (at 3200 cm^{-1}) showed relaxation dynamics faster than the duration of the pulse itself (<100 fs). Also the thermalization time-scales for all the sub-ensembles are demonstrated to be slightly longer than at the neat water-air interface (~ 1 ps). Further experiments with different kinds of lipid monolayer-water interfaces (positively-charged DPTAP, zwitterionic DPPC, DPPE) demonstrated that indeed the strongly hydrogen-bonded sub-ensemble of water molecules have sub-pulse T_1 relaxation time-scales (of the order of ≤ 50 fs) whereas the dynamics of those sub-ensembles with medium and weaker hydrogen-bond strengths are dominated by a Förster-type transfer as at the neat water-air interface.

In a separate study, the structure and dynamics of water in contact with a monolayer of artificial lung surfactant (LS), composed of four types of lipids (DPPC, DPPG, tripalmitin and cardiolipin) and a 21 amino acid peptide, were investigated using both static VSFG and TRSFG spectroscopy. In this study, the dynamic responses of only the sub-ensemble of strongly hydrogen-bonded water molecules (i.e. at 3200 cm^{-1}) interfacing with three systems were investigated: a monolayer of the pure lipid that is dominant in the LS mixture (DPPC), a monolayer of the four lipids, and a monolayer of the four lipids including the LS protein. Although the static VSFG spectra of all three systems are similar, remarkable differences are demonstrated in the vibrational energy relaxation mechanisms between the pure DPPC/water system and the mixtures. In contrast to the sub-pulse relaxation dynamics (T_1), observed for the DPPC/water interface, the LS mixture with and without the peptide show evidences that the relaxation dynamics are primarily dominated by a Förster-type vibrational energy transfer even for the sub-ensemble of strongly hydrogen-bonded water molecules, thus demonstrating the underlying structural differences of interfacial water in these different types of interfaces.

In the final chapter, the energy flow dynamics in model membrane-water interfaces were investigated by TRSFG. In this study, the vibrational relaxation dynamics of C-H stretch modes (CH_3 and CH_2 stretch modes) in the lipid alkyl chains were investigated. The results reveal that incoherent

energy transfer occurs from excited CH_2 groups to the terminal CH_3 groups. Evidences for strong anharmonic coupling between different CH_2 and CH_3 modes were demonstrated. Relaxation and energy transfer processes within the lipid alkyl chain occurs on (sub-)picosecond timescales. Studies of the dynamics on different lipid phases (gel or liquid crystalline phase) reveal a marked independence of the dynamics on the precise molecular conformation of the lipids. In addition, the energy transfer dynamics between membrane-bound water and lipids are also demonstrated, in which the transfer of heat between water and lipids occurs remarkably fast: heat is transferred across the monolayer, from the polar head group region of the lipid to the end of the alkyl chain, within 1 ps. These results demonstrate the potential of using ultrafast surface-specific TRSFG spectroscopy to investigate biomolecular dynamics at (model) membrane surfaces.

Samenvatting

De biologische membranen die de buitengrenzen van levende cellen vormen, bestaan voornamelijk uit een dubbele, zelfvormende laag van fosfolipiden. Fosfolipiden zijn amfifiele moleculen, waarin de hydrofiele kopgroep dipolair of geladen is, terwijl de hydrofobe staart gevormd wordt door een apolaire alkylketen. Zodra deze moleculen in contact komen met water vormen ze zich spontaan tot een dubbellaag, met de polaire kopgroepen in contact met watermoleculen en de apolair staarten bij elkaar, zo ver mogelijk van het water vandaan. In werkelijkheid bestaat een biologisch membraan echter niet enkel uit deze lipide dubbellaag. De laag fosfolipiden biedt namelijk ook het noodzakelijke platform voor een grote verscheidenheid aan membraan-geassocieerde eiwitten. Samen begeleiden en organiseren ze de talrijke complexe reacties die het cellulaire massa-energie balans en de chemische communicatie van en naar de cel controleren, waarmee ze de cel in staat stellen te leven. Maar ook de fosfolipiden en eiwitten tezamen kunnen de complexe structuur en functionaliteit van het membraan niet volledig verklaren. De rol van het omringende water voor het functioneren van het membraan in het verleden vaak is vaak beschreven als een effectief dielectrisch medium waarbinnen de cel functioneert. Het is echter bekend dat de eigenschappen van het membraan sterk afhankelijk zijn van de details van de moleculaire interacties met water. Het hydrateren van de fosfolipiden heeft belangrijke gevolgen voor de structuur en het functioneren van het membraan zelf. De dynamiek van hydratatie en de kracht van interacties tussen water en lipiden zijn bijvoorbeeld nauw gerelateerd aan de moleculaire ordening van de lipiden. Zodoende is de structuur en het functioneren van het membraan afhankelijk van de interacties tussen lipiden, eiwitten en de nabije watermoleculen. Maar omdat de watermoleculen die het membraan kunnen beïnvloeden een laag vormen van slechts enkele moleculen dik ($\sim 5 \text{ \AA}$), is het technisch zeer uitdagend om deze laag direct waar te nemen en zo een beter beeld te krijgen van de bijdrage van het water op de eigenschappen van membranen.

In dit proefschrift wordt de niet-lineaire optische methode vibrational sum frequency generation (VSFG) spectroscopie gebruikt om de structuur van fosfolipiden en het aangrenzende water in een modelmembraan direct te observeren. Het aantrekkelijke van de techniek is dat deze zeer specifiek informatie over het oppervlak levert. Omdat de focus van dit onderzoek de interactie tussen lipiden en water behelst, is een enkele laag lipiden op water een goed model voor een membraan. De specificiteit van de gebruikte techniek voor oppervlakken berust op het gegeven dat aan een grensvlak de

symmetrie is gebroken, waardoor het tweede-orde optische proces sum frequency generation (SFG) kan plaatsvinden. Door twee gefocuseerde laserstralen in ruimte en tijd te laten overlappen, kan een sum frequency (SF) spectrum worden gegenereerd dat alleen afkomstig is van de moleculen aan het grensvlak. Wanneer de optische frequentie van een van de laserstralen wordt afgestemd (in het mid-infrarood) op een specifieke, vibrationele resonantie van deze moleculen, waarbij de andere laserstraal niet resonant is, wordt het SF-signaal versterkt. Door de frequentie van de eerste laserstraal te variëren kan zo het infrarood (IR) spectrum van de moleculen aan het oppervlak verkregen worden. Zoals reeds bekend is van IR absorptie-spectroscopie, kunnen tal van structurele eigenschappen worden onderzocht door het IR-spectrum te observeren onder verschillende omstandigheden - bijvoorbeeld onder variatie van temperatuur, oplosmiddel, of zuurgraad. Volgens hetzelfde principe kan VSFG ons informatie verstrekken over moleculen aan een grensvlak. Maar omdat zowel IR- als VSFG-spectroscopie een tijdsgemiddelde nemen geven deze spectra alleen het gemiddelde van de moleculaire structuur weer, waarbij dynamische, structurele informatie die in de spectra verscholen kan zitten, verloren gaat. Dit is precies wat er gebeurt wanneer de VSFG-metingen aan een water-lucht of aan een water-lipide grensvlak worden uitgevoerd: de statische VSFG-spectra van deze interfaces zijn over het algemeen breed, en zonder noemenswaardig detail. De verscheidene grensvlakken die in dit proefschrift bestudeerd worden variëren van een simpel water-lucht grensvlak tot een model van een longmembraan, bestaande uit vier verschillende soorten fosfolipiden en een polypeptide van 21 aminozuren. Voor al deze media lijken de VSFG-spectra van het water aan het grensvlak erg op elkaar.

Soortgelijke observaties van brede en ongedetailleerde IR-spectra van watermoleculen in de *bulk* fase leidden op den duur tot de ontwikkeling van ultrasnelle infrarood pump-probe lasertechnieken. Met deze technieken, is veel informatie verzameld over de structurele dynamica van bulk water. In een typisch IR pump-probe experiment zorgt een zeer intense ultrakorte IR pump-puls (~ 100 fs pulsduur), met een frequentie afgestemd op bijvoorbeeld de O-H strek vibratie van water, voor excitatie van die vibratie. Hierna wordt met een IR probe-puls de relaxatie van de vibrationele verstoring bekeken op verschillende tijdstippen na de excitatie. Zodoende kunnen spectra worden opgenomen binnen een tijdsduur van slechts ~ 100 fs. De ultrasnelle spectrale veranderingen reflecteren de ultrasnelle structurele veranderingen. Op basis van deze IR pump-probe techniek, werd toegepast op *bulk* systemen, is de nieuwe, IR pump - VSFG probe methode ontwikkeld die de kern vormt van dit proefschrift, waarin de VSFG-spectra van water moleculen aan *grensvlakken* opgenomen kunnen worden op verschillende tijdstippen na een IR-excitatie. In deze methode wordt, naast de twee SF-genererende laserstralen, gebruik gemaakt van een ultrakorte (~ 100 fs), gepulste IR laser van hoge intensiteit die met de andere bundels samenvalt op het grensvlak en die een variabele vertraging heeft met betrekking tot de SF-genererende probe laserstraal. Een aantal modellen van biologische grensvlakken is bestudeerd met deze IR pump - VSFG probe methode (ook aangeduid met time-resolved SFG, TRSFG).

In het eerste onderzoek werd de TRSFG-techniek gebruikt om het water-lucht grensvlak te bestuderen, waarbij IR-pump en probe frequenties gelijk werden gehouden. Het statische VSFG-spectrum van de O-H waterstofbrug-oscillatoren van dit grensvlak is breed ($3200\text{-}3500\text{ cm}^{-1}$) en mo-

gelijk inhomogeen verbreed: bij 3200 cm^{-1} is het sub-ensemble van O-H oscillatoren sterk verbonden door waterstofbruggen, terwijl deze verbindingen bij 3500 cm^{-1} zwak zijn. Toch werd aangetoond dat de dynamische TRSFG-relaxatie onafhankelijk is van het sub-ensemble van de beschouwde watermoleculen. Omdat de relaxatie-dynamica van deze twee zeer verschillende sub-ensembles gelijk zijn, doen ze denken aan het waargenomen gedrag voor water in bulkvorm. Net als in de bulk worden de TRSFG relaxatie-dynamica gedomineerd door een ultrasnelle (~ 50 fs) vibrationele energieoverdracht van het Förster-type tussen naburige moleculen. Hierdoor worden verscheidene ensembles ultrasnel aangeslagen, en verliest het systeem heel snel zijn geheugen voor de polarisatierichting van de excitatie. Hetzelfde mechanisme viel te herkennen in het water aan het oppervlak. Inderdaad blijken de tijdschalen van relaxatie van de bulk goed onze TRSFG-data te kunnen beschrijven, met $T_1=200$ fs and $T_{\text{thermalisatie}}=500$ fs. Bovendien toont polarisatie-afhankelijke TRSFG aan dat de excitatie zich snel verspreid, in overeenstemming met de hypothese dat relaxatie zich voltrekt zoals in de bulk. Zodoende hebben we laten zien dat water aan een oppervlak en in bulk niet van elkaar te onderscheiden zijn ten gevolge van de hoge efficiëntie van Förster- energieoverdracht tussen de watermoleculen.

In ons tweede onderzoek werd TRSFG gebruikt om het grensvlak tussen een enkele laag fosfolipiden en water te beschouwen, om zo onderscheid te kunnen maken tussen enerzijds de effecten van interacties tussen water en de kopgroep en anderzijds de effecten die simpelweg ontstaan door begrenzing van de bulk, zoals bij het water-lucht grensvlak. Het gebruikte lipide was 1,2 Dimyristoyl Glycero-3-Phospho-L-Serine (DMPS, natriumzout), met een negatief geladen kopgroep. We hebben laten zien dat de TRSFG-dynamica bij het lipide-water grensvlak inderdaad verschilden van die aan het water-lucht grensvlak. Hoewel de sub-ensembles met zwakke tot middelmatige waterstofbrugverbindingen ($3300\text{-}3500\text{ cm}^{-1}$) gelijksoortige T_1 dynamica vertoonden als die aan het lucht-water grensvlak, waren er voor het sub-ensemble met sterk gebonden watermoleculen (rond 3200 cm^{-1}) relaxatiedynamica te zien die sneller waren dan de pulsduur zelf (<100 fs). Ook bleek de tijdschaal van thermalisatie voor alle sub-ensembles ietwat langer te zijn dan aan het water-lucht grensvlak (~ 1 ps). Vervolgexperimenten met verschillende typen fosfolipiden (positief geladen DPTAP, zwitterionisch DPPC, DPPE) lieten zien dat het het sterk gebonden sub-ensemble van watermoleculen inderdaad T_1 -relaxatietijden heeft korter dan de pulsduur (in de orde van ≤ 50 fs), terwijl voor de dynamica van de sub-ensembles met zwakkere waterstofbruggen een Förster-type overdracht de overhand heeft, zoals ook bij het water-lucht grensvlak te zien is.

In een onafhankelijk onderzoek werden de structuur en dynamica van water in contact met een enkele laag van oppervlakte-actieve stoffen van de long (lung surfactant, LS) - bestaande uit vier soorten lipiden (DPPC, DPPG, tripalmitin and cardiolipin) en een peptide van 21 aminozuren - onderzocht door middel van zowel statische VSFG- als TRSFG-spectroscopie. In dit onderzoek werd gekeken naar de dynamica van alleen het sub-ensemble met sterke waterstofbrugverbindingen (rond 3200 cm^{-1}), grenzend aan drie systemen van elk een enkele laag lipiden: een laag van het lipide dat het meest voorkomt in het LS-mengsel (DPPC), een laag van de vier lipiden, en een laag van de vier lipiden met daarin ook het LS-eiwit. Hoewel de statische VSFG-spectra voor elk van de drie systemen vergelijkbaar zijn, werden opmerkelijke verschillen aangetoond in de relaxatiemechanismen van

vibrationele energie tussen het pure DPPC-water systeem en de twee mengvormen. In tegenstelling tot de (T_1) relaxatiedynamica van het DPPC-water grensvlak, die opnieuw sneller zijn dan de pulsduur, waren er aanwijzingen dat de dynamica voor de twee LS-mengvormen voornamelijk worden beheerd door een Förster-type vibrationele energieoverdracht. Dat dit zelfs het geval was voor het sub-ensemble van sterk gebonden watermoleculen duidt op onderliggende structurele verschillen van de interactie van het water aan het grensvlak met deze verschillende lipidesystemen.

In het laatste hoofdstuk wordt het gebruik van TRSFG bij het onderzoek naar de dynamica van energiestromen op het grensvlak van modelmembranen en water beschreven. In dit onderzoek wordt gekeken naar de vibrationele relaxatiedynamica van de C-H strek-vibratie (CH_3 en CH_2 strek-vibraties) in de alkylketens van de lipiden. De resultaten onthullen dat een incoherente energieoverdracht plaatsvindt vanuit de aangeslagen CH_2 -groepen naar de CH_3 groepen aan de uiteinden van de ketens. Tevens werden aanwijzingen gevonden voor een sterke anharmonische koppeling tussen verschillende CH_2 - en CH_3 -vibraties. Relaxatie en processen van energieoverdracht binnen de alkylketen vinden plaats binnen een tijdsduur van een picoseconde. Metingen bij verschillende fasetoestanden van de lipiden (gelfase of vloeibaar-kristalfase) onthullen dat de dynamica duidelijk onafhankelijk is van de precieze moleculaire structuur van de lipiden. Daarnaast zijn dynamica van energieoverdracht tussen aan het membraan gebonden water en lipiden getoond waarin de overdracht van warmte tussen water en lipiden zich opmerkelijk snel voltrekt: warmte begeeft zich door de monolaag, van de polaire kopgroep van de lipiden tot het uiteinde van de alkylketen, binnen een tijdsduur van 1 ps. Deze resultaten onthullen het potentieel van het gebruik van ultrasnelle, oppervlakgevoelige TRSFG spectroscopie in het doorgronden van biomoleculaire dynamica in (modellen van) membraanoppervlakken.

Dankwoord

The challenging task of completing this thesis couldn't have been accomplished without the motivation and selfless support of some of the most nicest individuals I've ever met. Here I would like to take the opportunity to thank everyone at the Biosurface Spectroscopy Group at AMOLF for providing me with the essential artillery towards the realization of this thesis and making my stay a total experience. Firstly, although words fall short, I wish to thank Mischa for providing me not only the opportunity to work in his group but also for motivating me all along as a friend and appreciating my efforts, and most importantly by being critical of my experimental results. He has taken me by the hand, whether be it carrying my boxes from Amsterdam Centraal to my apartment upon my arrival in this country or be it teaching me the art of public scientific oratory. I thank Mischa for all that I've learnt under his tutelage. It's been a great experience to have worked with Marc and Ellen in building the time-resolved SFG setup while I would like to thank Niels for helping in automating it. It was certainly a painful task which couldn't have been accomplished without keeping up the humour and playing all kinds of odd songs at odd hours in the lab! I would also like to thank Dr. Martin Sterrer (at the Fritz Häber Institute, Berlin) for accompanying me in my first late night scientific escapades. Without you guys, I couldn't have worked for 48 hour shifts - which soon became a habit - and helped me carry on even after you guys left AMOLF. I would also like to thank Maria and Sjors for not only introducing me to SFG but also for being very supportive through thick and thin and keeping the lab environment stress-free, especially by raising the optical table by 10 cms ;-). Wish you all the best Maria on your PhD defense next week! Thanks Euan, Mattijs and Joep for being my first office mates - it was totally awesome! Euan - thanks for opening my eyes towards my understanding of surfaces from a completely tangential perspective - An analysis of the forces required to drag sheep over various surfaces (Applied Ergonomics, Volume 33, Issue 6, November 2002, Pages 523-531) - the range of surfaces used in the study were corrugated aluminum sheets to barbed wire! Also thanks Euan for sending emails from my account to Mischa - how to whack your boss in 13 ways (it's 20 nowadays) and almost jeopardizing my job here! Mattijs - thanks for introducing me to the Anarchist's Cookbook - if you ever come across a bomb made of tomatoes, cucumbers, lemon and vinegar, you know whom to look for ;-). Joep - thanks for your relentless efforts to getting me hooked on to Britney. Your efforts have definitely paid off by

transforming my hate for her into indifference towards her - that's really a BIG step! Jens - it was great working with you through the nights on the 2D-SFG setup and we shall remember the *best song in the world*, especially the refrain "We are but Men"! Susumu - thanks for everything you did in the last year of my PhD. I'm sorry if the time-resolved SFG setup has sapped all life force from you - but let me tell you, no one can be as able an heir to the time-resolved throne (if something like that exists) as yourself. Also it seems you're in a better position to be the editor-in-chief for our New Journal of PAIN (Polarization Anisotropy at INterfaces). Thanks Klaas, Gianluca, Katrin and James for all the pep-talk and preserving the general camaraderie in the group; although Klaas' contribution to the Bonn group camaraderie is only half. Thanks Ronald - for being my office-mate and flat-mate for most of the period of my stay here. Our nightly escapades to various parties mostly with terrible music and warm 1 Euro beer, dealing with evil old neighbours, house-cleaning fights and interviewing strange applicants for the room at Krammerstraat would be some of the memories that'll tag along with me. Kramer - thanks for the wonderful discussions we've had, treading across almost every topic under the sun from the depths of Antarctic ice-cores to flying my dream craft SR-71. Also thanks for helping me out with this thesis - it would take much longer if you hadn't been so kind to help me in general LaTeX formatting issues. Issues - think 'bout it, just think 'bout it! I shall always cherish the silly discussions over lunch, the numerous coffee breaks, the thirsty Thursdays and the curry/Bollywood evenings at my place with the Bakker-Bonn group including Han-Kwang, Maaikje, Peter, Domenico, Yves, Rutger, the Christians, Jocelyn and Eric. I wish all the younglings in the Biosurface Spectroscopy group, the very best in their endeavours at AMOLF and beyond - Thuy, Steven, Ruben and Cho-Shuen. Ruben, you have the extra responsibility of keeping the moronic traditions in our office since you have the honor of being Euan's successor (chair/desk-wise). I must say that my stay in the Netherlands, wouldn't probably be half as enjoyable without you guys! I must also thank all my Indian friends in the city - Rajoy, Rajesh, Rajat, Ritika, Onkar, Nilanjan, Sumedha, Shishir, Nayantara and Ganesh - for all the good times we've had together. It was particularly great to have Rajat here after our Delhi University days, some 8-9 years ago. You guys made this place my second home. Keep rockin'. Just like every building has a very strong foundation, the success of this PhD thesis should also be attributed to the reliable and strong support groups at AMOLF - including the E&I, the design workshop and the Personnel department. Particularly I would like to thank Hinco his selfless support in everything from fixing the air-co to the beastly YLF laser from time to time while seriously jeopardizing his beer sessions in Leiden. Ernst, Ad de Snaijer, Iliya Cerjak, Duncan, Idsart and Ilja Stavenuiter have also been extremely helpful and prompt with some of my mechanical and electronics design demands. I must also mention the help I received from the Leiden Institute of Chemistry, especially Dr. Johan Bakker and Jose Dijkzeul with placing my orders and general administrative issues. Thanks guys! Last but not the least, I shall remain indebted to my mum, dad and my younger brother in Delhi for not only being patient with me and my scientific endeavours but also being my spiritual strength that drove me all along, despite the physical distance of 7000 kilometres! I shall never forget the sacrifices you made to give me the best in life despite the situations we've been through and I promise to keep up to your expectations. For one, I dedicate this thesis to you. I love you all.

Curriculum Vita

Avishek Ghosh was born in London, U.K. in 1979. He moved to India along with his parents in 1984. He completed his primary, secondary and senior secondary education from Tagore International School (East of Kailash) in Delhi in 1998, with a distinction in Mathematics. He went on to study Chemistry in St. Stephen's College at the University of Delhi and received his Bachelor of Science degree with Honours in 2001. Further he went on to complete his Master of Science degree in Chemistry at the Indian Institute of Technology in Delhi in 2003. He spent a year (2004-2005) at the Max-Planck Institut für Quantenoptik in Garching (München) before joining Universiteit Leiden in April 2005. Most of his work presented in this thesis were performed in Prof. Mischa Bonn's Biosurface Spectroscopy group at the FOM-Instituut voor Atoom- en Molecuulfysica (AMOLF), located in the Science Park in Amsterdam. Currently he's still working at AMOLF on some ongoing projects. He shall be moving to the Advanced Light Source at Lawrence Berkeley National Labs in CA (USA), by the end of 2009, as a Postdoctoral Fellow. His future work is directed towards Ultrafast X-ray Spectroscopy. Some of his hobbies are music, photography and playing squash. His parents live in the National Capital Territory of Delhi in India and his younger brother has recently joined a Ph.D. programme in the Department of Earth and Environmental Science at the University of Rochester, NY (USA).

lipid vibrational SFG energy data bulk relaxation shown IR interface excited membrane VSFG pump probe molecules frequency water

signal surface generation DPPC CH₂ CH₃ cm⁻¹ CH₃ DPPC generation T₁₂ CH₂ Frequency DOPC

relaxation interface pump probe molecules frequency water

excited membrane VSFG pump probe molecules frequency water

state polarization stretch

time-resolved

water

lipid surface vibrational SFG energy data bulk relaxation shown IR interface excited membrane VSFG pump probe molecules frequency water

excited membrane VSFG pump probe molecules frequency water

state polarization stretch

time-resolved

water

Stellingen

- Ultrafast dynamics studies of interfacial water molecules at the air-water interface show that surface water behaves very similarly to bulk water in terms of its vibrational dynamics. (This thesis, Chapter 3)
- Ultrafast dynamics studies of lipid membrane-water interfaces show that membrane-bound water molecules are different from the ones in bulk water or those at the air-water interface. (This thesis, Chapter 4).
- Stacks of (partially) hydrated lipid bilayers do not necessarily present good model systems for biological membranes. Specifically, the dynamics of water molecules incorporated in hydrated lipid bilayer stacks are very different from those at the interface of bulk water and lipids. (Volkov *et al.*, *Phys. Rev. Lett.* 99, 78302, 2007; this thesis, Chapter 4 and 5).
- The generic understanding of the complexity of biological membrane function has largely overlooked the role of membrane-bound water, owing to the technical challenges in probing a water layer as thin as $\sim 5 \text{ \AA}$ – leading to a convenient, yet insufficient assumption that the interfacial water is simply an effective dielectric continuum around the membrane system.
- The two peaks in the SFG spectrum of surface water at 3200 and 3450 cm^{-1} were initially proposed to be the result of “ice-like” and “liquid-like” water species existing at the surface. SFG experiments on isotopically diluted water however proves that the two-peak feature in the spectrum can be best explained if the *dip* in the spectrum is the result of a Fermi resonance between the bend overtone and the stretch fundamental modes of the water molecule and not due to different species of water at the surface. (Sovago *et al.*, *Phys. Rev. Lett.* 100, 173901, 2008).
- SFG spectroscopy although a powerful tool in the surface science community, must be used in conjunction with other traditional surface techniques, in order to understand the true nature of surfaces and interfaces.
- Although SFG spectroscopy is highly surface-sensitive (sensitive to ~ 1 monolayer of matter), the efficacy of the technique largely depends on the kind of surfaces it is being used to probe: if the material symmetry is maintained to a large extent into the bulk from the surface, SFG will be sensitive only where the symmetry breaks, i.e. a few monolayers beneath the actual surface.
- SFG spectral intensities of interfacial water at charged lipid monolayers are much larger than those at zwitterionic or neutral lipid monolayers, primarily due to the second-order $\mathbf{P}^{(2)}$ of the interfacial water being enhanced by a bulk $\chi^{(3)}$ response originating from the DC-field provided by the *sheet* of charged head-groups. (This thesis, Chapter 4).
- By extending the time-resolved SFG setup, mentioned in this thesis, to a twodimensional SFG setup, one can address the molecular vibrational couplings and their evolution in real-time, in a very surface-specific manner. (Bredenbeck *et al.*, *J. Am. Chem. Soc.* 130(7), 2152, 2008).
- The concept of “Stellingen” is archaic and environmentally unfriendly since it takes up an extra piece of paper which people usually don’t read or it gets lost somewhere down the line.